METRANS Transportation Center
USC CSULB

METRANS RESEARCH PROJECT

Project 03-17

ANALYTICAL AND EXPERIMENTAL STRUCTURAL SYSTEM IDENTIFICATION USING VARIABLE STIFFNESS AND DAMPING DEVICES

FINAL REPORT

June 2007

Prof. Erik A. Johnson
Principal Investigator, Associate Professor
Department of Civil and Environmental Engineering
University of Southern California

Dr. Mohamed I.S. Elmasry
Arab Academy for Science & Technology and Maritime Transport, Alexandria, Egypt
(Formerly, Graduate Rsrch. Asst., Civil & Env. Engrg., University of Southern California)

ANALYTICAL AND EXPERIMENTAL STRUCTURAL SYSTEM IDENTIFICATION USING VARIABLE STIFFNESS AND DAMPING DEVICES

Prof. Erik A. Johnson
Principal Investigator, Associate Professor
Department of Civil and Environmental Engineering
University of Southern California

Mohamed I.S. Elmasry
Arab Academy for Science & Technology and Maritime Transport, Alexandria, Egypt
(Formerly, Graduate Rsrch. Asst., Civil & Env. Engrg., University of Southern California)

ABSTRACT

Structural health monitoring (SHM) is the process of monitoring structural health and identifying damage existence, severity and location. Clear needs for SHM exist for various types of civil structures; *e.g.*, approximately 25% of U.S. bridges are rated as deficient and require significant expenditures to rebuild or replace them (FHWA, 2002). Yet, the dominant method for monitoring the health of civil structures is manual visual inspection. Global vibration-based SHM techniques have been studied, but no approach has been well established and accepted due to limitations of ambient excitation for most civil structures and the small sensitivity of global vibration characteristics to damage. One approach that may alleviate some of the SHM difficulties for civil structures is using variable stiffness and damping devices (VSDDs) — controllable passive devices that received significant study for vibration mitigation — to improve damage estimates. In addition to providing near optimal structural control strategies for vibration mitigation, these low-power and fail-safe devices can provide parametric changes to increase global vibration measurement sensitivity for SHM.

This report proposes using VSDDs in structures to improve SHM, and demonstrates the benefits analytically and experimentally in contrast with conventional passive structures. A 2DOF bridge structure model and two shear building models (2DOF and 6DOF), are used as test beds to study the VSDD approach analytically in the context of an iterative parametric frequency domain identification. Using data from multiple VSDD configurations, and using multiple channels of data, a least-squares error formulation is used to estimate unknown structural parameters. The improvements in identification are quite effective when adding high effective levels of stiffness or damping to a structural system, though the resulting VSDD forces are small due to the low levels of ambient excitation. The VSDD approach is also studied using the Eigenvalue Realization Algorithm. In the experimental part of this study, a 2DOF shear building structure is excited using a small shaking table and the building parameters are identified. Results show that using VSDDs in identification gives parameter estimates that have more accurate means and smaller variations than the conventional structure approach.

Keywords: structural health monitoring, variable stiffness and damping devices, parametric frequency-domain identification, damage detection.

DISCLAIMER

The contents of this report reflect the views of the authors, who are responsible for the facts and the accuracy of the information presented herein. This document is disseminated under the sponsorship of the U.S. Department of Transportation, the University Transportation Centers Program, and the California Department of Transportation in the interest of information exchange. The U.S. Government and the California Department of Transportation assume no liability for the contents or use thereof. The contents do not necessarily reflect the official views or policies of the State of California or the U.S. Department of Transportation. This report does not constitute a standard, specification, or regulation.

ACKNOWLEDGMENTS

The authors gratefully acknowledge the partial support of this work by the U.S. Department of Transportation through the National Center for Metropolitan Transportation Research (METRANS), and by the National Science Foundation under CAREER grant 00-94030.

TABLE OF CONTENTS

LIST OF TABLES

LIST OF FIGURES

1 INTRODUCTION

Detecting damage in structures at an early stage, before they deteriorate, is vital to protecting structures. Generally, damage may be caused by acute events, such as earthquakes and other natural disasters, or by long-term degradation from environmental effects and human use (and abuse). Whatever the cause, structural damage can threaten both danger to human life and risk huge economic losses. Consequently, a process that can detect damage as early as possible would be extremely useful. The process of monitoring structural health and identifying damage existence, severity and location is generally termed *structural health monitoring* (SHM). Chang (1999) defined structural health monitoring to be an "autonomous [system] for the continuous monitoring, inspection, and damage detection of [a structure] with minimum labor involvement."

Fig. 1-1. Beam-column connection damage (Kiremedjian, 1999)

Fig. 1-2. Cracks through column flange and extending into web (Hall, 1995)

Fig. 1-3. Plastic hinging at top of column (Hall, 1995)

The SHM process includes system identification as a major step. Thus, high fidelity modeling and accurate response estimation are required to monitor the changes of structural characteristics and response and, subsequently, predict the onset of failure or the expected remaining life. With identification at different points in time — periodically or shortly after natural disasters — changes in these characteristics may be monitored. With damage models, changes in structural characteristics are used to predict damage severity and location. This study proposes using smart, controllable passive devices such as Variable Stiffness and Damping devices (VSDDs) in structures to improve SHM, and demonstrates the benefits over conventional passive structures.

1.1 SHM Benefits, Difficulties and Suggestions

Robust SHM systems are essential needs for both building and bridge structures: significant expenditures were reported after the 1994 Northridge and the 1995 Kobe earthquakes in inspecting hidden damage in joints of steel buildings for damage (*e.g.*, Fig. 1-1 to Fig. 1-3) (Mita, 1999); a recent report to the U.S. Congress by the Federal Highway Administration (FHWA, 2002) indicates that approximately 25% of the bridges in the U.S. are rated as deficient and will require huge annual expenses for repair (Patten *et al.*, 1999).

One approach to SHM is based on global vibration methods. Many global vibration SHM studies assume a class of mathematical models that may represent the actual structure. Generally, studies have focused on identifying changes in modal parameters obtained from measured vibration response; state-of-the-art surveys of global vibration SHM techniques applied to civil

engineering are given by Doebling *et al.* (1996, 1998). Unfortunately, no global technique has been well established and accepted as an overall successful approach (Sanayei *et al*., 1998). This may be attributed to several reasons including (*i*) models cannot exactly predict the full behavior of real structures, (*ii*) periodic environmental effects, such as thermally-induced variations, may mask the effects of damage on global vibration characteristics, (*iii*) measurement noise can cause significant variation from one test to the next, (*iv*) excitation is limited to ambient sources for most civil structures, and (*v*) the sensitivity of global vibration characteristics to damage may be small. These all lead to variations in the identified model parameter characteristics that are not due to true changes in the structure, raising uncertainty in damage estimates (Vanik *et al*., 2000).

Using forced structural response strategies, some of the aforementioned problems can be overcome: *e.g.*, for structures with embedded active vibration control systems, the actuators can be used to enhance damage detection by tuning the actuation signals to directly increase closed-loop damage sensitivity of global vibration characteristics (Ray and Tian, 1999). However, large actuation devices are not being used in a continuous manner for civil structures (except a few isolated cases in Asia) due to large power requirements, concerns about stability and so forth, rendering them impractical for damage mitigation or SHM of civil structures.

As a consequence, in order to perform SHM, one is restricted to analyzing response to ambient excitation that takes a number of forms (*e.g.*, wind, traffic, waves and microtremors). Ambient excitation has several advantages over approaches using forced vibration response. For low amplitude excitations typically experienced during ambient vibration, most structural systems are well characterized with linear models. Further, continuous ambient vibration tests can be performed at a very low cost. However, due to small structural response under such ambient excitations, measurement signal-to-noise ratios are small enough to make SHM difficult.

One approach that may help alleviate some of the SHM difficulties for civil structures would be to use "smart" variable stiffness and damping devices (VSDDs) — controllable, low-power and fail-safe passive devices that have received significant study for vibration mitigation (Spencer and Sain, 1997; Symans and Constantinou, 1999) — in a synergistic manner to provide internal parametric changes to affect sensitivity to damage. Further, the integration of smart damping and SHM can exploit, in a synergistic manner, the common aspects of both technologies as seen in the flowcharts in Fig. 1-4.

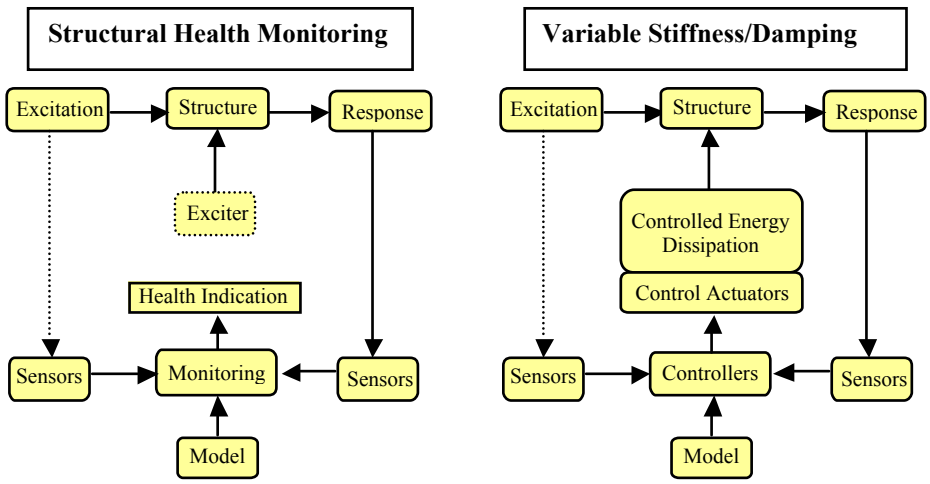

Fig. 1-4. SHM and variable stiffness/damping flow charts

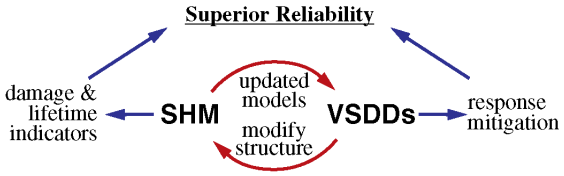

Fig. 1-5. Mutual benefits of SHM and VSDDs

VSDDs can adjust the behavior of a structure by real-time modification of stiffness and damping at discrete points within the structure. By commanding different behavior for each VSDD in a structure, multiple structural configurations can be tested, each of which can be designed to increase the sensitivity to damage in different portions of the structure (see Fig. 1-5).

1.2 Overview of the VSDD/SHM Research Studied Herein

This study proposes using VSDDs in structures to improve SHM, and demonstrates the benefits in contrast with conventional passive structures. The focus herein is introducing a better approach for estimating the structural dynamic parameters through the use of variable stiffness and damping devices. The study is divided into two parts. The first part is an analytical study of the benefits of applying VSDDs in SHM. The second part studies the VSDD approach benefits from an experimental perspective. Since controllable stiffness/damping devices are used to give the parametric changes necessary for improved monitoring, the structural models must be *control-oriented* dynamic models — *i.e.*, low-order models that still capture most of the salient dynamic characteristics of a real structure, particularly in locations of the controllable devices and in the frequency ranges driven by the excitation.

Using different identification techniques to investigate the use of VSDDs for SHM gives a broad view of how VSDDs are useful. In this study, the VSDDs are first investigated in the context of parametric frequency domain identification methods to determine structural parameters. An iterative method, previously proposed in METRANS report 01-10 (Johnson and Elmasry, 2003), is used first; this identification method expresses the structural system transfer functions in terms of the unknown structural parameters, and then iteratively uses a procedure to minimize the numerators of the error between the theoretical transfer function and the measured ones (in each iteration, using the denominator evaluated using the previous parameter estimates). Then, another parametric frequency domain method, denoted INVFLS herein, is introduced. INVFLS first identifies the polynomial coefficients of the transfer functions, using a multi-input multi-output extension, developed herein, to the `invfreqs` function in MATLAB for single-input single-output transfer functions; then, INVFLS obtains the structural parameters from direct relations with the polynomial coefficients. In addition, one subspace identification method, the Eigensystem Realization Algorithm (ERA) technique, is also used to study the benefits of the VSDD approach over the conventional structure approach. The numerical examples herein use a fairly noisy signal to challenge the methods.

In the analytical part (Chapters 3, 4 and 5), several structures are studied, with one or more VSDDs installed. First, two degree-of-freedom (2DOF) and then six-degree-of-freedom (6DOF) shear building structural models are studied, each in several configurations: the 2DOF structure with a VSDD in (*i*) the first story, (*ii*) the second story, and (*iii*) both stories, and the 6DOF building with VSDDs in the first three stories. Then, a 2DOF bridge structure model (Erkus *et al.*, 2002) is studied with a VSDD attached in the bearing layer between the pier and the deck. In each case, the VSDD is chosen to act as an ideal variable stiffness/damping device, with one of

several discrete stiffness/damping values. These devices are located in the structures in the form of lateral bracing or, in the bridge example, in the isolation layer between the bridge deck and the pier supports.

Using the least squares approach on the modified version of the error in transfer functions with known starting guesses, both using VSDD and conventional identification techniques give parameter estimates. METRANS report 01-10 (Johnson and Elmasry, 2003) introduced one approach for estimating structural parameters using low force levels in the VSDDs — up to 40% of the stiffness/damping of the corresponding story. While the previous study demonstrated that VSDDs can improve damage characterization, giving more accurate mean estimates and smaller estimate mean square errors, its improvements were modest. However, Chapter 3 in this study shows that the VSDD approach with higher levels of additional stiffness/damping, several times that of the corresponding stories, dramatically improves the estimate accuracy, reducing identification error significantly compared to the conventional structure approach. The VSDD force levels are shown to be quite reasonable and well within the capabilities of VSDDs developed to date.

In addition, Chapter 4 shows that using a two-stage least squares identification — first identifying the coefficients of the transfer function polynomials and then the structural parameters — gives results slightly better than the conventional approach. Moreover in Chapter 5, using the ERA technique, it is found that the root mean square error (RMSE) of the estimated structure stiffnesses is also reduced, indicating more accurate results.

In the experimental part of this study (Chapter 6), a 2DOF shear building structure, composed of vertical aluminum plates and horizontal plexi-glass plates, with weak springs elements in the diagonal bracing, is the test bed of the study. A small shake-table excites the structure to replicate ambient ground motion. The ground acceleration takes two forms: a band limited white noise and a filtered band limited white noise. The effects of VSDDs in the structure are replicated by adding a set of stiff springs in the diagonal bracing. The outcome of the experimental study is found to validate the improvements exhibited in the analytical study. The VSDD approach gives better means and smaller variations, whereas the conventional structure approach indicated less confidence in its results.

Finally, the conclusions (Chapter 7) summarize the results and provide some thoughts on future directions of this work.

2 SUMMARY OF PREVIOUS WORK

The contents of this METRANS report 03-17 follow the initial study in the METRANS report 01-10 (Johnson and Elmasry, 2003). METRANS report 01-10 studied the effectiveness of using variable stiffness and damping devices (VSDDs) to improve estimates of structural parameters for structural health monitoring and damage detection. VSDDs are controllable passive devices that have been shown to have significant potential for mitigating structural response to natural hazards. Previous work in METRANS report 01-10 demonstrated that VSDDs also have strong promise for use in SHM as well. Since VSDDs can be commanded to exert various force time histories, the response of a structure may be altered through the parametric changes effected by the VSDDs.

METRANS report 01-10 investigated VSDD/SHM by identifying structural parameters — mass, stiffness and damping coefficients — based on measured absolute acceleration transfer function data, using a parametric frequency-domain least-squares identification method. For each numerical example and configuration, the structural parameters were identified, first with one or more VSDDs in the structure, and then with no VSDDs. In all cases, simulated sensor noise was added to the exact transfer function to replicate the noisy transfer functions that are typically obtained through standard experimental techniques. In each VSDD configuration, data is collected while the VSDDs are commanded to act in one of several discrete stiffness or damping modes, with different noise corrupting each subsequent data set. To make for a fair comparison, the conventional structure approach was provided with the same amount of data. The variation in identified structural parameters due to the effects of random noise were studied by performing these identifications a number of times, each with a different random seed to generate the noise, giving a measure of both the mean and the variance of the structural parameter estimates.

While the VSDD approach is applicable to a wide variety of structural identification methodologies, it was studied in METRANS 01-10 in the context of a least-squares identification using the frequency-domain transfer function representation of the input/output dynamics of a structure. It was shown that one commonly-used simplification of this identification method gives biased results, and an alternate iterative approach is shown to give superior results. A summary of the iterative least squares numerator (ILSN) method from METRANS 01-10 is introduced in the following section.

2.1 Iterative-Least Squares Numerator Method (ILSN)

The transfer functions generally are defined by the ratio between the Fourier transforms of the output and input signals. For example, consider a linear structural model of the form:

$$\mathbf{M}\ddot{\mathbf{x}} + \mathbf{C}_d\dot{\mathbf{x}} + \mathbf{K}\mathbf{x} = \mathbf{b}f\ , \qquad \mathbf{y} = \mathbf{C}_1\mathbf{x} + \mathbf{C}_2\dot{\mathbf{x}} + \mathbf{d}f + \mathbf{v} \tag{2-1}$$

where $\mathbf{M}$, $\mathbf{K}$, and $\mathbf{C}_d$ are the mass, stiffness and damping matrices of the system, and $\mathbf{C}_1$, $\mathbf{C}_2$, and $\mathbf{d}$ are the output influence matrices for the displacement, velocity and the external scalar force f. Similarly, one can write the model in state-space form

$$\begin{aligned} \dot{\mathbf{q}} &= \tilde{\mathbf{A}}\mathbf{q} + \tilde{\mathbf{B}}f \\ \mathbf{y} &= \mathbf{C}\mathbf{q} + \mathbf{D}f + \mathbf{v} \end{aligned} \tag{2-2}$$

where $\mathbf{q} = [\mathbf{x}^T\ \dot{\mathbf{x}}^T]^T$ is the state vector, $\tilde{\mathbf{A}}$ is the system state matrix that is dependent on the mass, damping, and stiffness matrices, $\tilde{\mathbf{B}}$ is the input influence matrix, $\mathbf{C}$ is the output influence

matrix**,** and **D** is the direct transmission matrix. In both equations, f is an excitation force, and **y** is an $M \times 1$ vector of measured responses corrupted by $M \times 1$ sensor noise vector **v**.

Thus, the system can be represented by the $M \times 1$ transfer function matrix $\mathbf{H}(j\omega)$. Each element of $\mathbf{H}(j\omega)$ can be expressed as the ratio of numerator and denominator polynomials at a certain frequency with coefficients depending on matrices in Eqs. (2-1) or (2-2). The transfer function vector from a single input to the outputs can, consequently, be written in polynomial ratio form as:

$$\mathbf{H}(j\omega) = \mathbf{B}(j\omega) / A(j\omega) \tag{2-3}$$

where $\mathbf{B}(j\omega)$ and $A(j\omega)$ are the numerator and denominator polynomials

$$\begin{aligned} B_m(j\omega) &= b_{n_B-1}^{(m)}(j\omega)^{n_B-1} + b_{n_B-2}^{(m)}(j\omega)^{n_B-2} + \ldots + b_0^{(m)} \\ A(j\omega) &= \quad (j\omega)^{n_A} + a_{n_A-1}(j\omega)^{n_A-1} + \ldots + a_0 \end{aligned} \tag{2-4}$$

where the b's and a's are real coefficients.

Assuming that the transfer function has been determined experimentally through standard procedures from measured input and output data (Bendat and Piersol, 2000), the experimental transfer function matrix, expressed as

$$\hat{\mathbf{H}}(j\omega_p), \; p = 1, 2, \ldots, \; n_\omega \tag{2-5}$$

is known at n_ω discrete frequency points. Therefore, the difference between the estimated theoretical transfer function $\mathbf{H}(j\omega)$ and the actual experimental one $\hat{\mathbf{H}}(j\omega)$ represents the error equation, which is then used in the parameter identification process.

For a structure with one or more variable stiffness and/or damping devices, the properties of which are determined through a local control system, some of the coefficients in the transfer function polynomials may be adjusted through changing the VSDD control algorithms. Thus, it is convenient to introduce notation to explicitly state that the transfer function polynomials are functions of unknown structural parameters, denoted by the vector $\boldsymbol{\theta}$, which are to be estimated, and of known controllable structural parameters, denoted by the vector $\boldsymbol{\kappa}$. The transfer function expression can, then, be written as explicit function of these unknown and known structural parameters

$$\mathbf{H}(j\omega) = \mathbf{B}(j\omega, \boldsymbol{\theta}, \boldsymbol{\kappa}) / A(j\omega, \boldsymbol{\theta}, \boldsymbol{\kappa}) \tag{2-6}$$

For a given structural model, the A and **B** polynomials are specific known functions of their parameters. Substituting the measured TF in place of the exact TF leaves a residual error **e** that may be defined by

$$\mathbf{e}(j\omega_p, \boldsymbol{\theta}, \boldsymbol{\kappa}) = \frac{\mathbf{B}(j\omega_p, \boldsymbol{\theta}, \boldsymbol{\kappa}) - A(j\omega_p, \boldsymbol{\theta}, \boldsymbol{\kappa})\hat{\mathbf{H}}(j\omega_p, \boldsymbol{\kappa})}{A(j\omega_p, \boldsymbol{\theta}, \boldsymbol{\kappa})} \tag{2-7}$$

A conventional least-squares approach may be adopted to solve this problem, forming a global square error

$$\Delta^2(\boldsymbol{\theta}) = \sum_{p=1}^{n_\omega} \mathbf{e}^*(j\omega_p, \boldsymbol{\theta}, \boldsymbol{\kappa}) \cdot \mathbf{e}(j\omega_p, \boldsymbol{\theta}, \boldsymbol{\kappa}) = \sum_{p=1}^{n_\omega} \left| \mathbf{e}(j\omega_p, \boldsymbol{\theta}, \boldsymbol{\kappa}) \right|^2 \tag{2-8}$$

where $(\cdot)^*$ denotes complex conjugate transpose. The optimal choice of the unknown parameters is found by minimizing the square error — *i.e.*, take the partial derivatives of the square error Eq. (2-8) with respect to the elements of unknown vector $\boldsymbol{\theta}$, set the derivatives equal to zero, and solve the resulting (generally nonlinear) equations. However, if there are known controllable structural parameters in a structure with multiple configurations — which is the case when using VSDDs — the square error equation can be augmented by using several combinations of known controllable structural parameters

$$\boldsymbol{\Delta}^2(\boldsymbol{\theta}) = \sum_k \sum_{p=1}^{n_\omega} \mathbf{e}^*(j\omega_p, \boldsymbol{\theta}, \boldsymbol{\kappa}_k) \cdot \mathbf{e}(j\omega_p, \boldsymbol{\theta}, \boldsymbol{\kappa}_k) \tag{2-9}$$

where the symbol $\boldsymbol{\kappa}_k$ denotes one of multiple distinct sets of parametric changes to the structure. The error is, then, minimized simultaneously for all configurations.

Because the residual error **e** in Eq. (2-7) is a ratio of polynomials, the square error in Eq. (2-9) is an extremely complex function of the unknown parameters $\boldsymbol{\theta}$. Thus, to avoid bias, and to avoid the difficulty in solving the least-squares problem for the standard error measure **e**, an *iterative* method is adopted, using an approximation to the denominator in Eq. (2-7).

Assume that iteration i begins with a starting approximation $\hat{\boldsymbol{\theta}}_{i-1}$ to the unknown parameter vector $\boldsymbol{\theta}$; then, the denominator of Eq. (2-7) is estimated based on the vector $\hat{\boldsymbol{\theta}}_{i-1}$ of estimated parameters and is no longer a function of these unknowns, but only in the frequency and the multiple distinct sets of parametric changes to the structure

$$\hat{A}_i(j\omega_p, \boldsymbol{\kappa}_k) \equiv A(j\omega_p, \hat{\boldsymbol{\theta}}_{i-1}, \boldsymbol{\kappa}_k) \tag{2-10}$$

The error is, thus, formed as:

$$\hat{\mathbf{e}}_i(j\omega_p, \boldsymbol{\theta}, \boldsymbol{\kappa}_k) = \frac{\mathbf{B}(j\omega_p, \boldsymbol{\theta}, \boldsymbol{\kappa}_k) - A(j\omega_p, \boldsymbol{\theta}, \boldsymbol{\kappa}_k)\hat{\mathbf{H}}(j\omega_p, \boldsymbol{\kappa}_k)}{\hat{A}_i(j\omega_p, \boldsymbol{\kappa}_k)} \tag{2-11}$$

and the squared error takes the form

$$\boldsymbol{\Delta}_i^2(\boldsymbol{\theta}) = \sum_k \sum_{p=1}^{n_\omega} \hat{\mathbf{e}}_i^*(j\omega_p, \boldsymbol{\theta}, \boldsymbol{\kappa}_k) \cdot \hat{\mathbf{e}}_i(j\omega_p, \boldsymbol{\theta}, \boldsymbol{\kappa}_k) \tag{2-12}$$

Minimizing the sum of the square error in Eq. (2-12) will result in an updated estimate $\hat{\boldsymbol{\theta}}_i$ to the unknown parameter vector $\boldsymbol{\theta}$. The iterations continue until the relative differences between $\hat{\boldsymbol{\theta}}_{i-1}$ elements and the corresponding elements of $\hat{\boldsymbol{\theta}}_i$ are all below some threshold. (Absolute or relative norms of the difference could also be used.) A maximum number of iterations may also be set to stop the algorithm in the case that the iterative method does not converge (though this termination criterion was not required in this study as convergence always occurred within a limited number of iterations). This iterative least-squares identification, with and without VSDDs, was applied to several numerical examples: a bridge pier/deck model and two shear building models. A summary of these examples follows.

2.2 Numerical Test Beds

In METRANS 01-10 (Johnson and Elmasry, 2003) as well as in Chapters 3–5 of this report, three numerical examples are used as test beds of the VSDD/SHM approach. This section describes these examples.

2.2.1 Two Degree-of-Freedom Shear Building Model

Consider the two degree-of-freedom (2DOF) shear building structure model shown in Fig. 2-1. The structure is subject to ambient excitation from the ground. Absolute acceleration measurements of the ground, $\ddot{x}_g$, and of the two floors, $(\ddot{x}_1 + \ddot{x}_g)$ and $(\ddot{x}_2 + \ddot{x}_g)$, are used to generate a 2×1 experimental transfer function at n_ω distinct frequency values. (Note that x_1 and x_2 herein denote the displacements of the floors relative to the ground.) Let the unknown parameter vector be given by:

$$\boldsymbol{\theta} = \left[\begin{array}{ccccc} \frac{k_1}{m_1} & \frac{k_2}{m_2} & \frac{c_1}{m_1} & \frac{c_2}{m_2} & \frac{m_2}{m_1} \end{array} \right]^T \tag{2-13}$$

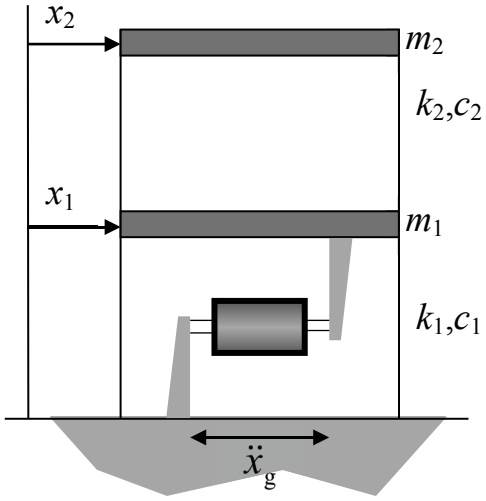

Fig. 2-1. 2DOF shear building model

A VSDD that can provide a number of distinct stiffness levels is located in the first, second, or both stories of the structure. The VSDD is installed in the lateral bracing of the structure and the mechanical properties of the dampers are modified according to control algorithms, which utilize the measured response of the structure. The device is considered ideal and semiactive; *i.e.*, it can generate the desired forces with no delay and with no actuator dynamics (Ramallo *et al*., 2000).

Therefore, the known controllable vector is related to the stiffness of a variable stiffness device such that

$$\boldsymbol{\kappa} = \kappa = k_{VSDD} / m_1 \tag{2-14}$$

or to the damping coefficient of a variable damping device

$$\boldsymbol{\kappa} = \kappa = c_{VSDD} / m_1 \tag{2-15}$$

Then, the theoretical transfer function can be written in the polynomial form as:

$$\mathbf{H}(j\omega, \kappa) = \left[\begin{array}{cc} \frac{B_1(j\omega, \boldsymbol{\theta}, \kappa)}{A(j\omega, \boldsymbol{\theta}, \kappa)} & \frac{B_2(j\omega, \boldsymbol{\theta}, \kappa)}{A(j\omega, \boldsymbol{\theta}, \kappa)} \end{array} \right]^T \tag{2-16}$$

The parameter identification methods discussed in the previous section can then be applied. The explicit reference to m_1 has dropped out of the transfer function polynomials; it is assumed here that of all the parameters, only m_1 is known. Different VSDD locations in the structure are studied in order to investigate the best way of using these VSDDs to improve SHM through better identification of the structural model parameters. Accordingly, this example is also solved considering a VSDD located in the second story of the structure and in both stories as well, as shown in Fig. 2-2 and Fig. 2-3.

In the numerical examples of this model, the masses and stiffnesses are taken of unit magnitude and the damping coefficients are taken as 0.05 kN·s/m.

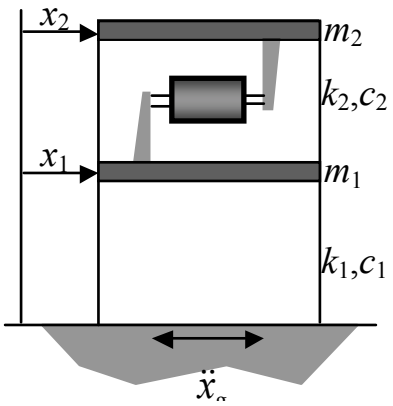

Fig. 2-2. VSDD in 2nd story of 2DOF model

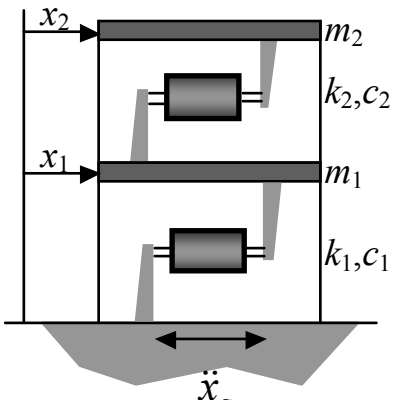

Fig. 2-3. VSDDs in both stories of 2DOF model

2.2.2 Two Degree-of-Freedom Pier-Deck Bridge Model

Consider a bridge structure such as the one shown in Fig. 2-4, which is a typical elevated highway bridge that consists of decks, bearings, and piers. The behavior of the bridge deck and piers, with a bearing between them, while complex, can be well approximated with the simple 2DOF model shown in Fig. 2-6*c*. This 2DOF model may be used to represent a passive system with rubber bearings if the girder is continuous with one pier and one bearing, or for several piers and bearings with identical properties. Also, this model can be used for VSDD systems if the devices are attached as shown in Fig. 2-5 and commanded to provide identical force levels. It is assumed in this problem that the pier mass m_1 is known.

Fig. 2-4. High occupancy vehicle (HOV) lanes during construction (ADOT, 2001)

The theoretical polynomial transfer function matrix $\mathbf{H}(j\omega,\kappa)$ is defined similarly to Eq. (2-3) where, here, $B_1(j\omega,\boldsymbol{\theta},\kappa)/A(j\omega,\boldsymbol{\theta},\kappa)$ is the transfer function between the ground acceleration and the absolute acceleration of the pier and $B_2(j\omega,\boldsymbol{\theta},\kappa)/A(j\omega,\boldsymbol{\theta},\kappa)$ is the transfer function between the ground acceleration and that of the bridge deck. The unknown parameter vector $\boldsymbol{\theta}$ is defined similarly to Eq. (2-13). The vector of known parameters $\boldsymbol{\kappa}$ denotes the additional stiffness and/or damping added through the VSDD connected between the pier and the deck. In the simulations, the installed VSDD is assumed to provide additional stiffness or damping at various discrete levels.

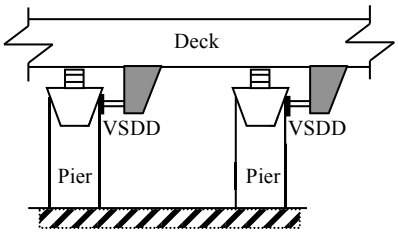

Fig. 2-5. VSDD placement in bridge

Numerical parameters for this model, drawn from Erkus *et al.* (2002), are considered as an illustrative example: k_1 = 15.791 MN/m, k_2 = 7.685MN/m, m_1 = 100 Mg (tons), m_2 = 500 Mg, c_1 = 125.6 kN·s/m, and c_2 = 196 kN·s/m.

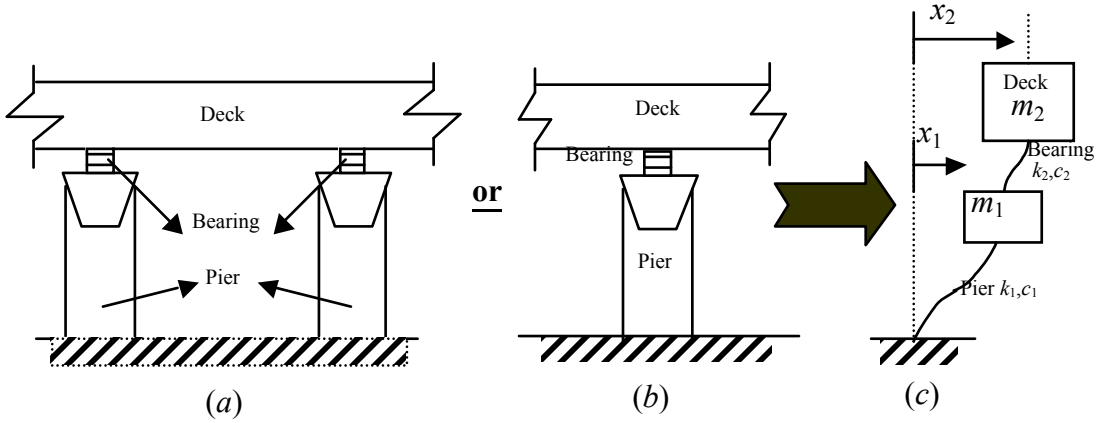

Fig. 2-6. 2DOF bridge model

2.2.3 Six Degree-of-Freedom Shear Building Model

To demonstrate that these methods can be extended to more complex problems, a six degree-of-freedom shear building model is also studied. This 6DOF model system identification was solved using variable stiffness VSDDs and a conventional structure (no VSDDs). In simulation, each installed VSDD is assumed to provide additional stiffness at various discrete levels. The VSDD devices included in the structure are also considered ideal; *i.e.*, they can generate the desired forces with no delay and with no actuator dynamics. In this problem, the VSDDs are considered to be located in the first three stories only, as shown in Fig. 2-7.

In the numerical example of this 6DOF model, the stiffnesses and masses are taken as unity and the damping coefficients are taken as 0.05 kN·s/m. The masses are assumed known *a priori*. The unknown parameter vector $\boldsymbol{\theta}$ for the six degree-of-freedom model is, then, a set of unknown stiffness k_i and damping c_i coefficients as follows:

$$\boldsymbol{\theta} = [\ k_1 \quad k_2 \quad k_3 \quad k_4 \quad k_5 \quad k_6 \quad c_1 \quad c_2 \quad c_3 \quad c_4 \quad c_5 \quad c_6\ ]^{\mathrm{T}} \qquad (2\text{-}17)$$

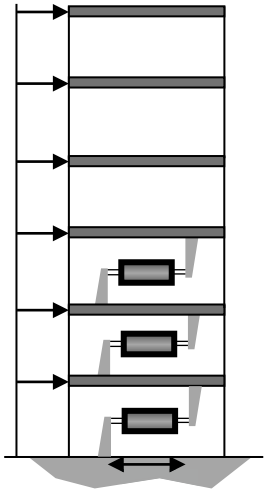

Fig. 2-7. 6DOF model with VSDDs in first three stories

2.3 Prior Results

The results in METRANS report 01-10 definitely showed that there is the potential for VSDDs to make a real contribution to structural health monitoring. When a VSDD acts as a discrete multi-level damping element with coefficient smaller than that of the structure, only little improvement is gained over the conventional structure approach, probably due to the very low force levels for damping VSDDs. In contrast, the discrete stiffness behavior, with small VSDD stiffness, is shown to modestly improve estimates of the structure stiffness and damping coefficients, particularly for the more complex numerical example with several VSDDs. However, since the response to ambient excitation sources is, generally, quite low, the force levels of the VSDDs in the previous study were very small — in fact, orders of magnitude smaller than the forces the structure is designed to withstand and two orders of magnitude smaller than the peak forces capable with current VSDD technology. Consequently, the VSDDs, especially in the discrete damping mode, were less effective than would likely occur if they were commanded to use larger force levels (but still moderate compared to the structural capacity).

Thus, the contents in Chapter 3 of this report, METRANS 03-17, demonstrate that larger force levels will give further improvement in identifying structural parameters. Moreover, to show the general applicability of using VSDDs in structural identification (*i.e.*, it is not just useful in the context of the iterative least squares identification discussed in Chapter 3), Chapters 4 and 5 study the effectiveness of using the VSDDs approach when different identification methods are used. Finally, an experimental verification of the analytical results is detailed in Chapter 6.

3 PARAMETRIC FREQUENCY DOMAIN IDENTIFICATION USING LARGER VSDD STIFFNESS/DAMPING FORCES

3.1 Introduction

To improve the advantages of the VSDD approach, larger VSDD stiffness/damping levels may be used. This Chapter studies and verifies the effect of adding higher levels of VSDD stiffness or damping to a structural system for improving the system identification process. The iterative least squares (ILSN) method is used for identification of parameters in the numerical test beds described in Chapter 2. The primary test bed here is the 2DOF bridge model, however, some results for the 2DOF and 6DOF shear building models are also given.

3.2 2DOF Bridge Model

Previous studies in METRANS report 01-10 (Johnson and Elmasry, 2003) investigated the effects of VSDDs operating in variable stiffness or damping modes on the 2DOF bridge model; however, the levels of stiffness or damping of the VSDD device were limited to 0%, 10%, 20%, 30%, and 40% of that of the isolator between the bridge deck and the pier. In contrast, the VSDDs in this section are assumed to: (*i*) add {0,1,2,3,4} times the bearing stiffness, (*ii*) add {0,5,10,15,20} times the bearing stiffness, (*iii*) add {0,25,50,75,100} times the bearing damping, and (*iv*) add {0,100,200,300,400} times the bearing damping. The structure stiffness and damping estimates from 100 response time histories, using conventional and VSDD approaches, are shown in Fig. 3-1 and the statistics in Table 3-1. Fig. 3-1*a*,*b*,*e*,*f* show the stiffness estimates and Fig. 3-1*c*,*d*,*g*,*h* show the damping estimates. Contour lines of 1σ, 2σ and 3σ are shown with solid lines.

Increasing the level of stiffness that the VSDD induces at the isolator level decreases dramatically the variation of the relative error of stiffness coefficients estimation as shown in Fig. 3-1*a*,*b*. In addition, the variation of the relative error of the damping coefficients estimation, as seen in Fig. 3-1*c*,*d*, improves considerably compared to cases of lower levels of induced VSDD stiffness, though the improvement is limited and the damping coefficient estimation error is up to 5–10%. For the case of varying VSDD damping, it is shown in Fig. 3-1*e*,*f* that the estimation of the stiffness coefficients are improved by increasing the damping levels. Moreover, the variation of the relative error decreases dramatically at highest level of damping (Fig. 3-1*f*).

Table 3-1. Estimate Means and Root Mean-Square Error Percentage for 2DOF Pier-Deck Bridge Model Using Highest Levels of Induced Stiffness or Damping

VSDD Loc.	Struct. Param.	Exact Values	Mean			RMSE(%)		
			No VSDD	Add k_{VSDD}	Add c_{VSDD}	No VSDD	Add k_{VSDD}	Add c_{VSDD}
One VSDD in the bearing between deck and pier	k_1 [MN/m]	15.791	15.726	15.791	15.791	1.634	0.034	0.013
	k_2 [MN/m]	7.685	7.507	7.683	7.685	3.484	0.160	0.027
	c_1 [kN·s/m	125.6	110.8	124.8	125.4	17.931	1.499	1.846
	c_2 [kN·s/m	196	192.8	203.2	195.7	5.390	4.492	1.625
	m_2 [tons]	100	98.29	100	100	2.398	0.030	0.035

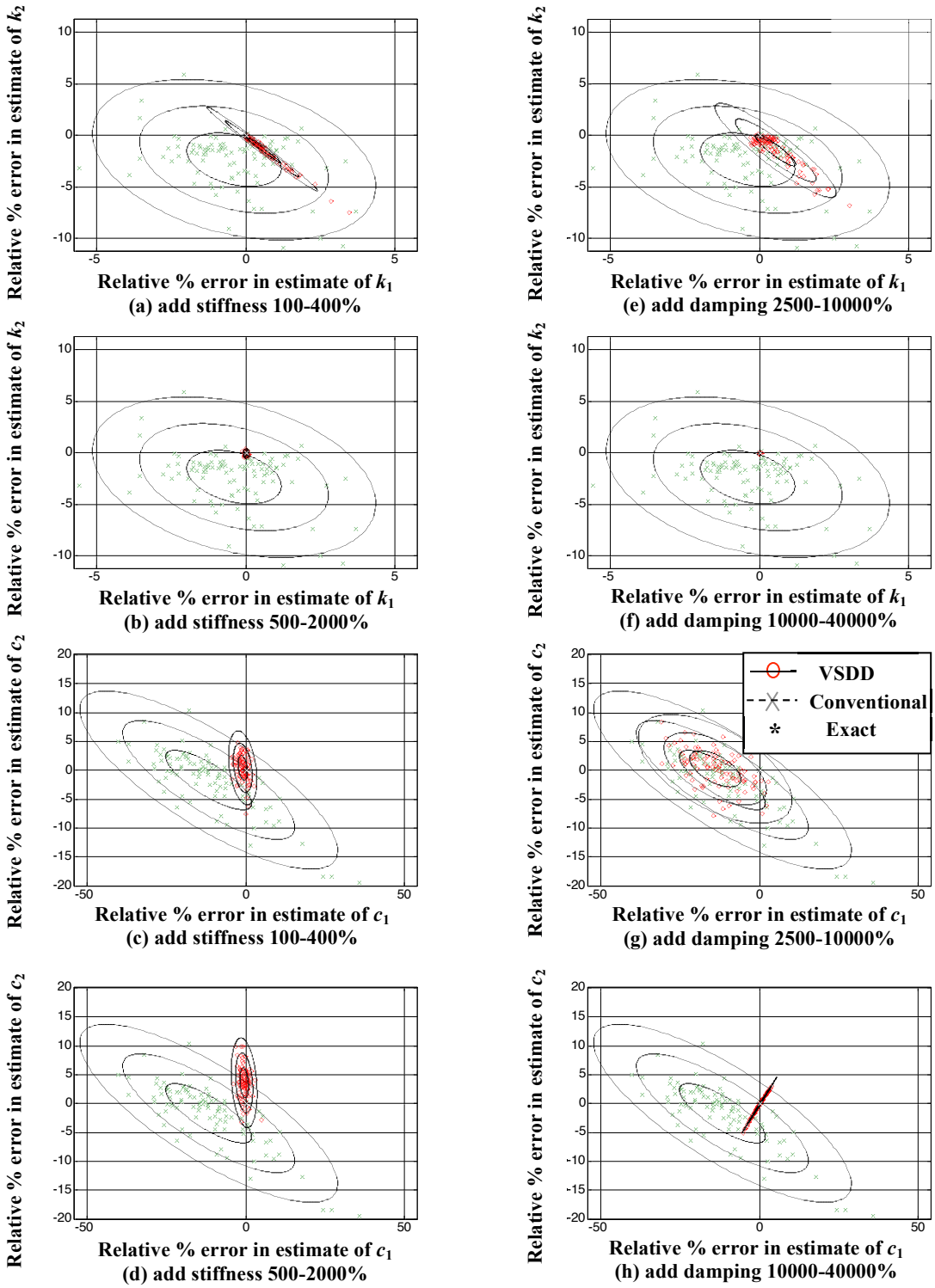

Fig. 3-1. Comparison of stiffness and damping estimate error levels for higher VSDD induced stiffness/damping for 2DOF bridge model

The damping estimates are also improved considerably, though the variation of the relative error tends to have a linear trend with a maximum error of 5% of the damping coefficients of the system as shown in Fig. 3-1*g*,*h*. Table 3-1 shows the mean and percent root mean square error (RMSE) of the estimates for configurations (*ii*) and (*iv*) — *i.e.*, with the highest levels of effective stiffness and effective damping, respectively.

One initial reaction to this approach is that the stiffness/damping levels sound *quite* unreasonable. However, it must be understood that these are **effective** levels of stiffness and damping forces exerted during low-level ambient excitation. Thus, the actual forces are well within the capabilities of current VSDDs and quite small compared to the structure load capacity.

To verify that the force levels are reasonable, the response of the structure to a low-level earthquake excitation (Kanai-Tajimi filtered white noise with a 0.002*g* root mean square (RMS) ground acceleration) is computed. With the VSDD producing 20 times the bearing stiffness, the RMS pier and deck drifts are 1.5 mm and 0.125 mm, respectively; RMS absolute pier and deck accelerations are 0.0037*g* and 0.0041*g*, respectively; and RMS VSDD force is 19.2 kN. This force level is quite small relative to the masses (500 ton deck, 100 ton pier). Meanwhile, with the VSDD producing 400 times the bearing damping, the RMS pier and deck drifts are 1.44 mm and 0.074 mm, respectively; RMS absolute accelerations are 0.003*g* at both deck and pier; and the RMS VSDD force is about 15 kN, which is also small compared to the masses. In contrast, when no VSDDs are used, the RMS pier and deck drifts are 0.85 mm and 1.61 mm, respectively; RMS absolute pier and deck accelerations are 0.0032*g* and 0.0025*g,* respectively. Thus, the VSDD forces used here are quite modest and induce little change in the magnitude of structural response.

3.3 2DOF Shear Building Model with Larger VSDD Forces

The identification results for the 2DOF shear building also showed considerable improvement by increasing the additional stiffness level induced by the VSDDs. The identification results introduced here add VSDD stiffness that is {0,5,10,15,20} times the stiffness of the corresponding story or VSDD damping that is {0,100,200,300,400} times the damping of the corresponding story. The improvements are well demonstrated in Table 3-2.

By using higher levels of induced VSDD stiffness/damping, faster convergence in the identification code is observed. Using the true parameter vector as an initial starting guess for the iterative procedure, the algorithm converges, generally in 3–5 iterations, to estimates that are fairly accurate.

The results in Table 3-2 for a single VSDD in the first story show that the identification of the stiffness in the first story is quite accurate using both conventional and VSDD approaches. On the other hand, the means of all other identified structural parameters are better when using the VSDD approach. The results in Table 3-2 indicate that the root mean square errors are reduced by more than two times for the second story stiffness, and by nearly ten times for the second story damping coefficient by varying VSDD stiffness with these higher force levels.

For the case of an initial parameter vector that is 20% higher (in all components) than the exact values, 100 separate estimates were computed. Fig. 3-2, showing the variation of the identified stiffnesses using higher levels of induced VSDD stiffness, indicates that the VSDD approach did very well compared to the conventional structure approach that shows large bias and variation. Similar results are observed in the identified damping coefficients of the first and second stories, as shown in Fig. 3-3. Both Fig. 3-2 and Fig. 3-3 show approximate one-, two- and three-sigma (standard deviation) curves for the two approaches.

Table 3-2. Estimate Means and Root Mean Square Error for 2DOF Shear Building Model

VSDD Loc.	Struct. Param.	Exact Values	Mean			RMSE (%)		
			No VSDD	Add k_{VSDD}	Add c_{VSDD}	No VSDD	Add k_{VSDD}	Add c_{VSDD}
One VSDD in 1st story (exact guesses)	k_1	1.0000	0.9999	0.9993	0.9980	0.078	0.288	0.428
	k_2	1.0000	0.9955	0.9985	0.9966	0.994	0.443	0.710
	c_1	0.0500	0.0519	0.0495	0.0495	8.646	4.160	5.553
	c_2	0.0500	0.0449	0.0497	0.0496	14.303	1.422	2.799
	m_2	1.0000	0.9982	0.9987	0.9967	0.417	0.413	0.716
One VSDD in 1st story (offset guesses)	k_1	1.0000	1.0368	0.9993	*	4.174	0.289	*
	k_2	1.0000	0.9953	0.9985	*	1.021	0.445	*
	c_1	0.0500	0.0520	0.0495	*	9.759	4.167	*
	c_2	0.0500	0.0482	0.0497	*	12.403	1.424	*
	m_2	1.0000	1.0343	0.9987	*	3.958	0.416	*
One VSDD in 2nd story (Exact guesses)	k_1	1.0000	0.9999	1.0022	1.0004	0.078	0.272	0.099
	k_2	1.0000	0.9955	0.9835	0.9989	0.994	1.877	0.581
	c_1	0.0500	0.0519	0.0501	0.0500	8.646	2.758	2.429
	c_2	0.0500	0.0449	0.0465	0.0467	14.303	9.952	9.946
	m_2	1.0000	0.9982	0.9949	0.9990	0.417	0.587	0.195
VSDDs in 1st and 2nd stories (Exact guesses)	k_1	1.0000	0.9999	1.0001	1.0002	0.078	0.125	0.093
	k_2	1.0000	0.9955	0.9996	0.9989	0.994	0.092	0.234
	c_1	0.0500	0.0519	0.0500	0.0499	8.646	1.934	2.296
	c_2	0.0500	0.0449	0.0498	0.0495	14.303	2.303	2.889
	m_2	1.0000	0.9982	0.9999	0.9993	0.417	0.027	0.173

** Note: some VSDD damping entries were never studied with offset guesses.*

For a VSDD in the second story, the results resemble those with a VSDD in the first story only, yet the improvement is more reflected when varying VSDD damping only. Moreover, the variation of the stiffness estimate of the 1st story is reduced compared to a VSDD in the first story only (Table 3-2).

With VSDDs in both stories of the structure, Fig. 3-4 and Fig. 3-5 show that the variation of the stiffness identification of the second story is clearly decreased and improved. The mean of the first story stiffness estimate is quite similar to that of the conventional approach case, as shown in Table 3-2. However, some improvement in the variation of the stiffness of the first story, compared to the case of a VSDD in the first and second stories only, can be observed. Generally, the variations are improved compared to any of the previous cases of a single VSDD in the structure such that it is now one tenth that of the conventional approach case for the second story stiffness and nearly one fifth for the damping coefficients in both stories, though the variance of the identified stiffness coefficient in the first story rises slightly compared to the conventional structure approach.

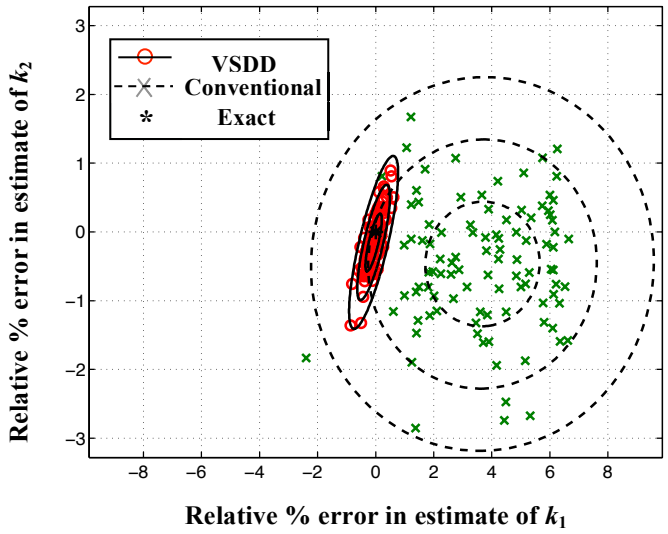

Fig. 3-2. Stiffness estimate error levels for the iterative method with offset start for 2DOF model with VSDD in 1st story only (varying stiffness case)

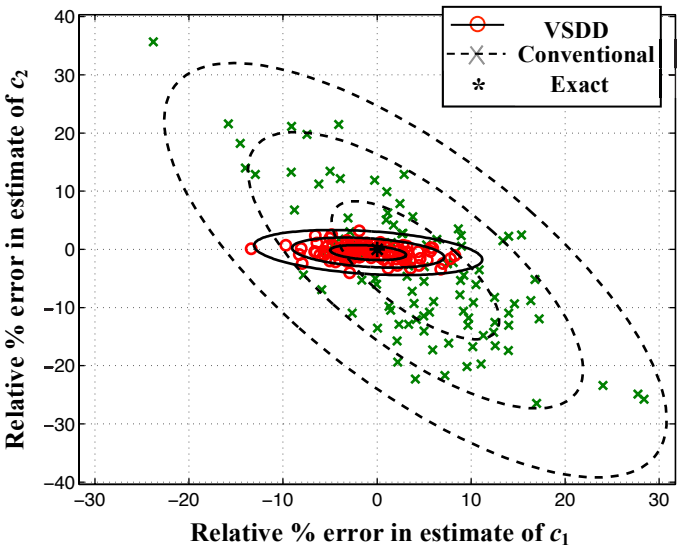

Fig. 3-3. Damping estimate error levels for the iterative method with offset start for 2DOF model with VSDD in 1st story only (varying stiffness case)

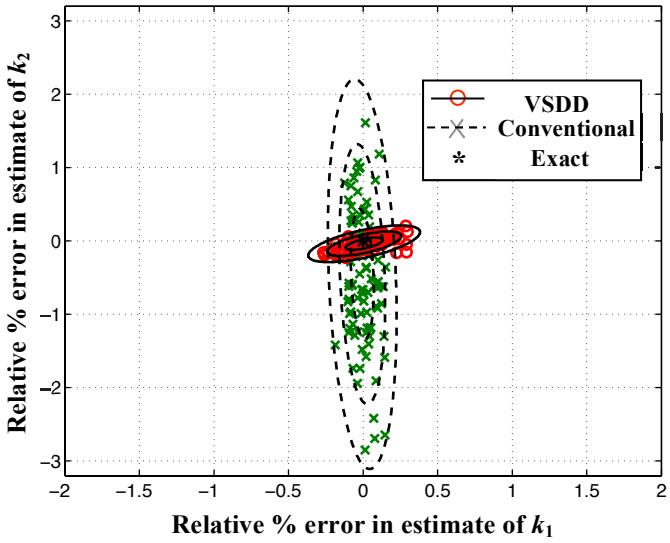

Fig. 3-4. Stiffness error levels for the iterative method with exact start for 2DOF model with VSDD in both 1st and 2nd stories (varying stiffness case)

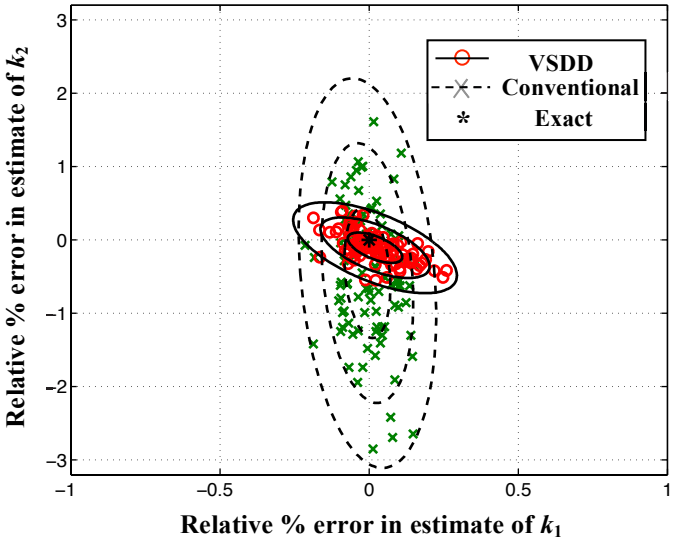

Fig. 3-5. Stiffness error levels for the iterative method with exact start for 2DOF model with VSDD in both 1st and 2nd stories (varying damping case)

3.4 6DOF Shear Building Model

The 6DOF model system identification in this section is solved for the variable stiffness VSDD and the conventional structure (no VSDDs) approaches, using the iterative least squares (ILSN) method with exact starting guesses of the unknown parameters. The VSDDs are located in the first three stories only. The masses are assumed known *a priori*. In simulation, each installed VSDD is assumed to provide additional stiffness at four discrete levels: {0,5,10,15} times the corresponding story stiffness.

Table 3-3 shows the improvement in the estimates of the stiffness and damping coefficients when using VSDDs in the structural model. Also, it is quite evident that the variations are dramatically reduced — up to 12 times for stiffness estimate in the 6th story and up to nearly 23 times in the damping estimates. The results here confirm the improvements observed previously for the lower-order 2DOF shear building model and the 2DOF bridge model.

Table 3-3. Estimate Means and Mean-Square Error Percentage for 6DOF Shear Building Model (Varying Stiffness)

VSDD Loc.	Structural Parameters	Exact Values	Mean		RMSE(%)	
			No VSDD	Varying k	No VSDD	Varying k
Three VSDDs in 1st, 2nd, and 3rd stories	k_1	1.0000	1.0003	1.0000	0.183	0.036
	k_2	1.0000	0.9996	1.0000	0.105	0.071
	k_3	1.0000	1.0001	0.9999	0.163	0.083
	k_4	1.0000	1.0002	1.0000	0.220	0.020
	k_5	1.0000	0.9999	1.0000	0.172	0.026
	k_6	1.0000	0.9995	1.0000	0.144	0.011
	c_1	0.0500	0.0511	0.0500	5.399	0.783
	c_2	0.0500	0.0491	0.0501	3.877	1.444
	c_3	0.0500	0.0496	0.0496	4.698	2.028
	c_4	0.0500	0.0502	0.0500	7.321	0.296
	c_5	0.0500	0.0492	0.0500	3.748	0.267
	c_6	0.0500	0.0496	0.0500	4.587	0.202

3.5 Summary

This chapter demonstrated that using VSDDs with effective stiffness or damping larger than that of the structure can significantly decrease the error in structural parameter estimates. Since this approach would be used with small ambient excitation, the VSDD forces are quite moderate. Thus, this VSDD approach is a viable improvement for structural parameter identification compared to the conventional structure approach.

4 VSDD APPROACH USING THE INVFREQS-LEAST SQUARES METHOD

4.1 Introduction

The INVFREQS-Least Squares (INVFLS) method is a frequency domain identification method, based on a polynomial form of the transfer function and a least squares error approach. The method is composed of two stages. The first stage, called the INVFREQS stage, estimates the coefficients of polynomials of the transfer functions of structural systems. The second, also by least squares, estimates the structural parameters, such as stiffness and damping coefficients, from direct relations with the coefficients of the transfer function polynomials. The INVFREQS stage for single-input single-output (SISO) systems already exists as the MATLAB® function `invfreqs`. In this study, the first stage is extended to single-input multi-output (SIMO) and multi-input multi-output (MIMO) systems. To explain the method, the application to SISO systems is explained thoroughly and, then, the extension to SIMO and MIMO systems is introduced. The second stage, using a least squares technique to find the structure parameters, is then discussed. A numerical example with the 2DOF shear building model is used to demonstrate that the VSDD approach provides stiffness estimates superior to those from the conventional passive structure.

4.1.1 INVFREQS Method for SISO System

To explain the general derivation of this method, a SISO system is a good start. Generally, the transfer function $H(j\omega)$ for a SISO system can be represented as a fraction with a numerator polynomial of order n_B divided by a denominator polynomial of order n_A. Let $\boldsymbol{\theta}$ be a vector of the coefficients of these polynomials

$$\boldsymbol{\theta} = [\ a_{n_A-1} \quad a_{n_A-2} \quad \ldots \quad a_0 \ \big|\ b_{n_B} \quad b_{n_B-1} \quad \ldots \quad b_0\ ]^{\mathrm{T}} \tag{4-1}$$

The polynomials and the transfer function can, then, be written explicitly as a function of the parameters

$$\begin{aligned} A(j\omega,\boldsymbol{\theta}) &= \quad (j\omega)^{n_A} + a_{n_A-1}(j\omega)^{n_A-1} + \ldots + a_0 \\ B(j\omega,\boldsymbol{\theta}) &= b_{n_B}(j\omega)^{n_B} + b_{n_A-1}(j\omega)^{n_B-1} + \ldots + b_0 \\ H(j\omega,\boldsymbol{\theta}) &= B(j\omega,\boldsymbol{\theta}) / A(j\omega,\boldsymbol{\theta}) \end{aligned} \tag{4-2}$$

By measuring the output response for known input excitation, an experimental transfer function $\hat{H}(j\omega)$ may be obtained. The residual error between the theoretical and experimental transfer functions can, consequently, be defined as:

$$e(j\omega,\boldsymbol{\theta}) = \frac{B(j\omega,\boldsymbol{\theta}) - A(j\omega,\boldsymbol{\theta})\hat{H}(j\omega)}{A(j\omega,\boldsymbol{\theta})} \tag{4-3}$$

Minimizing this error directly at all frequencies can be numerically difficult; however, a first estimate of the parameters that minimize the error can be found by minimizing the error in the numerator of Eq. (4-3)

$$\tilde{e}(j\omega,\boldsymbol{\theta}) = [b_{n_B}(j\omega)^{n_B} + \ldots + b_0] - \hat{H}(j\omega)[(j\omega)^{n_A} + a_{n_A-1}(j\omega)^{n_A-1} + \ldots + a_0] \tag{4-4}$$

Then, rearranging the components of Eq. (4-4) as

$$\begin{aligned}&(j\omega)^{n_A-1}a_{n_A-1}\hat{H}(j\omega)+(j\omega)^{n_A-2}a_{n_A-2}\hat{H}(j\omega)+\ldots+a_0\hat{H}(j\omega)\\&-(j\omega)^{n_B}b_{n_B}-(j\omega)^{n_B-1}b_{n_B-1}-\ldots-b_0=-(j\omega)^{n_A}\hat{H}(j\omega)-\tilde{e}(j\omega,\boldsymbol{\theta})\end{aligned} \tag{4-5}$$

which, when evaluated at n_ω distinct frequencies, can be expressed in matrix form

$$\mathbf{D}\boldsymbol{\theta}=\mathbf{v}-\tilde{\mathbf{e}} \tag{4-6}$$

where $\mathbf{D}$ is the $n_\omega\times(n_B+n_A+1)$ matrix

$$\mathbf{D}=\left[\begin{array}{ccc|ccc}(j\omega_1)^{n_A-1}\hat{H}(j\omega_1) & \cdots & \hat{H}(j\omega_1) & -(j\omega_1)^{n_B} & -(j\omega_1)^{n_B-1} & \cdots & -1\\ \vdots & & \vdots & \vdots & \vdots & & \vdots\\ (j\omega_{n_\omega})^{n_A-1}\hat{H}(j\omega_{n_\omega}) & \cdots & \hat{H}(j\omega_{n_\omega}) & -(j\omega_{n_\omega})^{n_B} & -(j\omega_{n_\omega})^{n_B-1} & \cdots & -1\end{array}\right] \tag{4-7}$$

and $\mathbf{v}$ and $\tilde{\mathbf{e}}$ are the $n_\omega\times 1$ vector

$$\begin{aligned}\mathbf{v}&=\left[\begin{array}{ccc}-(j\omega_1)^{n_A}\hat{H}(j\omega_1) & \cdots & -(j\omega_{n_\omega})^{n_A}\hat{H}(j\omega_{n_\omega})\end{array}\right]^{\mathrm{T}}\\ \tilde{\mathbf{e}}&=\left[\begin{array}{ccc}e(j\omega_1,\boldsymbol{\theta}) & \cdots & e(j\omega_{n_\omega},\boldsymbol{\theta})\end{array}\right]^{\mathrm{T}}\end{aligned} \tag{4-8}$$

Minimizing the squared error vector $\left|\tilde{\mathbf{e}}\right|^2=\tilde{\mathbf{e}}^*\tilde{\mathbf{e}}$, with respect to the vector of unknown coefficients $\boldsymbol{\theta}$, gives

$$\begin{aligned}\frac{\partial\tilde{\mathbf{e}}^*\tilde{\mathbf{e}}}{\partial\boldsymbol{\theta}}&=\frac{\partial}{\partial\boldsymbol{\theta}}((\mathbf{D}\boldsymbol{\theta}-\mathbf{v})^*(\mathbf{D}\boldsymbol{\theta}-\mathbf{v}))=\frac{\partial}{\partial\boldsymbol{\theta}}(\boldsymbol{\theta}^{\mathrm{T}}\mathbf{D}^*\mathbf{D}\boldsymbol{\theta}-\boldsymbol{\theta}^{\mathrm{T}}\mathbf{D}^*\mathbf{v}-\mathbf{v}^*\mathbf{D}\boldsymbol{\theta}+\mathbf{v}^*\mathbf{v})\\&=2(\mathbf{D}^*\mathbf{D}\boldsymbol{\theta}-\mathbf{D}^*\mathbf{v})^{\mathrm{T}}=\mathbf{0}^{\mathrm{T}}\end{aligned} \tag{4-9}$$

where $(\cdot)^*$ denotes complex conjugate transpose. For the system to be causal, all coefficients should be real. Thus, the vector of unknown coefficients $\boldsymbol{\theta}$ can be obtained with

$$\boldsymbol{\theta}=[\mathbf{D}^*\mathbf{D}]^{-1}\mathrm{Re}[\mathbf{D}^*\mathbf{v}] \tag{4-10}$$

The Re(·) should not be necessary theoretically but it eliminates, in numerical computation, small imaginary components resulting from floating-point round off. Thus, Eq. (4-10) gives initial estimates of the transfer function coefficients. The stability of the estimated system is checked by calculating the roots of the estimated denominator polynomial, $\hat{A}(j\omega)$, and verifying the roots have negative real parts.

An iterative technique is then used to refine the estimates by reducing the residual transfer function error, in terms of the estimated polynomials $\hat{B}(j\omega)$ and $\hat{A}(j\omega)$,

$$\hat{e}(j\omega)=\hat{B}(j\omega)\big/\hat{A}(j\omega)-\hat{H}(j\omega) \tag{4-11}$$

The estimated coefficients of the numerator and denominator polynomials are not yet the best estimates. Therefore, each of the coefficients of $\hat{B}(j\omega)$ and $\hat{A}(j\omega)$ has error Δb and Δa, respectively. In other words, the estimated polynomials equal the exact polynomials plus some error such that:

$$\hat{B}(j\omega) = (b_{n_B} + \Delta b_{n_B})(j\omega)^{n_B} + (b_{n_B-1} + \Delta b_{n_B-1})(j\omega)^{n_B-1} + \ldots + (b_0 + \Delta b_0) \tag{4-12}$$

$$\hat{A}(j\omega) = (j\omega)^{n_A} + (a_{n_A-1} + \Delta a_{n_A-1})(j\omega)^{n_A-1} + \ldots + (a_0 + \Delta a_0) \tag{4-13}$$

Substituting Eqs. (4-12) and (4-13) into Eq. (4-11) and simplifying, results in

$$\begin{aligned} \hat{e}(j\omega)\hat{A}(j\omega) = &\left[(b_{n_B} + \Delta b_{n_B})(j\omega)^{n_B} + \ldots + (b_0 + \Delta b_0)\right] \\ &-\hat{H}(j\omega)\left[(a_{n_A-1} + \Delta a_{n_A-1})(j\omega)^{n_A-1} + \ldots + (a_0 + \Delta a_0)\right] \end{aligned} \tag{4-14}$$

The right hand side of Eq. (4-14) can be divided into two parts: one includes the coefficients of the actual polynomials and the other formed of the error coefficients

$$\begin{aligned} \hat{e}(j\omega)\hat{A}(j\omega) = &B(j\omega) - \hat{H}(j\omega)A(j\omega) + [\Delta b_{n_B}(j\omega)^{n_B} + \ldots + \Delta b_0] \\ &-\hat{H}(j\omega)[\Delta a_{n_A-1}(j\omega)^{n_A-1} + \ldots + \Delta a_0] \end{aligned} \tag{4-15}$$

For the exact actual $B(j\omega)$ and $A(j\omega)$, the first two terms in the right hand side of Eq. (4-15) cancel and, thus, the resulting equation of the error is

$$\hat{e}(j\omega) = \frac{1}{\hat{A}(j\omega)}\left\{\left[\Delta b_{n_B}(j\omega)^{n_B} + \ldots + \Delta b_0\right] - \hat{H}(j\omega)\left[\Delta a_{n_A-1}(j\omega)^{n_A-1} + \ldots + \Delta a_0\right]\right\} \tag{4-16}$$

The new residual error Eq. (4-16) is used for the evaluation of the error coefficients. This is done by rewriting Eq. (4-16) in a matrix form such that

$$\Delta\mathbf{D}_{n_\omega \times (n_B+n_A+1)} \Delta\boldsymbol{\theta}_{(n_B+n_A+1)\times 1} = \hat{\mathbf{e}}_{n_\omega \times 1} \tag{4-17}$$

where the error coefficients vector $\Delta\boldsymbol{\theta}$ is

$$\Delta\boldsymbol{\theta} = \left[\begin{array}{cccc:cccc} \Delta a_{n_A-1} & \Delta a_{n_A-2} & \ldots & \Delta a_0 & \Delta b_{n_B} & \Delta b_{n_B-1} & \ldots & \Delta b_0 \end{array}\right]^{\mathrm{T}} \tag{4-18}$$

and the matrix $\Delta\mathbf{D}$ is defined as

$$\Delta\mathbf{D} = \left[\begin{array}{ccc:ccc} -\frac{(j\omega_1)^{n_A-1}\hat{H}(j\omega_1)}{\hat{A}(j\omega_1)} & \cdots & -\frac{\hat{H}(j\omega_1)}{\hat{A}(j\omega_1)} & \frac{(j\omega_1)^{n_B}}{\hat{A}(j\omega_1)} & \frac{(j\omega_1)^{n_B-1}}{\hat{A}(j\omega_1)} & \cdots \quad \frac{1}{\hat{A}(j\omega_1)} \\ \vdots & \vdots & & \vdots & \vdots & \vdots \quad \vdots \\ -\frac{(j\omega_i)^{n_A-1}\hat{H}(j\omega_i)}{\hat{A}(j\omega_i)} & \cdots & -\frac{\hat{H}(j\omega_i)}{\hat{A}(j\omega_i)} & \frac{(j\omega_i)^{n_B}}{\hat{A}(j\omega_i)} & \frac{(j\omega_i)^{n_B-1}}{\hat{A}(j\omega_i)} & \cdots \quad \frac{1}{\hat{A}(j\omega_i)} \\ \vdots & \vdots & & \vdots & \vdots & \vdots \quad \vdots \\ -\frac{(j\omega_{n_\omega})^{n_A-1}\hat{H}(j\omega_{n_\omega})}{\hat{A}(j\omega_{n_\omega})} & \cdots & -\frac{\hat{H}(j\omega_{n_\omega})}{\hat{A}(j\omega_{n_\omega})} & \frac{(j\omega_{n_\omega})^{n_B}}{\hat{A}(j\omega_{n_\omega})} & \frac{(j\omega_{n_\omega})^{n_B-1}}{\hat{A}(j\omega_{n_\omega})} & \cdots \quad \frac{1}{\hat{A}(j\omega_{n_\omega})} \end{array}\right] \tag{4-19}$$

Premultiplying both sides of Eq. (4-17) by the complex conjugate transpose $\Delta\mathbf{D}^*$, taking the real parts and solving for the error coefficients vector $\Delta\boldsymbol{\theta}$,

$$\Delta\boldsymbol{\theta} = [\Delta\mathbf{D}^*\Delta\mathbf{D}]^{-1}\mathrm{Re}[\Delta\mathbf{D}^*\hat{\mathbf{e}}] \tag{4-20}$$

The calculation of error coefficients helps in finding a general direction to better estimate the transfer function coefficients. The new resulting coefficients vector $\boldsymbol{\theta}_{\text{mod}}$ is equal to the sum of the initial estimates vector $\boldsymbol{\theta}$ and the error coefficients vector $\Delta\boldsymbol{\theta}$. For enhancement however, a check is performed on the evaluated error coefficients $\Delta\boldsymbol{\theta}$ before adding them to the initial estimates $\boldsymbol{\theta}$. In the check, the new modified coefficients will be represented as

$$\boldsymbol{\theta}_{\text{mod}} = \boldsymbol{\theta} + k(\Delta\boldsymbol{\theta}) \tag{4-21}$$

where k is to be determined as follows. First, calculate the squared residual error $\hat{\mathbf{e}}^*\hat{\mathbf{e}}$ from the first step in Eq. (4-11) for all frequencies

$$\hat{\mathbf{e}}^*\hat{\mathbf{e}} = \left[\frac{\hat{B}(j\omega_i)}{\hat{A}(j\omega_i)} - \hat{H}(j\omega_i)\right]^* \left[\frac{\hat{B}(j\omega_i)}{\hat{A}(j\omega_i)} - \hat{H}(j\omega_i)\right] \tag{4-22}$$

The result is then compared to the modified squared residual error $\hat{\mathbf{e}}^*_{\text{mod}}\hat{\mathbf{e}}_{\text{mod}}$

$$\hat{\mathbf{e}}^*_{\text{mod}}\hat{\mathbf{e}}_{\text{mod}} = \left[\frac{\hat{B}_{\text{mod}}(j\omega_i)}{\hat{A}_{\text{mod}}(j\omega_i)} - \hat{H}(j\omega_i)\right]^* \left[\frac{\hat{B}_{\text{mod}}(j\omega_i)}{\hat{A}_{\text{mod}}(j\omega_i)} - \hat{H}(j\omega_i)\right] \tag{4-23}$$

where $\hat{A}_{\text{mod}}(j\omega_i)$ and $\hat{B}_{\text{mod}}(j\omega_i)$ are computed using $\boldsymbol{\theta}_{\text{mod}}$ and $k = 1$. If $\hat{\mathbf{e}}^*\hat{\mathbf{e}}$ is smaller than $\hat{\mathbf{e}}^*_{\text{mod}}\hat{\mathbf{e}}_{\text{mod}}$, then $\boldsymbol{\theta}_{\text{mod}}$ is recalculated from Eq. (4-21) by taking k equivalent to half of its previous value. The comparison is repeated between $\hat{\mathbf{e}}^*\hat{\mathbf{e}}$ and $\hat{\mathbf{e}}^*_{\text{mod}}\hat{\mathbf{e}}_{\text{mod}}$ until the latter is smaller. After the check is fulfilled, another loop of recalculating the error coefficients vector $\Delta\boldsymbol{\theta}$ is applied. In the new loop, the old vector $\boldsymbol{\theta}_{\text{mod}}$ is considered like the initial estimate in Eq. (4-11). These loops of evaluation of $\Delta\boldsymbol{\theta}$ and modification of the estimated coefficients are repeated until the norm of the error coefficients vector becomes smaller than a tolerance factor

$$\left\|\Delta\boldsymbol{\theta}\right\| \le tol \tag{4-24}$$

This tolerance factor is dependent on the sensitivity that the user requires.

4.1.2 INVFREQS Method for SIMO and MIMO Systems

For the case of SIMO and MIMO systems, a series of transfer functions is identified rather than the single one in the SISO case. Each transfer function represents the ratio between one of the inputs and one of the outputs. The global transfer function matrix is formed such that each column corresponds to one of the inputs, and each row to one of the outputs.

Consider a system that is subjected to M excitation inputs and has L measured outputs. Then, the transfer function from the m^{th} input to the l^{th} output of the system is expressed as

$$H_{l,m}(j\omega) = B_{l,m}(j\omega) / A_m(j\omega) \tag{4-25}$$

where the denominator polynomial $A_m(j\omega)$ of the transfer functions of all measured outputs is considered unique for a single input, and the numerator polynomial $B_{l,m}(j\omega)$ is considered unique for each input/output combination. Accordingly, the residual error between the polynomial transfer function and the corresponding experimental transfer function $\hat{H}_{l,m}(j\omega)$ is defined as

$$e_{l,m}(j\omega) = \frac{B_{l,m}(j\omega) - A_m(j\omega)\hat{H}_{l,m}(j\omega)}{A_m(j\omega)} \tag{4-26}$$

where

$$B_{l,m}(j\omega) = b_{n_B(l,m)}^{(l,m)}(j\omega)^{n_B(l,m)} + b_{n_B(l,m)-1}^{(l,m)}(j\omega)^{n_B(l,m)-1} + \ldots + b_0^{(l,m)} \tag{4-27}$$

$$A_m(j\omega) = (j\omega)^{n_A(m)} + a_{n_A(m)-1}^{(m)}(j\omega)^{n_A(m)-1} + \ldots + a_0^{(m)} \tag{4-28}$$

Simplifying the residual error Eq. (4-26) gives an equation for each input/output transfer function, similar to Eq. (4-3) in SISO systems case where $n_A(m)$ and $n_B(l,m)$ are the orders of polynomials $A_m(j\omega)$ and $B_{l,m}(j\omega)$, respectively. However, in contrast with SISO systems, the residual error in the SIMO/MIMO case is defined as a vector error for transfer functions from a single input to all related outputs

$$\mathbf{err}^{(m)}(j\omega) = \begin{bmatrix} [b_{n_B(1,m)}^{(1,m)}(j\omega)^{n_B(1,m)} + \ldots + b_0^{(1,m)}] - [(j\omega)^{n_A(m)} + \ldots + a_0^{(m)}]\hat{H}_{1,m}(j\omega) \\ \vdots \\ [b_{n_B(L,m)}^{(L,m)}(j\omega)^{n_B(L,m)} + \ldots + b_0^{(L,m)}] - [(j\omega)^{n_A(m)} + \ldots + a_0^{(m)}]\hat{H}_{L,m}(j\omega) \end{bmatrix} \tag{4-29}$$

Eq. (4-29) can be set in a matrix form as

$$\mathbf{D}_{Ln_\omega \times (\sum_l n_B(m,l)+n_A(m)+L)}^{(m)} \tilde{\mathbf{x}}_{(\sum_l n_B(m,l)+n_A(m)+L)\times 1}^{(m)} = \mathbf{V}_{Ln_\omega \times 1}^{(m)} - \mathbf{err}_{Ln_\omega \times 1}^{(m)} \tag{4-30}$$

where the vector $\mathbf{V}$ for the m^{th} input is defined as

$$\mathbf{V}_{Ln_\omega \times 1}^{(m)} = \left[\begin{array}{c} (j\omega_1)^{n_A(m)}\hat{H}_{1,m}(j\omega_1) \\ \vdots \\ (j\omega_{n_\omega})^{n_A(m)}\hat{H}_{1,m}(j\omega_{n_\omega}) \\ \hdashline \vdots \\ \hdashline (j\omega_1)^{n_A(m)}\hat{H}_{L,m}(j\omega_1) \\ \vdots \\ (j\omega_{n_\omega})^{n_A(m)}\hat{H}_{L,m}(j\omega_{n_\omega}) \end{array}\right]^{\mathrm{T}} \tag{4-31}$$

and $\mathbf{D}$ is a matrix that is defined for m^{th} input as

$$\mathbf{D}^{(m)} = \begin{bmatrix} \bar{\mathbf{D}}_1^{(m)} & \tilde{\mathbf{D}}_1^{(m)} & \mathbf{0} & \cdots & \mathbf{0} \\ \bar{\mathbf{D}}_2^{(m)} & \mathbf{0} & \tilde{\mathbf{D}}_2^{(m)} & & \vdots \\ \vdots & \vdots & \ddots & \ddots & \mathbf{0} \\ \bar{\mathbf{D}}_L^{(m)} & \mathbf{0} & \cdots & \mathbf{0} & \tilde{\mathbf{D}}_L^{(m)} \end{bmatrix} \tag{4-32}$$

where submatrices $\bar{\mathbf{D}}_l^{(m)}$ are given by

$$\bar{\mathbf{D}}_l^{(m)} = \begin{bmatrix} (j\omega_1)^{n_A(m)-1}\hat{H}_{l,m}(j\omega_1) & (j\omega_1)^{n_A(m)-2}\hat{H}_{l,m}(j\omega_1) & \cdots & \hat{H}_{l,m}(j\omega_1) \\ (j\omega_2)^{n_A(m)-1}\hat{H}_{l,m}(j\omega_2) & (j\omega_2)^{n_A(m)-2}\hat{H}_{l,m}(j\omega_2) & & \hat{H}_{l,m}(j\omega_2) \\ \vdots & \vdots & & \vdots \\ (j\omega_{n_\omega})^{n_A(m)-1}\hat{H}_{l,m}(j\omega_{n_\omega}) & (j\omega_{n_\omega})^{n_A(m)-2}\hat{H}_{l,m}(j\omega_{n_\omega}) & \cdots & \hat{H}_{l,m}(j\omega_{n_\omega}) \end{bmatrix} \tag{4-33}$$

and block matrices $\tilde{\mathbf{D}}_l^{(m)}$ that sit along a diagonal in $\mathbf{D}^{(m)}$ are

$$\tilde{\mathbf{D}}_l^{(m)} = \begin{bmatrix} -(j\omega_1)^{n_B(l,m)} & -(j\omega_1)^{n_B(l,m)} & \cdots & -1 \\ -(j\omega_2)^{n_B(l,m)} & -(j\omega_2)^{n_B(l,m)} & \cdots & -1 \\ \vdots & \vdots & \ddots & \vdots \\ -(j\omega_{n_\omega})^{n_B(l,m)} & -(j\omega_{n_\omega})^{n_B(l,m)} & \cdots & -1 \end{bmatrix} \tag{4-34}$$

and $\boldsymbol{\theta}^{(m)}$, the vector of the coefficients of the numerator and denominator polynomials of all transfer functions from the m^{th} input to all L outputs is

$$\boldsymbol{\theta}^{(m)} = \left[\begin{array}{ccc:ccc:c:ccc} a_{n_A-1}^{(m)} & \cdots & a_0^{(m)} & b_{n_B(1,m)}^{(1,m)} & \cdots & b_0^{(1,m)} & \cdots & b_{n_B(L,m)}^{(L,m)} & \cdots & b_0^{(L,m)} \end{array} \right]^{\mathrm{T}} \tag{4-35}$$

Similarly to SISO systems, the vector of unknown coefficients $\boldsymbol{\theta}^{(m)}$ is evaluated from

$$\boldsymbol{\theta}^{(m)} = [\mathbf{D}^{(m)*}\mathbf{D}^{(m)}]^{-1}\mathrm{Re}[\mathbf{D}^{(m)*}\mathbf{V}^{(m)}] \tag{4-36}$$

The procedure described by Eq. (4-29) to Eq. (4-36) computes the initial approximate estimation part of the INVFREQS method for SIMO systems case. For MIMO systems, the same procedure is executed M times to obtain the transfer functions with respect to each input. The stability of the estimated system is checked by calculating the roots of the estimated denominator polynomial for each input m, $A_m(j\omega)$, and verifying that the real parts of the roots are negative.

The iterative part of INVFREQS method for SIMO and MIMO systems considers the estimated vector $\boldsymbol{\theta}$ as an initial estimate. Similarly to SISO case, the estimated coefficients of the transfer function polynomials are assumed biased by an error where,

$$\hat{B}_{lm}(j\omega) = [b_{n_B(l,m)}^{(l,m)} + \Delta b_{n_B(l,m)}^{(l,m)}](j\omega)^{n_B(l,m)} + \ldots + [b_0^{(l,m)} + \Delta b_0^{(l,m)}] \tag{4-37}$$

$$\hat{A}_m(j\omega) = (j\omega)^{n_A(m)} + [a_{n_A(m)-1}^{(m)} + \Delta a_{n_A(m)-1}^{(m)}](j\omega)^{n_A(m)-1} + \ldots + [a_0^{(m)} + \Delta a_0^{(m)}] \tag{4-38}$$

where

$$\hat{a}_i^{(m)} = a_i^{(m)} + \Delta a_i^{(m)} \quad \text{and} \quad \hat{b}_i^{(l,m)} = b_i^{(l,m)} + \Delta b_i^{(l,m)} \tag{4-39}$$

By substituting the estimated polynomial coefficients, the vector error as defined in Eq. (4-29) is evaluated,

$$\hat{\mathbf{err}}^{(m)}(j\omega) = \begin{bmatrix} (\hat{b}_{n_B(1,m)}^{(1,m)}(j\omega)^{n_B(1,m)} + \ldots + \hat{b}_0^{(1,m)}) - \hat{H}_{1,m}(j\omega)((j\omega)^{n_A(m)} + \ldots + \hat{a}_0^{(m)}) \\ \vdots \\ (\hat{b}_{n_B(L,m)}^{(L,m)}(j\omega)^{n_B(L,m)} + \ldots + \hat{b}_0^{(L,m)}) - \hat{H}_{L,m}(j\omega)((j\omega)^{n_A(m)} + \ldots + \hat{a}_0^{(m)})] \end{bmatrix}$$

(4-40)

whereas by substituting Eqs. (4-37) and (4-38) into Eq. (4-29) gives a matrix form of the resulting equation similar to that in the SISO case

$$\Delta\mathbf{D}^{(m)}_{Ln_\omega\times(\sum_l n_B(m,l)+n_A(m)+L)}\Delta\boldsymbol{\theta}^{(m)}_{(\sum_l n_B(m,l)+n_A(m)+L)\times 1}=\mathbf{e\hat{r}r}^{(l,m)}_{Ln_\omega\times 1)} \tag{4-41}$$

The $\Delta\mathbf{D}$ matrix for m^{th} input is

$$\Delta\mathbf{D}^{(m)}=\begin{bmatrix}\Delta\bar{\mathbf{D}}_1^{(m)} & \Delta\tilde{\mathbf{D}}_1^{(m)} & \mathbf{0} & \cdots & \mathbf{0}\\ \Delta\bar{\mathbf{D}}_2^{(m)} & \mathbf{0} & \Delta\tilde{\mathbf{D}}_2^{(m)} & & \vdots\\ \vdots & \vdots & \ddots & \ddots & \mathbf{0}\\ \Delta\bar{\mathbf{D}}_L^{(m)} & \mathbf{0} & \cdots & \mathbf{0} & \Delta\tilde{\mathbf{D}}_L^{(m)}\end{bmatrix} \tag{4-42}$$

where submatrices $\Delta\bar{\mathbf{D}}_l^{(m)}$ are given by

$$\Delta\bar{\mathbf{D}}_l^{(m)}=\begin{bmatrix}\dfrac{(j\omega_1)^{n_A(m)-1}\hat{H}_{l,m}(j\omega_1)}{\hat{A}(j\omega_1)} & \dfrac{(j\omega_1)^{n_A(m)-2}\hat{H}_{l,m}(j\omega_1)}{\hat{A}(j\omega_1)} & \cdots & \dfrac{\hat{H}_{l,m}(j\omega_1)}{\hat{A}(j\omega_1)}\\ \dfrac{(j\omega_2)^{n_A(m)-1}\hat{H}_{l,m}(j\omega_2)}{\hat{A}(j\omega_2)} & \dfrac{(j\omega_2)^{n_A(m)-2}\hat{H}_{l,m}(j\omega_2)}{\hat{A}(j\omega_2)} & & \dfrac{\hat{H}_{l,m}(j\omega_2)}{\hat{A}(j\omega_2)}\\ \vdots & \vdots & & \vdots\\ \dfrac{(j\omega_{n_\omega})^{n_A(m)-1}\hat{H}_{l,m}(j\omega_{n_\omega})}{\hat{A}(j\omega_{n_\omega})} & \dfrac{(j\omega_{n_\omega})^{n_A(m)-2}\hat{H}_{l,m}(j\omega_{n_\omega})}{\hat{A}(j\omega_{n_\omega})} & \cdots & \dfrac{\hat{H}_{l,m}(j\omega_{n_\omega})}{\hat{A}(j\omega_{n_\omega})}\end{bmatrix} \tag{4-43}$$

and block matrices $\Delta\tilde{\mathbf{D}}_l^{(m)}$ that sit along a diagonal in $\Delta\mathbf{D}^{(m)}$ are

$$\Delta\tilde{\mathbf{D}}_l^{(m)}=\begin{bmatrix}\dfrac{-(j\omega_1)^{n_B(l,m)}}{\hat{A}(j\omega_1)} & \dfrac{-(j\omega_1)^{n_B(l,m)}}{\hat{A}(j\omega_1)} & \cdots & \dfrac{-1}{\hat{A}(j\omega_1)}\\ \dfrac{-(j\omega_2)^{n_B(l,m)}}{\hat{A}(j\omega_2)} & \dfrac{-(j\omega_2)^{n_B(l,m)}}{\hat{A}(j\omega_2)} & \cdots & \dfrac{-1}{\hat{A}(j\omega_2)}\\ \vdots & \vdots & \ddots & \vdots\\ \dfrac{-(j\omega_{n_\omega})^{n_B(l,m)}}{\hat{A}(j\omega_{n_\omega})} & \dfrac{-(j\omega_{n_\omega})^{n_B(l,m)}}{\hat{A}(j\omega_{n_\omega})} & \cdots & \dfrac{-1}{\hat{A}(j\omega_{n_\omega})}\end{bmatrix} \tag{4-44}$$

In case of SIMO systems, the vector of the error coefficients is defined as,

$$\Delta\boldsymbol{\theta}^{(m)}=\begin{bmatrix}\Delta a_{n_A(m)-1}^{(m)} & \cdots & \Delta a_0^{(m)} & \Delta b_{n_B(1,m)}^{(1,m)} & \cdots & \Delta b_0^{(1,m)} & \cdots & \Delta b_{n_B(L,m)}^{(L,m)} & \cdots & \Delta b_0^{(L,m)}\end{bmatrix}^{\mathrm{T}} \tag{4-45}$$

Then the error coefficients vector $\Delta\boldsymbol{\theta}^{(m)}$ is evaluated through the following equation,

$$\Delta\boldsymbol{\theta}^{(m)}=[\Delta\mathbf{D}^{(m)^*}\Delta\mathbf{D}^{(m)}]^{-1}\mathrm{Re}[\Delta\mathbf{D}^{(m)^*}\mathbf{e\hat{r}r}^{(m)}] \tag{4-46}$$

For MIMO systems, the same procedure is repeated M times to obtain the error coefficients of transfer functions with respect to each input. A similar convergence check to that explained for SISO systems is applied. These loops evaluating $\Delta\boldsymbol{\theta}$ and updating the estimated coefficients are repeated until the norm of the error coefficients vector becomes smaller than a tolerance factor as in Eq. (4-24).

4.1.3 Least Squares Estimation of Structural Parameters

The next task, then, is to use estimates of the polynomial coefficients of the transfer functions to obtain estimates of structural parameters such as stiffness and damping coefficients. This, however, requires knowledge of the direct relations between the transfer function coefficients and the structural parameters. To develop such relations, a method is used that is based on the conventional definition of the transfer function in the frequency domain.

By considering a state-space representation of a structural system

$$\dot{\mathbf{q}} = \tilde{\mathbf{A}}\mathbf{q} + \tilde{\mathbf{B}}f\,, \qquad \mathbf{y} = \mathbf{C}\mathbf{q} + \mathbf{D}f + \mathbf{v} \tag{4-47}$$

where $\mathbf{q} = [\ \mathbf{x}^{\mathrm{T}} \quad \dot{\mathbf{x}}^{\mathrm{T}}\ ]^{\mathrm{T}}$ is the state vector, $\tilde{\mathbf{A}}$ is the system state matrix, which is dependent on the mass $\mathbf{M}$, damping $\mathbf{C}_{\mathrm{d}}$, and stiffness $\mathbf{K}$ matrices of the structural system

$$\tilde{\mathbf{A}} = \begin{bmatrix} \mathbf{0}_{n\mathrm{DOF}\times n\mathrm{DOF}} & \mathbf{I}_{n\mathrm{DOF}\times n\mathrm{DOF}} \\ \left(-\mathbf{M}^{-1}\mathbf{K}\right)_{n\mathrm{DOF}\times n\mathrm{DOF}} & \left(-\mathbf{M}^{-1}\mathbf{C}_{\mathrm{d}}\right)_{n\mathrm{DOF}\times n\mathrm{DOF}} \end{bmatrix} \tag{4-48}$$

and nDOF is the number of degrees of freedom of the system. The $\tilde{\mathbf{B}}$ matrix is the input influence matrix, $\mathbf{C}$ is the output influence matrix for the state vector $\mathbf{q}$, and $\mathbf{D}$ is the direct transmission matrix. In both equations, f is a scalar excitation force, and $\mathbf{y}$ is a $m\times 1$ vector of measured responses corrupted by $m\times 1$ sensor noise vector $\mathbf{v}$.

Thus, the system can be represented by the $m\times 1$ transfer function (TF) matrix $\mathbf{H}(j\omega)$, expressed as the ratio of numerator and denominator polynomials as

$$\mathbf{H}(j\omega) = \mathbf{B}(j\omega) / A(j\omega) \tag{4-49}$$

However, another definition of the TF that depends on the system state matrix $\tilde{\mathbf{A}}$ is,

$$\mathbf{H}(j\omega) = \mathbf{C}[(j\omega)\mathbf{I}_{(2\times n\mathrm{DOF})\times(2\times n\mathrm{DOF})} - \tilde{\mathbf{A}}]^{-1}\tilde{\mathbf{B}} + \mathbf{D} \tag{4-50}$$

Equating the right hand sides of Eqs. (4-49) and (4-50) gives

$$\mathbf{B}(j\omega) / A(j\omega) = \mathbf{C}[(j\omega)\mathbf{I}_{(2\times n\mathrm{DOF})\times(2\times n\mathrm{DOF})} - \tilde{\mathbf{A}}]^{-1}\tilde{\mathbf{B}} + \mathbf{D} \tag{4-51}$$

Knowing the structure of the system state matrix, the dependence of $\mathbf{C}$, the output influence matrix, on $\mathbf{M}$, $\mathbf{C}_{\mathrm{d}}$, and $\mathbf{K}$ matrices, and the dependence of the $\tilde{\mathbf{B}}$ and $\mathbf{D}$ on the type of the excitation force f, one can obtain a parametric representation of the coefficients of the numerator and denominator polynomials in terms of $\mathbf{M}$, $\mathbf{C}_{\mathbf{d}}$, and $\mathbf{K}$ matrices components which will be denoted $\boldsymbol{\theta}(\mathbf{M},\mathbf{C}_{\mathrm{d}},\mathbf{K})$.

Finally, the difference between the parametric forms of the coefficients of the polynomials, $\mathbf{B}(j\omega)$ and $A(j\omega)$, from Eq. (4-51) and the estimates of these coefficients obtained from the INVFREQS stage $\boldsymbol{\theta}_{\mathrm{final}}$, is defined as an error vector

$$\mathbf{error} = \boldsymbol{\theta}_{\mathrm{final}} - \boldsymbol{\theta}(\mathbf{M},\mathbf{C},\mathbf{K}) \tag{4-52}$$

Minimizing the sum of the square errors in Eq. (4-52) for all coefficients will result in an estimate to the unknown parameter vector that includes the stiffness and damping coefficients.

4.1.4 Some Applications and Results for INVFLS Method

The two degree-of-freedom (2DOF) shear building structure model in Chapter 2 is studied using the INVFLS method. The structure is subjected to ambient excitation from the ground. Absolute acceleration measurements at the ground, $\ddot{x}_g$, and at the two floors, $(\ddot{x}_1 + \ddot{x}_g)$ and $(\ddot{x}_2 + \ddot{x}_g)$, are used to generate a 2×1 experimental transfer function at n_ω distinct frequency values. The theoretical transfer function matrix is the same as in Chapter 2 where $\boldsymbol{\theta}$ is the vector of unknown structural parameters and $\boldsymbol{\kappa}$ is the vector of known parameters based on the VSDDs actions.

The experimental transfer functions are generated in MATLAB® as discussed in METRANS report 01-10 (Johnson and Elmasry, 2003). The sensor noise used in generating the five experimental VSDD transfer functions is the same as those used for the conventional structure approach for both the INVFLS and ILSN applications. The VSDD is installed in the lateral bracing of the structure. For comparison with the results from ILSN method, similar VSDD locations in the structure are studied: a VSDD in the first story of the structure, then only in the second story and, finally, in both stories. As in the previous sections, the results are compared to the conventional structure approach. It is assumed that, of all structural parameters, only the mass of the 1st story m_1 is known.

In the numerical model considered here, the floor masses and story stiffnesses are taken to be unity. The story damping coefficients are set to 0.05. The single VSDD is assumed to provide additional stiffness in the story at which it is located with five discrete stiffness levels, corresponding to an additional 0%, 10%, 20%, 30% and 40% stiffness; *i.e.*, $\kappa_1 = 0.0$, $\kappa_2 = 0.1$, …, $\kappa_5 = 0.4$ where, in this case, $\boldsymbol{\kappa} = \kappa = k_{VSDD} / m_1$. For this study, the number of evenly spaced frequency points, n_ω, is 251 when comparing results of VSDD approach and the conventional structure approach, and is 2001 when comparing the INVFLS and ILSN methods. (The ILSN study in the previous sections used only 51 frequency points; such a larger number of frequency points is used here since INVFREQS is non-parametric so it can handle the computation for a large number of frequencies in much shorter time than ILSN method.) In addition, picking a larger number of frequency points is done since the least squares solution in the ILSN method depends on more information than the least squares stage in case of INVFLS method. It is also assumed that the same noise level exists for the simulated experimental transfer functions.

The comparisons reported here are the differences between:

- The VSDD approach, using five experimental transfer function matrices, one per VSDD stiffness level, and
- The conventional structure approach with $\kappa = 0.0$ where the conventional approach uses a square error based on five separate experimental transfer functions.

4.1.5 Analysis of Results

The INVFLS method is found to be successful in estimating stiffness coefficients. However, the estimation of the damping coefficients exhibits large deviations from the exact values. The results are shown in Fig. 4-1 for a VSDD in the first story, in Fig. 4-2 for a VSDD in the second story, and in Fig. 4-3 for VSDDs in both stories. Based on 100 noisy patterns of the simulated transfer function, the results indicate that, for the VSDD approach, the relative error in the estimates of stiffness coefficients has a maximum standard deviation of 3% for the first story

and 1% for the second story. Meanwhile, the relative error in the estimates of the damping coefficients has a maximum standard deviation of 35% for the 1st story and 20% for the 2nd story.

Comparing the VSDD and conventional structure approaches, it is observed from Fig. 4-1, for one VSDD in the 1st story, that the stiffness coefficient estimate of the 1st story is improved by using VSDDs whereas better estimation of the 2nd floor stiffness coefficient is achieved using the conventional structure approach. The trend of the variation of the damping coefficients estimates, however, shows no clear difference between the two approaches.

For a VSDD in the 2nd story only, the stiffness estimates for both stories have smaller variations using VSDD approach. Also, the damping coefficients estimates for both stories, though still with large variations, show some modest improvement with the VSDD approach.

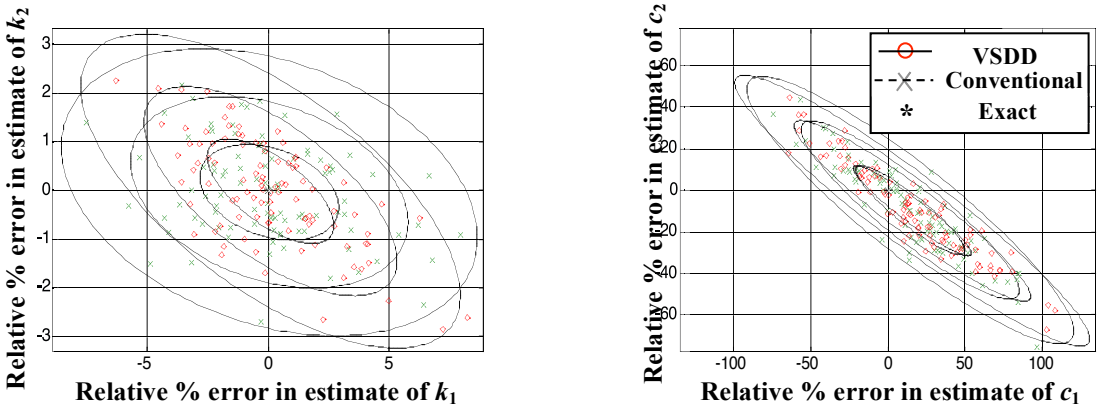

Fig. 4-1. Stiffness and damping estimate error levels for INVFLS method for 2DOF model with VSDD in 1st story only

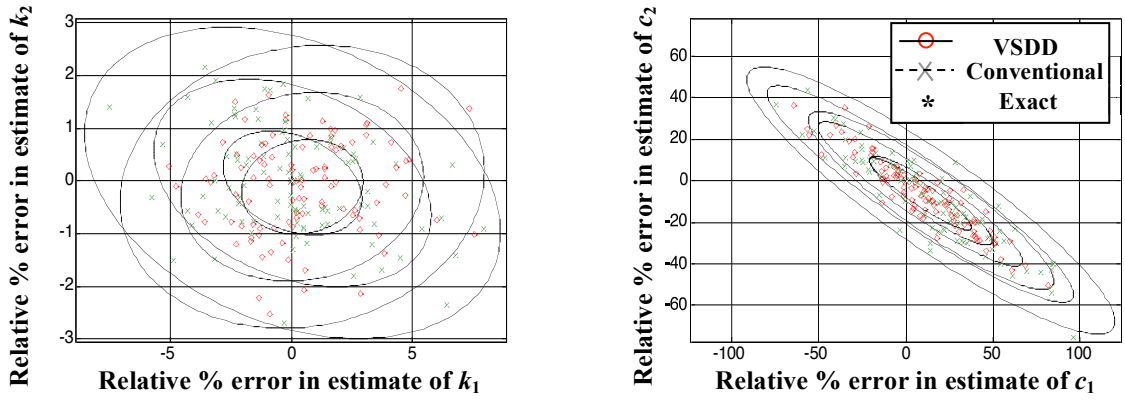

Fig. 4-2. Stiffness and damping estimate error levels for INVFLS method for 2DOF model with VSDD in 2nd story only

Using VSDDs in both stories, the variation of the stiffness coefficient estimate in the 2nd story is smaller than any other VSDD or conventional structure case. However, while the variation of the estimate of the stiffness coefficient of the 1st story is smaller than that of the conventional structure approach, locating a single VSDD in the 1st story or 2nd story only gives slightly smaller variation for the relative error of estimation as shown in Fig. 4-1 and Fig. 4-2.

The variation of the relative error of the damping estimates shows the same trend as using a VSDD in the 2nd story only.

By increasing the number of frequencies, n_ω, the results for stiffness and damping coefficients identification are improved. This is clear by comparing the results of INVFLS method in Fig. 4-1 to Fig. 4-3 to those in Fig. 4-4.

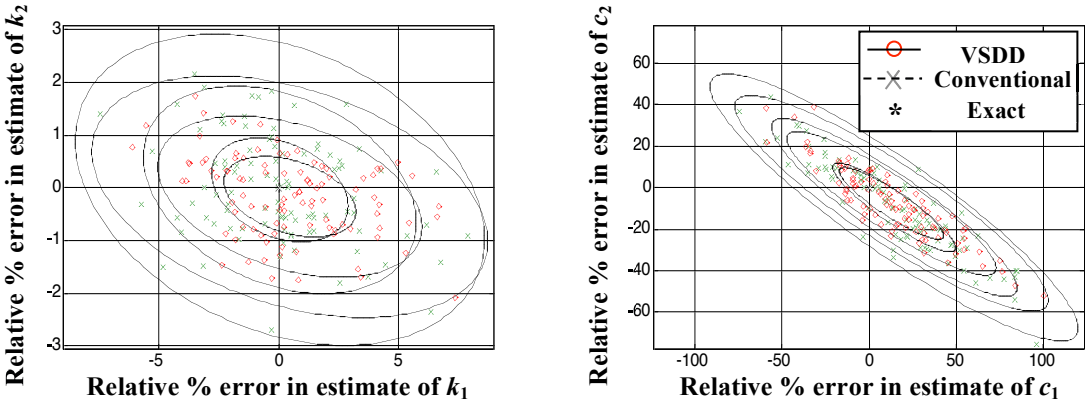

Fig. 4-3. Stiffness and damping estimate error levels for INVFLS method for 2DOF model with VSDDs in both stories

Comparing the results from the INVFLS method to those of ILSN method, shown in Fig. 4-4, one can observe that the ILSN method gives better estimates for the stiffness coefficients in the first story whereas INVFLS method gives better estimates for the stiffness coefficients of the second story. This is the case for all three VSDDs configurations in the 2DOF shear building structure.

However, the estimates of the damping coefficients are found to have less variation using the ILSN method for solving the identification problem. Nevertheless, Fig. 4-4 shows that the mean estimates for either stiffness or damping coefficients are always better using the INVFLS method. This may be attributed to the large number of frequency points used in the optimization problem in the INVFLS method. The INVFLS method also proved to consume much less computational time and converged faster to the results. This may be attributed to the fact that the INVFREQS stage of the INVFLS method uses a non-parametric numerical technique that is easily handled numerically, in contrast with the parametric problems in the ILSN method. Moreover, the application of the ILSN method requires some *a priori* initial guesses of the parameters to be estimated, whereas the INVFLS method has no such requirement and is able to estimate the stiffness parameters successfully with relatively small errors.

When it comes to choosing which method is applied on-site, the control designer should study the priorities whether absolute accuracy is more important than computation time or vice versa. Also, the designer should consider that using the ILSN method may require some prior guesses of the estimated parameters, which may require some experience. A good suggestion is to use the results of INVFLS method as an initial guess for the ILSN method.

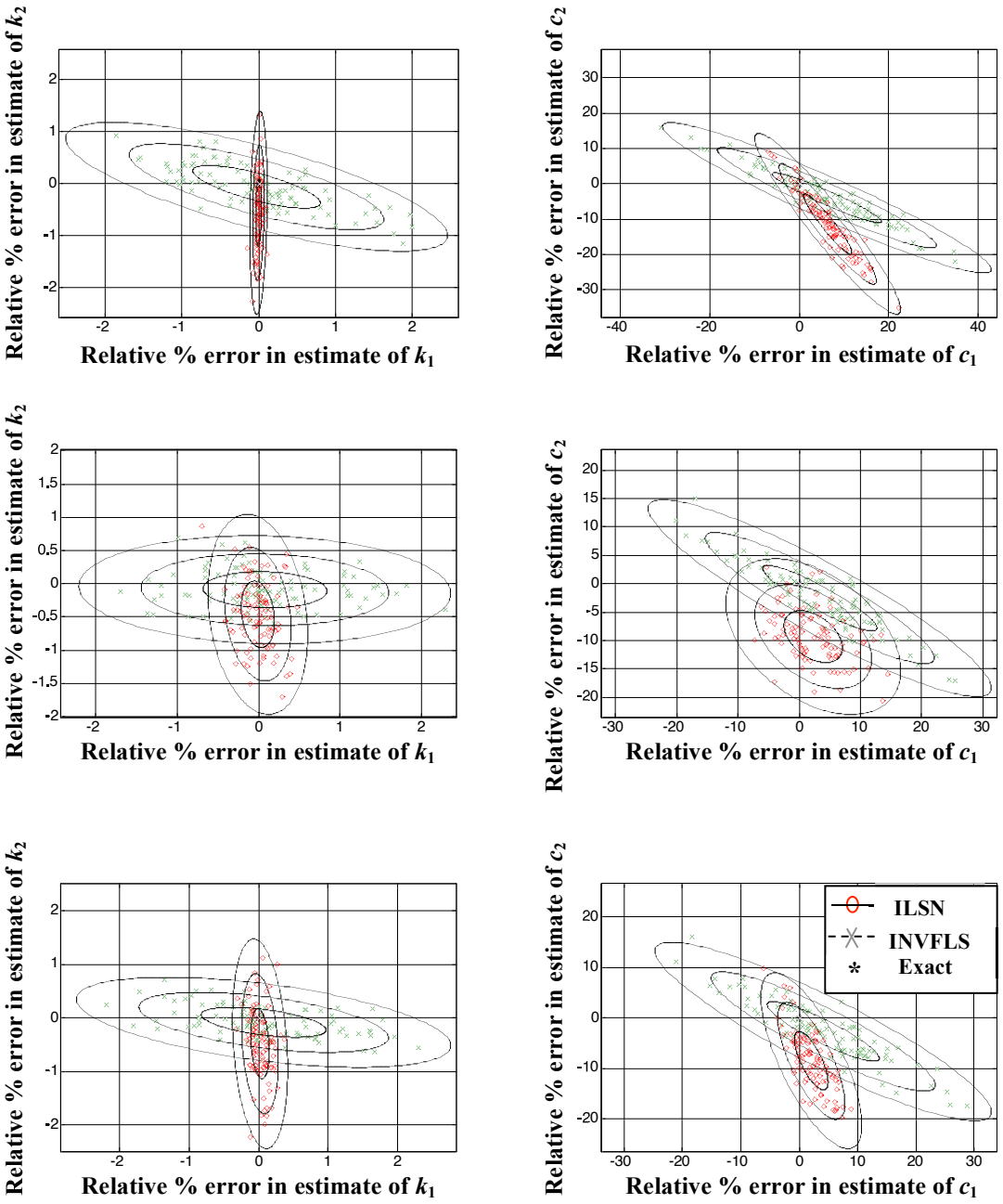

Fig. 4-4. Comparison of stiffness and damping estimate error levels between INVFLS and ILSN methods for 2DOF shear building model

5 VSDDs APPROACH IN THE CONTEXT OF SUBSPACE IDENTIFICATION

5.1 Introduction

The identification of modal parameters for structures from experimental data is sometimes carried out using methods that operate in the time domain. Typically, a curve is fit to free decay response data. This is based on a difference equation or state space mathematical model for the structure. In addition, the state space model has received considerable attention for system analyses and design in control and systems research during the last three decades. The basic development in state space realization is attributed to Ho and Kalman (1965) who introduced the important principle of minimum realization theory, which is the process of constructing a state space representation (Juang and Pappa, 1985). The Eigensystem Realization Algorithm (ERA), a modification and an extension to the minimum realization theory, was developed by Juang and Pappa (1985). The ERA is a state-space realization identification technique from noisy measurement data. Then, based on the identified state space model, the modal parameters can be obtained. This method is very effective in the identification of lightly damped structures (like many civil structures) and can also be applied to multi-input/multi-output systems. This chapter studies the improvement in identifying structural parameters (stiffness) using the ERA method for identification when VSDDs are included and commanded to induce additional stiffness.

5.2 Eigensystem Realization Algorithm

The Eigensystem Realization Algorithm (ERA) is a modal testing method (Juang and Pappa, 1985) developed at the NASA Langley research center. This state space method makes use of model overspecification in the initial stage in order to reduce bias. Spurious results are minimized by reducing an over-specified model order by singular value truncation. Moreover, a judicious choice of data and its proper arrangement in the block matrix can also be used to minimize the computational requirements of the method. The important features of the ERA method (Juang and Pappa, 1985) can be summarized in the following:

1. From the computational standpoint, simple numerical operations are needed.
2. The computational procedure is numerically stable.
3. The structural dynamics requirements for modal parameter identification and the control design requirements for a reduced state space model are satisfied.
4. Data from more than one test can be used simultaneously to efficiently identify closely spaced eigenvalues.
5. Computational requirements are moderate.

Generally, the ERA algorithm consists of two major parts, namely, the basic formulation of the minimum-order realization and the modal parameter computation. The technique begins by forming a block data matrix, obtained by deleting some rows and some columns of the generalized Hankel matrix of the pulse response (Markov Parameters), but maintaining the first block matrix intact. Singular value decomposition is then applied on the system Hankel matrix to compute the singular values and unitary matrices (all of the columns are orthonormal) of a system, which are subsequently used to determine the order of the system and to obtain a realization for the state space matrices. Natural frequencies, damping ratios, and mode shapes of the simulated structure can be obtained from the realized system matrix.

The system to be identified is assumed to be discrete-time, linear, and time invariant of the form:

$$\mathbf{x}(k+1) = \mathbf{A}\mathbf{x}(k) + \mathbf{B}\mathbf{u}(k), \qquad \mathbf{y}(k) = \mathbf{C}\mathbf{x}(k) \tag{5-1}$$

with $n_{\mathbf{u}}$ inputs and $n_{\mathbf{y}}$ outputs. The Markov (pulse response) parameters are given by:

$$\mathbf{Y}(0) = \mathbf{D}, \qquad \mathbf{Y}(k) = \mathbf{C}\mathbf{A}^{k-1}\mathbf{B}, \ k > 0 \tag{5-2}$$

where **A** is the discrete state matrix, **B** is the input influence matrix that characterizes the location and type of inputs, **C** is the output influence matrix for the state vector **x**, and **D** is the direct transmission matrix.

For the application in this chapter, the Markov parameters are measured in the time domain by introducing impulses to system inputs. Then, a generalized Hankel matrix **H**(k) of the Markov parameters is formed where **H**(k) is in the form:

$$\mathbf{H}(k) = \begin{bmatrix} \mathbf{Y}(k) & \mathbf{Y}(k+1) & \cdots & \mathbf{Y}(k+s) \\ \mathbf{Y}(k+1) & \mathbf{Y}(k+2) & \cdots & \mathbf{Y}(k+s+1) \\ \cdots & \cdots & \ddots & \cdots \\ \mathbf{Y}(k+r) & \mathbf{Y}(k+r+1) & \cdots & \mathbf{Y}(k+r+s) \end{bmatrix} \tag{5-3}$$

where r and s are arbitrary integers. The variables r and s are taken as 20–30 and 10 times, respectively, the assumed order of the system for best results (Caicedo *et al.*, 2004).

The generalized Hankel matrix is then evaluated for k=0. This is followed by performing a singular value decomposition on the Hankel matrix **H**(0)

$$\mathbf{H}(0) = \mathbf{P}\Sigma\mathbf{Q}^{\mathbf{T}} \tag{5-4}$$

where the **P** and **Q** matrices are unitary matrices (all of the columns are orthonormal), and the matrix Σ is the diagonal matrix of singular values. The order of the system will be apparent in the absence of noise because the first n singular values are non-zero while the rest are zeros or approximately zeros. When noise is present, the order may not be so clear and one must choose what order n to use. The smaller singular values in the diagonal of Σ correspond to computational or noise (non-physical) modes. Once the estimated order of the system is chosen, the rows and columns associated with the computational modes are eliminated to form condensed versions of the singular values and unitary matrices, Σ_n, $\mathbf{P}_n$, and $\mathbf{Q}_n$, respectively.

Using these truncated matrices, estimates of the state space matrices for the discrete-time structural model are found by using the formulas (Juang, 1994):

$$\hat{\mathbf{A}} = \Sigma_n^{-1/2}\mathbf{P}_n^{\mathrm{T}}\mathbf{H}(1)\mathbf{Q}_n\Sigma_n^{-1/2} \tag{5-5}$$

$$\hat{\mathbf{B}} = \Sigma_n^{1/2}\mathbf{Q}_n^{\mathrm{T}}\mathbf{E}_m \tag{5-6}$$

$$\hat{\mathbf{C}} = \mathbf{E}_n^{\mathrm{T}}\mathbf{P}_n\Sigma_n^{1/2} \tag{5-7}$$

where

$$\mathbf{E}_n^{\mathrm{T}} = \begin{bmatrix} \mathbf{I} & \mathbf{0} \end{bmatrix}, \qquad \mathbf{E}_m = \begin{bmatrix} \mathbf{I} & \mathbf{0} \end{bmatrix} \tag{5-8}$$

The eigenvalues and eigenvectors of the system can then be computed from the identified system matrix $\hat{\mathbf{A}}$ using a standard eigenvalue problem. The output matrix $\hat{\mathbf{C}}_n$ is used to transform the computed eigenvectors (corresponding to non-physical states in the identified model) to displacement at the floors of the structure using the equation

$$\tilde{\Phi} = \hat{\mathbf{C}}\hat{\Phi} \tag{5-9}$$

where $\tilde{\Phi}$ is the matrix of the output shapes and $\hat{\Phi}$ is the matrix of the eigenvectors of the state space matrix $\hat{\mathbf{A}}$. The ERA method was implemented using MATLAB®.

5.2.1 Least Squares Stiffness Estimation of the Eigenvalue Problem Solution

The structural parameters, especially the stiffness parameters, are the main interest herein. Thus, a technique that would evaluate such parameters from the modal parameters is required. The method used herein follows that of Caicedo *et al.* (2004), which is summarized as follows.

By considering a lumped mass system (such as a shear building model and the 2DOF bridge model) with n_d degrees of freedom, the mass matrix, **M**, and the stiffness matrix, **K**, are assumed to be of the form

$$\mathbf{M} = \begin{bmatrix} m_1 & 0 & \cdots & 0 & 0 \\ 0 & m_2 & \cdots & 0 & 0 \\ \vdots & \vdots & \ddots & \vdots & \vdots \\ 0 & 0 & \cdots & m_{n_\mathrm{d}-1} & 0 \\ 0 & 0 & \cdots & 0 & m_{n_\mathrm{d}} \end{bmatrix} \tag{5-10}$$

$$\mathbf{K} = \begin{bmatrix} k_1 + k_2 & -k_2 & \cdots & 0 & 0 \\ -k_2 & k_2 + k_3 & \ddots & \vdots & \vdots \\ 0 & \ddots & \ddots & -k_{n_\mathrm{d}-1} & 0 \\ \vdots & \cdots & -k_{n_\mathrm{d}-1} & k_{n_\mathrm{d}-1} + k_{n_\mathrm{d}} & -k_{n_\mathrm{d}} \\ 0 & \cdots & 0 & -k_{n_\mathrm{d}} & k_{n_\mathrm{d}} \end{bmatrix} \tag{5-11}$$

The eigenvalue problem of such a structure is (Chopra, 1995)

$$(\mathbf{K} - \lambda_j \mathbf{M})\boldsymbol{\phi}_j = 0 \quad \text{or} \quad \mathbf{K}\boldsymbol{\phi}_j = \lambda_j \mathbf{M}\boldsymbol{\phi}_j \tag{5-12}$$

where λ_j and $\boldsymbol{\phi}_j$ are the j^{th} eigenvalue and eigenvector of the structure, respectively.

Substituting the mass and stiffness matrices into the eigenvalue problem and reorganizing so that the stiffness coefficients can be assembled in a vector, results in

$$\Delta_j \mathbf{k} = \Lambda_j \tag{5-13}$$

where

$$\Delta_j = \begin{bmatrix} \varphi_{1,j} & \varphi_{1,j} - \varphi_{2,j} & 0 & \cdots & 0 \\ 0 & \varphi_{2,j} - \varphi_{1,j} & \varphi_{2,j} - \varphi_{3,j} & \cdots & 0 \\ \vdots & \vdots & \ddots & \ddots & \vdots \\ 0 & 0 & \cdots & \varphi_{n_d-1,j} - \varphi_{n_d-2,j} & \varphi_{n_d-1,j} - \varphi_{n_d,j} \\ 0 & 0 & \cdots & 0 & \varphi_{n_d,j} - \varphi_{n_d-1,j} \end{bmatrix} \tag{5-14}$$

and the stiffness vector $\mathbf{k}$ is

$$\mathbf{k} = [\ k_1 \quad k_2 \quad \ldots \quad k_n\ ]^{\mathrm{T}} \tag{5-15}$$

and the vector Λ is

$$\Lambda = [\ \varphi_{1,j}\lambda_j m_1 \quad \varphi_{2,j}\lambda_j m_2 \quad \ldots \quad \varphi_{n_d,j}\lambda_j m_{n_d}\ ]^{\mathrm{T}} \tag{5-16}$$

where $\varphi_{i,j}$ is the i^{th} element of the eigen vector $\boldsymbol{\phi}_j$.

Eq. (5-13) can be applied for each of the n_d eigenvalues and eigenvector pairs identified. Thus, by gathering all of the equations corresponding to Eq. (5-13) into one big matrix equation gives

$$\begin{bmatrix} \Delta_1 \\ \Delta_2 \\ \vdots \\ \Delta_n \end{bmatrix} \begin{bmatrix} k_1 \\ k_2 \\ \vdots \\ k_n \end{bmatrix} = \Delta\mathbf{k} = \Lambda = \begin{bmatrix} \Lambda_1 \\ \Lambda_2 \\ \vdots \\ \Lambda_n \end{bmatrix} \tag{5-17}$$

representing n_d^2 equations, which are used to solve for the vector $\mathbf{k}$ of stiffnesses by the relation

$$\mathbf{k} = \Delta^{-1}\Lambda \tag{5-18}$$

It is important to note that the matrix Δ is not square and, consequently, a pseudo-inverse of this matrix is computed to obtain a least squares estimate of the stiffnesses. Using multiple eigenvectors improves the resulting estimations.

5.2.2 Applying VSDD approach to the ERA method

In order to apply the VSDD approach to the ERA method, some assumptions are considered. The stiffnesses of VSDDs are assumed known for any desired configuration of VSDD stiffnesses. Once the identification process (of the structure including VSDDs) is complete, the added VSDD stiffness in each corresponding story is subtracted from the estimated stiffness parameter. Thus, the results are considered estimates of the structure's stiffnesses at this configuration of the VSDDs stiffnesses.

This can be expressed through the equation

$$k_{\text{actual}} = k_{\text{estimated}} - k_{\text{VSDD}} \tag{5-19}$$

Then, by applying the same operation for each case of the VSDD stiffness and obtaining the resulting corresponding stiffness estimates, a mean estimate of the stiffnesses for all different VSDD cases can be obtained. This can be expressed in the form of the equations

$$k_i = \frac{1}{n_\kappa} \sum_{k=1}^{n_\kappa} k_{i,\mathrm{VSDD}_k} \tag{5-20}$$

where n_κ is the number of the VSDD stiffness configuration cases.

5.2.3 Application to the 2DOF Bridge Model

The ERA approach with VSDDs is applied to the 2DOF bridge model discussed in METRANS 01-10 (Johnson and Elmasry, 2003) and in Chapter 2. The bridge stiffness and damping parameters are the same as in Chapter 2. The suggested technique is applied such that every realization of the stiffness parameters is averaged over 100 different patterns of noisy data. This is done 20 times to get statistics of the variation. The RMS noise level was taken as 10% of that of the original signal. The impulse response was generated in MATLAB® based on the exact parameters of the structure bridge structure. The additional stiffnesses induced by the VSDD are 0%, 125%, 250%, 375%, and 500% of the isolator stiffness. The system is assumed of the 4th order in the identification process, so the ERA algorithm chooses the first four singular values to represent the system. The arbitrary integers r and s are taken equivalent to 50 and 20, respectively. In addition, the state space system matrices **A**, **B**, **C**, and **D** are

$$\mathbf{A} = \begin{bmatrix} 0 & 0 & 1 & 0 \\ 0 & 0 & 0 & 1 \\ -\dfrac{(k_1+k_2)+k_{VSDD}}{m_1} & \dfrac{k_2+k_{VSDD}}{m_1} & -\dfrac{(c_1+c_2)}{m_1} & \dfrac{c_2}{m_1} \\ \dfrac{k_2+k_{VSDD}}{m_2} & -\dfrac{k_2+k_{VSDD}}{m_2} & \dfrac{c_2}{m_2} & -\dfrac{c_2}{m_2} \end{bmatrix} \tag{5-21}$$

$$\mathbf{B} = [\ 0 \quad 0 \quad 1/m_1 \quad 1/m_2\ ]^{\mathrm{T}} \tag{5-22}$$

$$\mathbf{C} = \begin{bmatrix} -\dfrac{(k_1+k_2)+k_{VSDD}}{m_1} & \dfrac{k_2+k_{VSDD}}{m_1} & -\dfrac{(c_1+c_2)}{m_1} & \dfrac{c_2}{m_1} \\ \dfrac{k_2+k_{VSDD}}{m_2} & -\dfrac{k_2+k_{VSDD}}{m_2} & \dfrac{c_2}{m_2} & -\dfrac{c_2}{m_2} \end{bmatrix} \tag{5-23}$$

$$\mathbf{D} = [\ 1/m_1 \quad 1/m_2\ ]^{\mathrm{T}} \tag{5-24}$$

5.2.4 Results of Identification Process

Fig. 5-1 shows the relative error in the stiffness estimates. It demonstrates that using a VSDD was beneficial in giving more accurate means of the estimated stiffnesses. In addition, the root mean square error (RMSE) of the identified stiffnesses in the first and second stories, with the VSDD approach, are about two-thirds and half, respectively, of those obtained through the conventional structure approach. Thus, it can be concluded that using VSDDs also has potential for improving the accuracy of sub-space techniques such as ERA method in identification.

Table 5-1. Estimate means and mean-square error percentage for 2DOF bridge model using ERA method (Varying stiffness)

	Exact	With VSDD		No VSDD	
		Mean (kN/m)	RMSE (%)	Mean (kN/m)	RMSE (%)
k_1	15791	15734.9	0.67	15651.65	0.99
k_2	7685	7692.5	0.73	7781.995	1.42

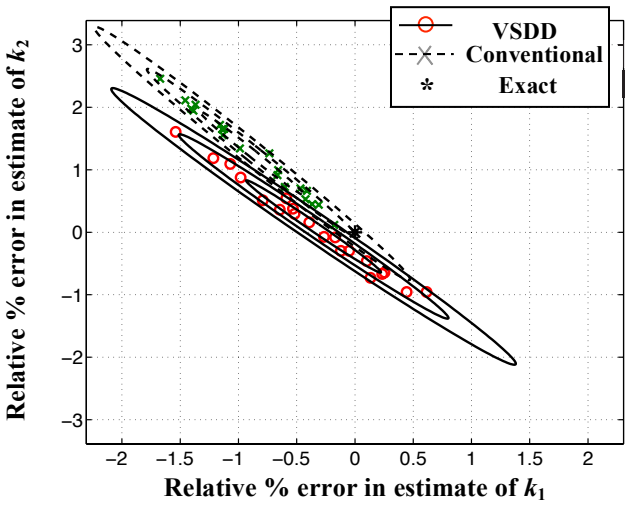

Fig. 5-1. Variation in the stiffness parameters of the pier and deck of the 2DOF Bridge system model

6 EXPERIMENTAL VERIFICATION OF THE BENEFITS OF VSDDs IN SHM

6.1 Introduction

Experimental investigations are essential to obtain a fundamental understanding of many phenomena. To verify the advantages gained by using VSDDs in structures for SHM, it is vital to identify these advantages in an experimental basis. This chapter introduces a laboratory experiment that replicates the effect of VSDDs on structures when used for SHM. A two degree-of-freedom (2DOF) experimental shear building structure is subjected to a band-limited white noise (BLWN) ground acceleration and a filtered band-limited white noise (FBLWN) through a small-scale shaking table. The acceleration of the table and the absolute accelerations of the first and second stories are recorded. The measurements are processed to obtain an identification of the stiffness of the first and second stories of the 2DOF structure before and after damage. The results verify the observations from the theoretical results in the previous chapters that the identification is improved by using VSDDs.

6.2 Experiment Description

In the area of control and SHM of civil structures, it is well recognized that experimental verification is necessary to focus research efforts in the most promising directions (Housner *et al.*, 1994a,b). Consequently, a small-scale shaking table experiment is performed to validate the analytical results that show the improvements to SHM when using VSDDs. A schematic of the experiment, where a two degree-of-freedom (2DOF) shear building structure is mounted on and fixed to a small shaking table, is shown in Fig. 6-1. Fig. 6-1 also shows the blue power module that passes the analog command voltage signals from the MultiQ (D/A, A/D converter) board to the table and passes back the accelerometer analog measurement signals. The experiment was built and run in the SHM and Control Lab at the University of Southern California (USC).

Fig. 6-1. The shaking table with the 2DOF shear building structure mounted on it

The components of the experiment, in general, include the shaking table, 2DOF shear building model, digital controller (MultiQ I/O) board, the power module for the table, PC computer, three accelerometers and two sets of steel springs necessary to replicate the various stiffness levels that would be achieved with VSDDs in a real-world application. The computer used in the experiment is a Windows 98 466MHz Pentium 3.

6.2.1 Experiment Steps

The experiment goal can be summarized in identifying damage in an experimental 2DOF structure composed of the shear building structure and two pairs of weak springs per floor, acting as bracing to the structure, as shown in Fig. 6-1. The damage in the structure will be effected by changing the stiffness of one of the two stories by removing a pair of the weak diagonal bracing springs.

The damage identification problem is solved once with no VSDDs included in the system (conventional structure) and then again when VSDDs exist in the system. In the course of the experiment, the additional forces induced by the VSDDs in the system are replicated by adding strong springs in the diagonal bracing with different configurations giving different stiffness levels. The identification process, in each damage case, is performed using four sets of measured ground and floor absolute accelerations data, obtained using four different configurations of the strong springs. For fairness in comparison, the conventional structure approach uses the same amount of measured data.

The 2DOF structure, during the experiment, is subjected to ambient ground excitation induced by the shake table. The ambient ground excitation is generated in two ways: by a band-limited white noise (BLWN) ground excitation with a cutoff frequency of approximately 20Hz, and by a filtered BLWN using the Kanai-Tajimi filter to simulate ground effects (Soong and Grigoriou, 1993; Ramallo *et al.*, 2002).

Once the data is obtained, the Iterative Least Squares Numerator (ILSN) identification method is then applied to estimate the stiffness coefficients for both floors of the 2DOF structure. This is done in a manner similar to the simulation study in Chapter 3. (The ILSN identification technique is not detailed here; the reader is referred to Chapter 2 for more information.) Finally, the identification results of the stiffnesses in both stories are compared, before and after damage occurs, both with VSDDs in the system and without VSDDs. The experimental results confirm the simulation observations showing more accurate damage assessment when using VSDDs.

6.2.2 Components of the Experiment

Before introducing the results, the properties and nature of each component of the experiment are detailed in the following subsections.

6.2.2.1 Shaking Table Properties

The key component of the experiment is a bench-scale shake table, shown in Fig. 6-2. The shaking table is a small-scale uniaxial earthquake simulator manufactured by Quanser Consulting Inc. The table is located in the SHM and Control Lab at the University of Southern California (USC). The specifications of the table have been developed to produce a unit that is effective for a wide variety of experiments for civil engineering structures. The table is computer-controlled with a user-friendly interface. The design specifications of the shaking table, as supplied by the manufacturer, are shown in Table 6-1.

The nominal operational frequency range of the simulator is 0–20 Hz. Because the shake table motor is inherently open loop unstable, position feedback, measured from the shake table motor, is employed to stabilize the table (Christenson *et al.*, 2003).

Fig. 6-2. Plan view of the shaking table

Table 6-1. Design Specifications of the Shaking Table

Specification	Value	Unit
Shake table system overall dimensions (L×W×H)	61×46×13	cm
Shake table system mass	27.2	kg
Table dimensions (payload area), (L×W)	46×46	cm
Maximum payload at 2.5*g*	15	kg
Peak Displacement	±7.5	cm
Operational bandwidth	20	Hz
Peak velocity	83.8	cm/s
Peak acceleration	24.5	m/s^2
Accelerometer range	±49	m/s^2
Accelerometer sensitivity	1/9.81	Vs^2/m
Lead screw spread pitch	12.7	mm/rev
Brushless servo motor power	745.7	W
Maximum continuous current	12.5	A
Motor maximum torque	1.65	N-m
Linear bearing load carrying capability	131.5	kg
Linear bearing life expectancy (total travel)	6350	km
Leadscrew encoder resolution	4096	counts/rev
	3.1	μm/count

6.2.2.2 Digital Controller

The digital controller, used in the experiment, is the MultiQ I/O board (http://www.quanser.com/English/html/solutions/fs_soln_hardware.html) with the WinCon (http://www.quanser.com/English/html/solutions/fs_soln_software_wincon.html) real time controller installed in a Windows computer. The MultiQ interface board is connected to the MultiQ I/O board by a ribbon cable, and to the power module that is, in turn, connected to the shake table. The extended terminal of the MultiQ interface board, as shown in Fig. 6-3, has 13 bit analog/digital (A/D) and 12 bit digital/analog (D/A) connections with eight input and eight output analog channels. Eight digital encoders are also available. The table control algorithm is developed using SIMULINK (1999) under MATLAB® 5.3 and executed in real time using the WinCon software. The SIMULINK code is converted to C++ code using the Real Time workshop in MATLAB® and interfaced through the WinCon software to run the control algorithms on the CPU of the PC (Quanser Consulting, 1995; Christenson *et al.*, 2003).

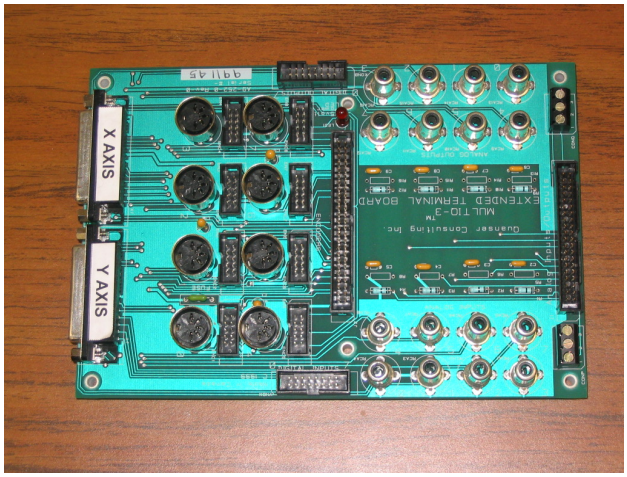

Fig. 6-3. Plan view of the extended terminal of the MultiQ interface board

6.2.2.3 2DOF Structure

A 2DOF shear building structure, shown in Fig. 6-1, is the test bed of this experiment. The structure is composed of two vertical aluminum plates in each story, with thick plexi-glass plates at the bottom, first and second stories of the structure to connect the vertical plates. The horizontal plexi-glass plates and the vertical aluminum plates are fixed to each other by three 8-32 UNC bolts in each side at each level. The interstory height is 490 mm.

The experimental structure also includes two pairs of weak steel springs located in each story as shown in Fig. 6-4. Including these weak springs as part of the experimental structure allows inducing damage in the structure, by removing one or two of these pairs, without damaging the original structure. Each pair of the weak springs represents about 7.38 % of the estimated stiffness of each story of the original structure.

Prior to experimentation, the 2DOF structure was disassembled so that its dimensions and measurements could be recorded. A caliper was used to measure the thickness of the structure's components. The lengths, widths, and heights were measured using a measuring tape with accuracy of 1/32 of an inch. An electronic scale, with measurement sensitivity 1 gm, was used to weigh each component of the structure. Table 6-2 lists the measured dimensions in centimeters

and masses in kilograms. It is important to note that the mass tabulated for the plexi-glass plate, also includes the mass of the screws, washers, fastener plates, and accelerometers located at the corresponding level. The weak springs are manufactured by Century Spring Corp. (Los Angeles) and have vendor stock #80039. The physical properties of the weak steel springs, as per the manufacturer's catalogue, are shown in Table 6-3.

Fig. 6-4. Front view of the experimental 2DOF structure including the added weak steel springs

Table 6-2. Measured Dimensions and Masses of the 2DOF Structure

	Mass (kg)	Length (cm)	Width (cm)	Thickness (cm)
Plexi-glass plate at shake table level	0.654	30.48	10.80	1.24
Plexi-glass plate at 1st story level	0.654	30.48	10.80	1.24
Plexi-glass plate at 2nd story level	0.654	30.48	10.80	1.24
Vertical Aluminum Plates (1st story)	0.236	50.17	10.80	0.18
Vertical Aluminum Plates (2nd story)	0.236	50.17	10.80	0.18

Table 6-3. Physical Properties of Weak Spring #80039 as per Manufacturer Catalogue

Stock No.	Outer Diameter (mm)	Length without Hooks (mm)	Stiffness (N/m)	Initial Tension (N)	Suggested Max. Deflection (mm)	Suggested Max. Load (N)
80039	2.39	25.40	90.00	0.30	37.00	3.60

For the sake of accuracy in the processing of results, the stiffnesses of the weak springs are verified by applying an additional test using a spring tester at the manufacturer main office (see

Appendix A for manufacturer test reports). The tests are applied on two pairs of the weak springs. One of the two pairs is the one removed from the first story to replicate damage there, and the other pair is the one removed from the second story to replicate damage there. The results of the tests are shown in Table 6-4. It is found that, based on the verification tests results, that the mean stiffness of the weak springs (#80039) is 83.11 N/m, which is less than that documented in the catalogue. Thus, a pair of the weak springs represents 7.38% of the estimated overall stiffness of each floor of the experimental 2DOF structure. The configurations of the weak springs pairs in the structure, in order to replicate damage in the structure, are shown in Table 6-5.

Table 6-4. Weak Spring (#80039) Stiffness Test Results Supplied by Manufacturer

Spring #80039	Location	Stiffness (N/m)
Sample 1	1st story	83.46
Sample 2	1st story	82.41
Sample 3	2nd story	82.06
Sample 4	2nd story	84.51

Table 6-5. Different Configurations of Spring Pairs in the 2DOF Structure to Replicate Damage in the Structure

	Case	Location	No. of Pairs
Induced Damage	No damage	1st story	2 pairs
		2nd story	2 pairs
	7.38% damage in 1st story	1st story	1 pair
		2nd story	2 pairs
	7.38% damage in 2nd story	1st story	2 pairs
		2nd story	1 pair

6.2.2.4 Accelerometers

The resulting response of the structure during the experiment is measured by accelerometers as shown in Fig. 6-5. One accelerometer is fixed to the table base level. Another two are fixed to each of the two stories in the middle bottom of the plexi-glass plates at each story. The range of the accelerometers is ± 5*g* with an output of ± 5 volts. Each accelerometer is connected via cable to the power module which is, in turn, connected to the MultiQ® unit.

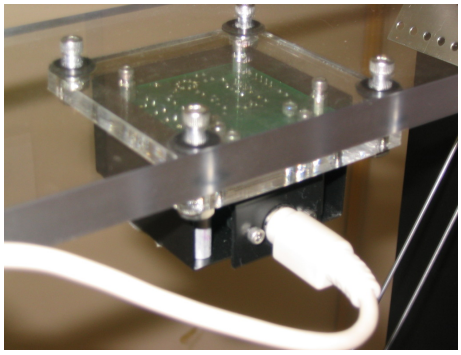

Fig. 6-5. Isometric view of the mounted accelerometer

6.2.2.5 Springs Representing VSDDs

The theoretical simulations in Chapter 3 (*e.g.*, the 2DOF bridge model problem) show that using higher VSDD stiffness to story stiffness ratio improves the results considerably. For the case of the experimental structure, the small cross-section of the aluminum plates limits the feasible added stiffness per floor because too much added vertical load could cause the vertical plates to buckle. Consequently, the springs used to represent the additional forces exerted by VSDD are chosen to have stiffness of the same order as that of the columns per story. Therefore, Century Spring Corp. spring stock number #80222 is chosen. The physical properties of this stiff spring, from the manufacturer catalogue, are shown in Table 6-6.

Fig. 6-6 shows the experimental structure with the stiff springs attached. Due to the short lengths of the springs, steel links are used to connect the springs to aluminum connections as shown in Detail A, Fig. 6-7, at each joint of the 2DOF structure. The springs are staggered across the depth of the structure, as shown in Detail B, Fig. 6-8, so that the springs do not rub against each other. To replicate the effect of varying forces by VSDDs, the stiff spring pairs are added in four configurations. Table 6-7 shows the different configurations of the stiff spring pairs in the 2DOF structure.

Table 6-6. Physical Properties, as per Manufacturer Catalogue, of Stiff Springs Used to Replicate the Effect of VSDD Forces

Stock No.	Outer Diameter (mm)	Length without Hooks (mm)	Stiffness (N/m)	Initial Tension (N)	Suggested Max. Deflection (mm)	Suggested Max. Load (N)
80222	4.57	69.90	840.00	3.00	37.00	34.00

Table 6-7. Different Configurations of Stiff Springs Pairs in the Two Stories of the 2DOF Structure

Configuration No.	No. of Pairs in 1st Story	No. of Pairs in 2nd Story
1	0	0
2	4	0
3	4	2
4	2	4

Table 6-8. Stiff Spring (#80222) Stiffness Test Results Supplied by Manufacturer

Spring #80222	Stiffness (N/m)
Sample 1	989.291
Sample 2	974.563
Sample 3	962.464
Sample 4	978.069
Sample 5	991.396
Sample 6	969.653
Sample 7	993.499
Sample 8	980.875
Sample 9	980.875
Sample 10	966.146
Sample 11	963.165
Sample 12	967.549

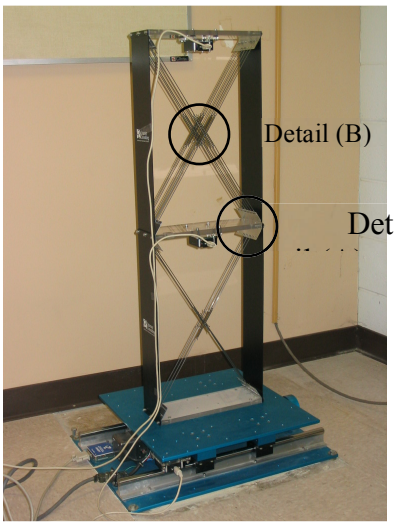

Fig. 6-6. Experimental structure with springs representing VSDDs

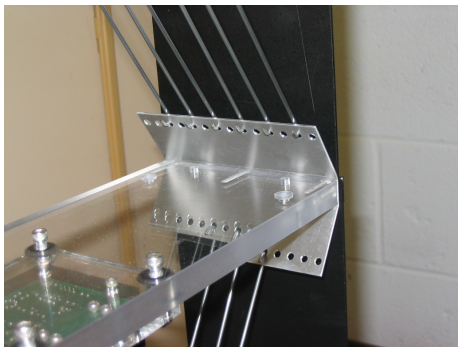

Fig. 6-7. Detail (A) showing aluminum connections and steel link

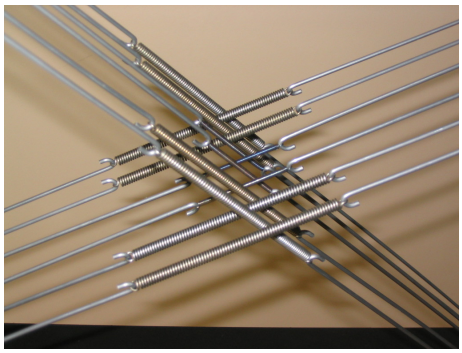

Fig. 6-8. Detail (B) showing staggered springs connected by steel link

The reason for even numbered spring pairs per configuration, in each story, is to minimize any coupling of the transverse modes with those of torsion. The results obtained in system identification with the stiff springs included in the structure are compared to the case without any stiff springs in either of the two stories (conventional structure).

Since an accurate estimate of the VSDD stiffness is required in the identification, spring stiffness tests are performed by the manufacturer on the stiff springs (#80222). (See Appendix A for the test report by the manufacturer.) During the experiment, a maximum of six pairs are required (Table 6-7). Thus, the twelve springs forming these six pairs are tested to obtain the stiffnesses as shown in Table 6-8. The results show differences from those documented in the manufacturer catalogue. The measured stiffnesses are the ones used in the identification process.

Where Table 6-7 shows four pairs of stiff springs in a story, they are samples 1,3,4,5,6,7,8, and 12 in Table 6-8. Where Table 6-7 shows two pairs, they are samples 2, 9, 10 and 11.

6.2.3 Modeling and Stiffness Calculations for the Experimental Structure

A critical precursor to SHM is the development of an accurate dynamic model of the structural system. For this study, the approach used for system identification is to construct a mathematical model to replicate the input/output behavior of the system (Dyke *et al.*, 1996). The model assumed here is a shear-building model. Thus, in the calculation of the stiffness for the

first and second floors, the total stiffness is considered the sum of the columns' stiffnesses and the additional equivalent stiffness due to spring pairs. Accordingly, the stiffness of each story is calculated from

$$k_{\text{story}} = \left(\sum^{n_c} k_{\text{col}} \right) + n_{\text{p}} \times 2 \times k_{\text{s}} \times \cos^2 \theta \tag{6-1}$$

where n_{c}=2 is the number of columns, k_{col} is the stiffness of each vertical aluminum plate. The stiffness of each spring is k_{s} and n_{p} is the number of spring connections pairs. θ is the angle of inclination of the spring, calculated from

$$\theta = \tan^{-1}(B / h) \tag{6-2}$$

where B is the horizontal width of the 2DOF structure and h is the interstory height of each story of the 2DOF structure.

E_{AL}, the modulus of elasticity of aluminum (material of the plates), is taken as 75GPa. All cross sections of the aluminum and plexi-glass plates are rectangular. Thus, the moment of inertia of each plate can be calculated from

$$I = \frac{bt^3}{12} \tag{6-3}$$

where t is the thickness of the plate and b is the plate width. Consequently, the stiffness matrix for the undamaged structure is

$$\mathbf{K} = \left[\frac{24 E_{\text{AL}} I_{\text{AL}}}{h^3} + 4 \times k_{80039} \times \cos^2 \theta \right] \begin{bmatrix} 2 & -1 \\ -1 & 1 \end{bmatrix} \tag{6-4}$$

where I_{AL} is the moment of inertia of each of the aluminum plates and k_{80039} is the stiffness of the stiff spring #80039. Note that this stiffness matrix is based on the measured dimensions and assumed material properties and may not be exact due to the difference between actual and assumed material properties and modeling idealization.

6.2.4 Generation of Simulated Ground Acceleration

During the shake table experiment, the laboratory structure is assumed subjected to ambient ground excitation induced by the shake table. The ambient ground excitation is generated in two ways: by a band-limited white noise (BLWN) ground excitation with a cutoff frequency of 20Hz and by a filtered band-limited white noise (FBLWN) using the Kanai-Tajimi filter (Soong and Grigoriou, 1993; Ramallo *et al.*, 2002). The procedure for obtaining each excitation type is explained in the following paragraphs.

6.2.4.1 Band-Limited White Noise (BLWN) Generation

The SIMULINK toolbox under MATLAB® 5.3 is used for designing the excitation model that commands the shake table to generate white noise ground acceleration. The software WinCon 3.1, supplied by the manufacturer of the shake table (Quanser), uses the SIMULINK toolbox to generate models and compile them using C++. Fig. 6-9 shows the BLWN acceleration generator model used in the experiment.

The generator model of white noise ground acceleration is designed such that a BLWN displacement is commanded to the shake table. Theoretically, the commanded white noise

displacement should produce BLWN acceleration. However, due to noise resulting from imperfections, frequency dependence of table dynamics and nonlinearities in the table system, this is not the case. Thus, the commanded BLWN displacement to the table should be filtered through some frequency domain filters in order to obtain the desired white noise ground acceleration, and to enforce table safety and limitations. Consequently, two filters (Filter_1 and Filter_2 in Fig. 6-9) are added to the designed generator SIMULINK model. The first filter (Filter_1) ensures that the power spectral density (PSD) of the resulting table acceleration has a constant magnitude in the frequency domain. The second filter (Filter_2) is a low pass filter that limits the effective frequency range of the table motion with a cutoff frequency at 20 Hz. For the safety of the table, the magnitude of the commanded displacement is scaled so as not to exceed one inch, and its magnitude is only allowed to ramp up at the start of the table motion.

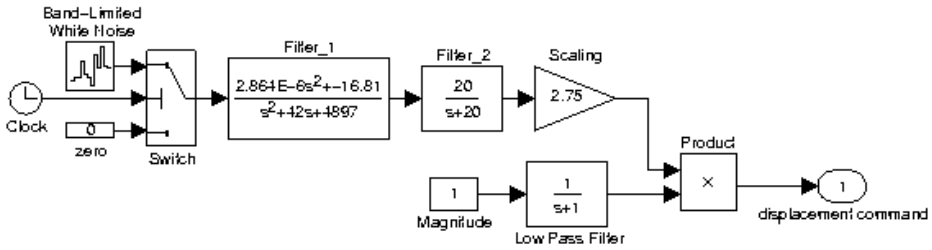

Fig. 6-9. SIMULINK model for generation of band-limited white noise ground acceleration using the shaking table

Fig. 6-10 shows a sample time history of the generated ground acceleration as measured by the accelerometer located on the table. The power spectral density (PSD) of this sample ground acceleration is shown in Fig. 6-11. (The sampling frequency is 1000 Hz.)

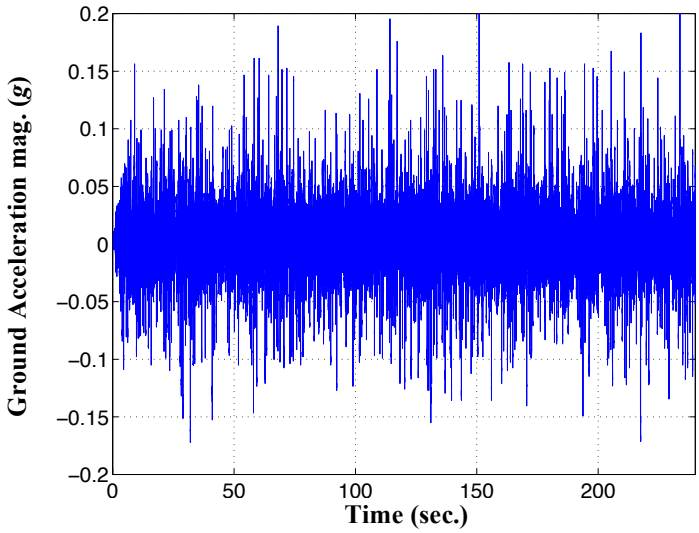

Fig. 6-10. Sample 4-minute realization of the band-limited white noise acceleration at table level

The Hanning window with an overlap of 75% between the consecutive data samples is used for the evaluation of the PSD. To obtain a correct PSD, the time history was detrended to remove any DC gains that may exist due to any static charges or manufacturing defects in the accelerometers.

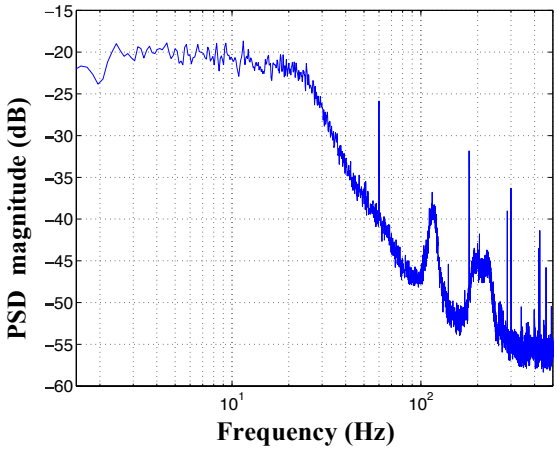

Fig. 6-11. PSD magnitude of the generated BLWN ground acceleration

6.2.4.2 Filtered Band-Limited White Noise (FBLWN) Generation

For a more realistic loading model to replicate ground motion, it is better to consider the effect of the soil on the propagation of ground vibrations. A good assumption for the experiment applied here is to consider the soil as a filter through which the vibrations pass before reaching the location of interest. This assumption, however, is complicated by the fact that the soil conditions and layers are different in different site locations. Thus, the approximation here considers a simple stationary representation of the soil that was originally proposed by Kanai (1957) and Tajimi (1960), who suggested that surface ground acceleration can be approximated by the motion of a simple oscillator with a concentrated mass supported by a linear spring and a dashpot and subjected to a white noise excitation (bedrock acceleration) of spectral density S_0. Thus, the power spectral density of the absolute surface ground acceleration becomes

$$S_g(\omega) = \frac{\omega_g^4 + 4\xi_g^2\omega_g^2\omega^2}{(\omega_g^2 - \omega^2)^2 + 4\xi_g^2\omega_g^2\omega^2} S_0 \tag{6-5}$$

where ω_g and ξ_g are the natural frequency and the damping ratio of the assumed oscillator determined by the characteristics of the local ground conditions. The intensity S_0 of the excitation is determined by the strength of the excitation waves (Soong and Grigoriou, 1993). The Kanai-Tajimi model is widely used as an earthquake excitation for engineering structures because of its ability to simulate earthquake-induced ground motions in a very simple way.

To use the Kanai-Tajimi model, the three parameters, namely ω_g, ξ_g, and S_0, are estimated from representative earthquake records by means of statistical estimation procedures. Thus, an approximation based on the study of frequency content of a number of two strong ground-motion records each in the USA and Japan is considered. In the experiment here, the natural frequency of the oscillator, ω_g, is taken equivalent to 17 rad/s; the oscillator damping ratio ξ_g is taken equivalent to 0.3 (Ramallo *et al.*, 2002). Fig. 6-12 shows the frequency response of this Kanai-Tajimi filter used in the experiment.

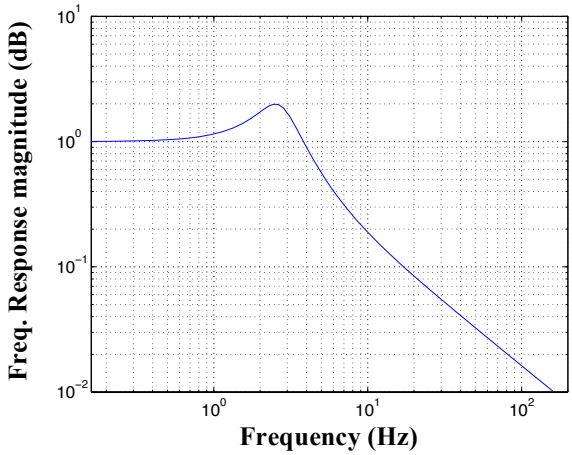

Fig. 6-12. Frequency response of the Kanai-Tajimi filter used in the experiment

6.2.5 Determination of the Transfer Function from Measurement Data and Identifying the Structure

The ILSN identification method (previously summarized in Chapter 2) used here attempts to match a parametric model of a transfer function to measured transfer function data. To apply the ILSN identification technique, the experimental transfer function needs to be obtained. Thus, based on the measurement acceleration I/O data (Bendat and Piersol, 2000), the transfer function from the ground acceleration excitation input to the absolute acceleration outputs at the first and the second stories can be evaluated. In the application here, the input $u(t)$ to the structure is the measured table (ground) accelerations data, and the measured first and second story accelerations are the outputs $y_1(t)$ and $y_2(t)$, respectively. The PSD of the acceleration input $u(t)$ is

$$S_{uu}(\omega) = U^*(\omega)U(\omega) \tag{6-6}$$

The cross-spectral density (CSD) function between the table acceleration and the measured story accelerations are

$$S_{y_1u}(\omega) = U^*(\omega)Y_1(\omega) \qquad \text{and} \qquad S_{y_2u}(\omega) = U^*(\omega)Y_2(\omega) \tag{6-7}$$

Finally, the transfer functions $H_1(\omega)$ and $H_2(\omega)$ from the ground acceleration input to the absolute accelerations of the two floors are evaluated from the ratio between the CSDs and PSD

$$H_1(\omega) = \frac{S_{y_1u}(\omega)}{S_{uu}(\omega)} \qquad \text{and} \qquad H_2(\omega) = \frac{S_{y_2u}(\omega)}{S_{uu}(\omega)} \tag{6-8}$$

Thus, having the experimental transfer functions, the ILSN technique can be used to obtain the values of the structural parameters by minimizing the residual error between the experimental and the theoretical parametric transfer functions.

6.3 Data Analysis

The main task of the experiment is to detect a small amount of damage (about 7.38% of the estimated story stiffness) located in one of the two stories of the structure. The accuracy of the identified damage is then compared between the cases when VSDDs are used in a structure and when they are not. The damage is defined as a loss in stiffness. There are two damage cases, one

where a pair of weak springs are removed from the first story (to simulate damage there), and one removing a pair of weak springs from just the second story.

6.3.1 Experimental Challenges and Solutions

The main task of the experiment is complicated by different factors. These difficulties include accuracy of modeling, nonlinearities in the experiment, the sensitivity of the accelerometers (sensor noise), and unmeasured vibrations coming from the ground under the table or from connecting cables. Moreover, the memory of the computer, used in the storage of the data, is limited. Consequently, the amount of data that can be stored is also limited. These problems add to the complexity of the identification problem.

To overcome some of these challenges, some actions were taken. For example, the experiment was performed in the basement of a building in order to minimize the ground vibrations under the table and to avoid building vibrations encountered in higher levels. Moreover, the level of excitation is kept small enough that the 2DOF structure response is linear and the weak and stiff springs in the bracings exhibit only elastic behavior. Further, the weak and stiff springs are pretensioned to nearly half their maximum elastic deflection so they are always in tension during the experiment and, thus, the bracing forces exerted by the springs never vanish. In addition, all flexible cables connected to the structure (such as those connected to the accelerometers) in the first and the second stories are banded and fixed to the structure, as shown in Fig. 6-4.

To ensure good structure modeling, the 2DOF structure is designed as a shear building where the moment of inertia of the plexi-glass plate is 327 times that of the aluminum vertical plate. Moreover, all weights and dimensions are accurately measured.

6.3.2 Data Processing

The excitation generator models of the table are designed to excite the structure for 3800 seconds continuously (the limits of memory in the laboratory computer). The stored data is divided into non-overlapping two-minute samples of data or six-minute samples of data; in both cases, ten seconds is omitted between each sample to eliminate coherence between successive samples. The data is split into a number of samples, each of which is used to generate one set of parameter estimates, in order to get a statistical distribution of the identified structure parameters. The sample duration is varied in order to observe the effect of the amount of data in each sample on the identification of the structure parameters. Each of the samples is processed in a separate identification problem for the unknown structure parameters, which are here assumed to be only the stiffness coefficients. Thus, it is assumed that the masses and damping coefficients of the two stories of the structure are known *a priori*. The masses of each of the two floors are considered equivalent to 1.125 kg. Based on the measurements recorded in Table 6-2. The logarithmic decrement method is used to obtain modal damping ratios of the 2DOF structure. The results of testing the damping ratios indicate a 1% damping in the first and second modes. In addition, the natural frequencies of the structure without adding the weak springs are measured and found to be 2.197 Hz and 6.24 Hz respectively. Consequently, the uncoupled damping coefficients for the two floors are computed to be 0.2 and 0.5 N·sec/m, respectively.

The ILSN method requires initial estimates of the unknown stiffness parameters. Using the dimensions of the aluminum vertical plates (Table 6-2) and assuming the modulus of elasticity of Aluminum to be 75 GPa, the initial estimates of the stiffnesses of the first and second stories (including the springs) are computed from Eq. (4-1) to be 657.94 N/m.

6.3.3 Damage Identification Results

The damage, within the context of this research, is defined as the loss in stiffness after damage. Thus, the mean and the standard deviation (STD) of the identified values of the first and second story stiffnesses, k_1 and k_2, respectively, are evaluated for the undamaged and damaged cases. Fig. 6-17 to Fig. 6-32 show the error in the identified first and second story stiffnesses, k_1 and k_2, relative to the assumed stiffnesses which are based on the material properties. This is done for both the undamaged and damaged cases; in both cases, a one-standard deviation ellipse is shown in the figures. The shift in the one-standard deviation ellipse, before and after damage, indicates damage quantity and location in any of the graphs. Moreover, Table 6-10 to Table 6-24 give the percentage of damage as the difference in stiffness between mean values of the identified stiffnesses, before and after damage, relative to the assumed values of the stiffnesses since it is a constant reference. In order to compare between the VSDD and conventional structure approaches, the resulting identified percentages of damage are compared to the exact ones.

6.4 Resulting Transfer Functions

To show the success of the ILSN identification technique in estimating the stiffness of the two stories of the 2DOF structure, the estimated theoretical TF of one two-minute sample and one six-minute sample data, based on the values of the identified stiffness parameters of these samples, are demonstrated here in contrast to their experimental counterparts (computed as per Section 6.2.5). This is applied for both the VSDD and conventional structure approaches, respectively. The TFs here represent a single sample case, either two-minute (Fig. 6-13 and Fig. 6-14) or six-minute (Fig. 6-15 and Fig. 6-16), for the undamaged structure when subjected to FBLWN ground excitation. The TF identification for the sample studied in this section is found to be successful for both the VSDD and the conventional structure approaches. This was not always the case for all samples when using the conventional structure approach.

6.4.1 Two-minute sample

As shown in Fig. 6-13 and Fig. 6-14, the identified theoretical TFs have done very well in tracing the experimental one for both the VSDD and the conventional structure approaches. This is the case despite the considerable noise in the experimental TFs. However, as will be shown in the coming sections, for the conventional structure approach, the identification is not always ideal.

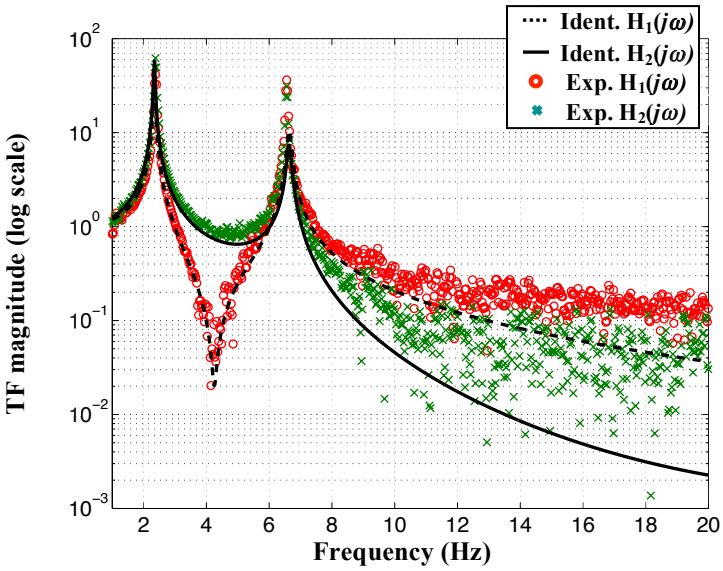

Fig. 6-13. Experimental transfer functions versus identified transfer functions of the 2DOF experimental structure without damage, using VSDDs approach, for one 2-min sample under FBLWN excitation

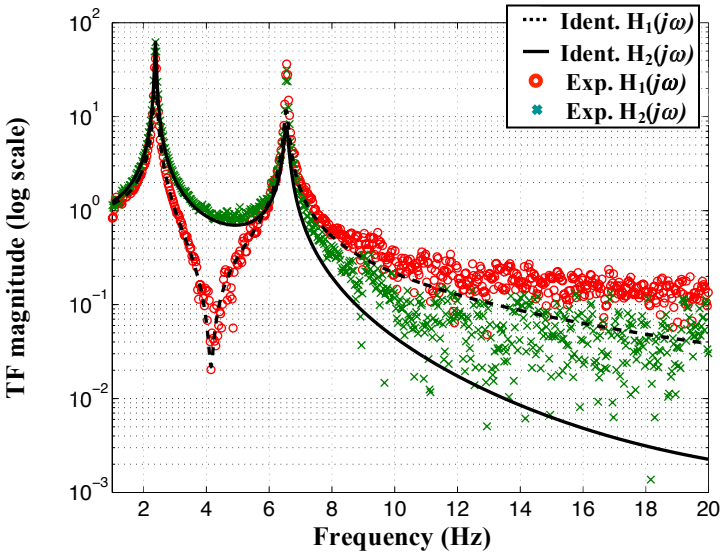

Fig. 6-14. Experimental transfer functions versus identified transfer functions of the 2DOF experimental structure without damage, using conventional structure approach, for one 2-min under FBLWN excitation

6.4.2 Six-minute sample

Similarly, the identified theoretical TFs, for the VSDD and conventional structure approaches, are successful in defining the system in one sample of the six minutes data samples as shown in Fig. 6-15 and Fig. 6-16. This is expected due to better averaging of the PSD of the inputs and the CSD functions between the inputs and the outputs for longer duration data samples. This, in turn, reduces the noise in the evaluated experimental TFs. However, this is not always the case for the conventional structure approach, as will be shown later.

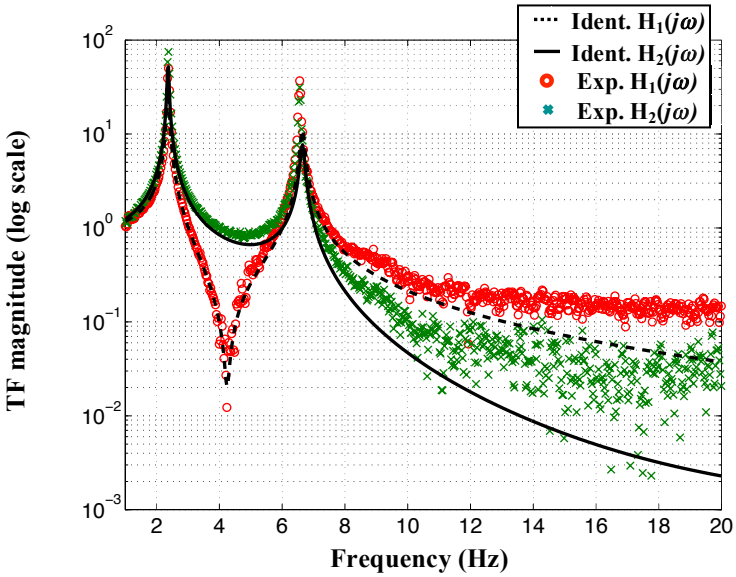

Fig. 6-15. Experimental transfer functions versus identified transfer functions of the 2DOF experimental structure without damage, using VSDDs approach, for one 6-min sample under FBLWN excitation

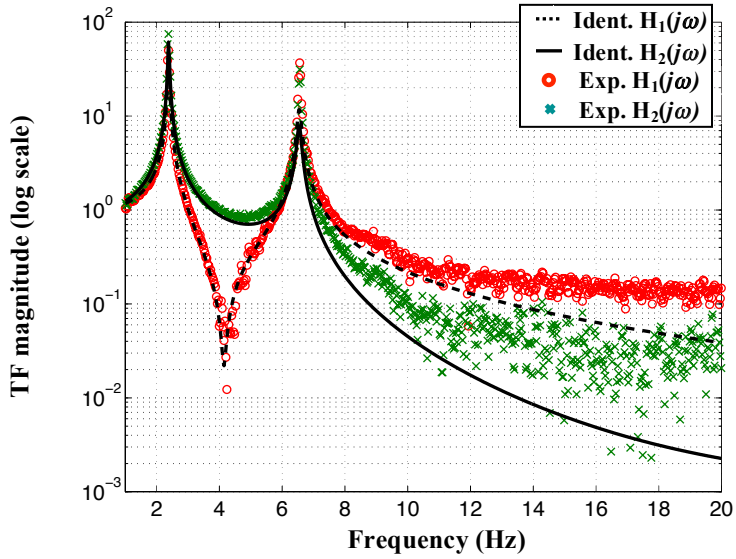

Fig. 6-16. Experimental transfer functions versus identified transfer functions of the 2DOF experimental structure without damage, using conventional structure approach, for one 6-min sample under FBLWN excitation

6.5 Damage Identification Results for BLWN Excitation

6.5.1 Two-Minute Data Samples

6.5.1.1 Damage in First Story

Fig. 6-17 and Fig. 6-18 show the results of the identification, with VSDDs and without, respectively, using two-minute samples for damage in the first story. Fig. 6-17 shows that the VSDD approach is successful in identifying the damage in the first story. In contrast, Fig. 6-18 indicates that the conventional structure approach is not successful in determining the damage; in fact, nearly half of the samples give quite inaccurate estimates for the undamaged stiffnesses. This, consequently, leads to a huge bias in the mean estimates of stiffnesses, and large variations, as shown in. In addition, one estimate after damage, using the conventional structure approach, gives a dramatically different result, exaggerating the variance. Table 6-10 shows that the damage is well estimated with relatively low variation using the VSDD approach whereas, in the conventional structure approach, the damage location is incorrect and the severity is exaggerated.

Table 6-9. Mean and COV† Estimates of the Identified Stiffnesses of the 2DOF Structure for Case of Damage in 1st Story (BLWN, 2 min)

	VSDDs Approach				Conventional Structure Approach			
	Before Damage		After Damage		Before Damage		After Damage	
	Mean (N/m)	COV (%)	Mean (N/m)	COV (%)	Mean (N/m)	COV (%)	Mean (N/m)	COV (%)
k_1	609.380	1.959	562.009	1.992	636.816	4.475	697.215	23.672
k_2	801.629	0.336	801.958	0.441	756.166	6.960	621.486	30.045

Table 6-10. Mean and STD Estimates of the Identified Damage for 2DOF Structure, Relative to Assumed Stiffnesses, in Case of Damage in 1st Story Only (BLWN, 2 min)

	Damage Location	Actual % of Damage	Relative Identified Damage	
			Mean(%)	STD(%)
VSDD App.	1st	7.36	7.20	2.49
	2nd	0	0.05	0.68
Conventional Structure App.	1st	7.36	-9.18	25.46
	2nd	0	20.47	29.49

† COV = Coefficient of Variation

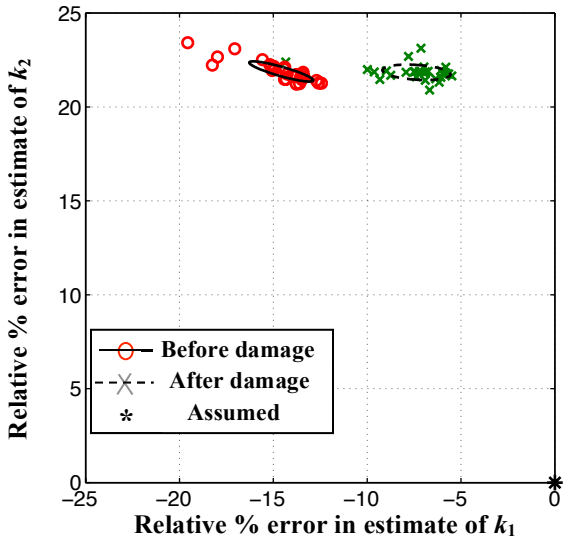

Fig. 6-17. Relative errors in identified stiffnesses of 2DOF structure to assumed ones, before and after damage in first story, (BLWN, 2-min samples, VSDDs approach)

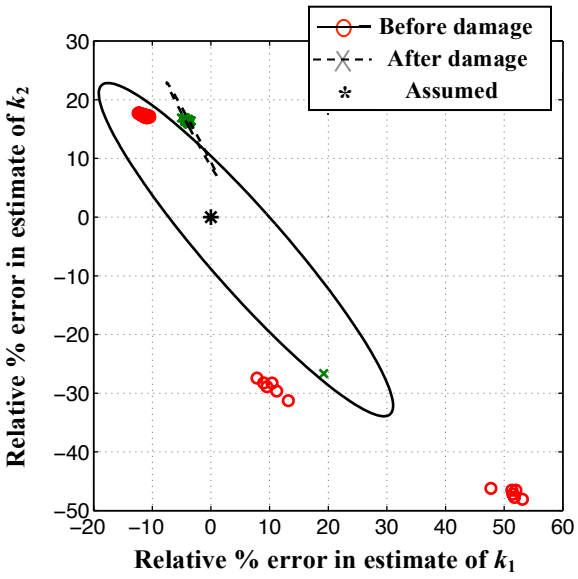

Fig. 6-18. Relative errors in identified stiffnesses of 2DOF structure to assumed ones, before and after damage in 1st story, (BLWN, 2-min samples, Conventional Structure approach)

6.5.1.2 Damage in Second Story

The damage in the second story is usually well identified for both the VSDD and the conventional structure approaches as demonstrated in Fig. 6-19 and Fig. 6-20. However, using the conventional structure approach, very inaccurate stiffness estimates occurred in one sample for the undamaged structure case, causing large variance as shown in Table 6-11. This, in turn, affects the credibility of the identified damage severity for the conventional structure approach. This is represented in Table 6-12 in terms of large standard deviation, bigger than the identified damage, leading to doubts about the results. In contrast, the VSDD approach supplied a good identification of damage in the second story with very small variation. Moreover, the indication of stiffening in the first story, identified after damage in both approaches, by the negative damage mean is suspect since the magnitude of stiffening is smaller than the standard deviation.

Table 6-11. Mean and COV Estimates of the Identified Stiffnesses of the 2DOF Structure for Case of Damage in 2nd Story (BLWN, 2 min)

	VSDDs Approach				Conventional Structure Approach			
	Before Damage		After Damage		Before Damage		After Damage	
	Mean (N/m)	COV (%)	Mean (N/m)	COV (%)	Mean (N/m)	COV (%)	Mean (N/m)	COV (%)
k_1	609.380	1.959	615.433	1.414	636.816	4.475	641.553	0.704
k_2	801.629	0.336	754.192	0.690	756.166	6.960	708.729	0.418

Table 6-12. Mean and STD Estimates of the Identified Damage for 2DOF Structure, Relative to Assumed Stiffnesses, in Case of Damage in 2nd Story Only (BLWN, 2 min)

	Damage Location	Actual % of Damage	Relative Identified Damage	
			Mean(%)	STD(%)
VSDD App.	1st	0	-0.92	2.25
	2nd	7.39	7.21	0.89
Conventional Structure App.	1st	0	-0.72	4.39
	2nd	7.39	7.21	8.01

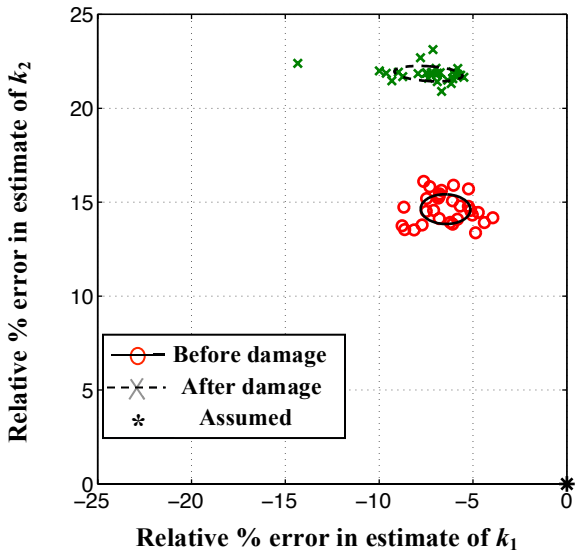

Fig. 6-19. Relative errors in identified stiffnesses of 2DOF structure to assumed ones, before and after damage in 2nd story, (BLWN, 2-min samples, VSDDs approach)

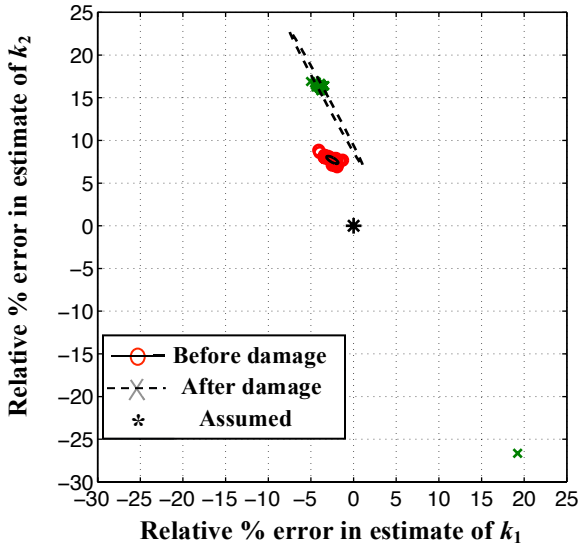

Fig. 6-20. Relative errors in identified stiffnesses of 2DOF structure to assumed ones, before and after damage in 2nd story, (BLWN, 2-min samples, Conventional Structure approach)

6.5.2 Six-Minute Data Samples

6.5.2.1 Damage in First Story

Both approaches, VSDD (Fig. 6-21) and conventional structure (Fig. 6-22), did extremely well in identifying the damage using six-minute samples when the damage is in the first story. This shows that a longer sample duration improved the results of both approaches, particularly for the conventional structure approach. However, the VSDD approach still give better means. The VSDD approach estimates the damage at 7.38% — very close to the exact of 7.36% — whereas the conventional structure approach gives 7.43%. In Table 6-14, the extra 0.97% stiffness estimated in the second story for the conventional structure approach case may be considered significant compared to the 0.29% standard deviation, in contrast with an insignificant 0.19% extra stiffness with a 0.36% standard deviation when using VSDDs.

Table 6-13. Mean and COV Estimates of the Identified Stiffnesses of the 2DOF Structure for Case of Damage in 1st Story (BLWN, 6 min)

	VSDDs Approach				Conventional Structure Approach			
	Before Damage		After Damage		Before Damage		After Damage	
	Mean (N/m)	COV (%)	Mean (N/m)	COV (%)	Mean (N/m)	COV (%)	Mean (N/m)	COV (%)
k_1	613.328	0.895	564.772	1.009	632.408	0.165	583.523	0.562
k_2	800.642	0.157	801.892	0.248	765.509	0.117	771.891	0.222

Table 6-14. Mean and STD Estimates of the Identified Damage for 2DOF Structure, Relative to Assumed Stiffnesses, in Case of Damage in 1st Story Only (BLWN, 6 min)

	Damage Location	Actual % of Damage	Relative Identified Damage	
			Mean(%)	STD(%)
VSDD App.	1st	7.36	7.38	1.20
	2nd	0	-0.19	0.36
Conventional Structure App.	1st	7.36	7.43	0.52
	2nd	0	-0.97	0.29

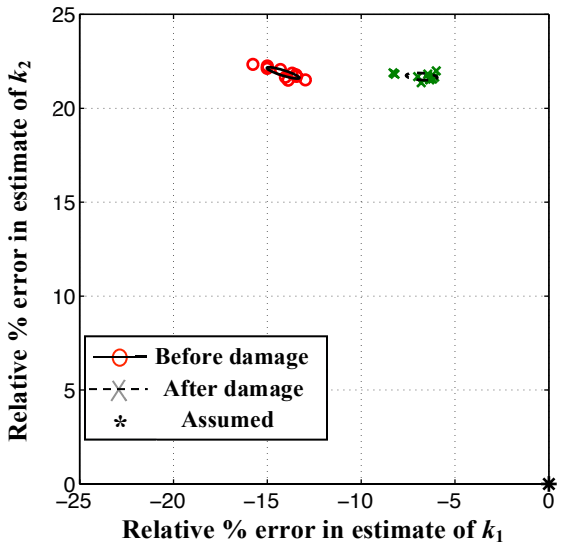

Fig. 6-21. Relative errors in identified stiffnesses of 2DOF structure to assumed ones, before and after damage in 1st story, (BLWN, 6-min samples, VSDDs approach)

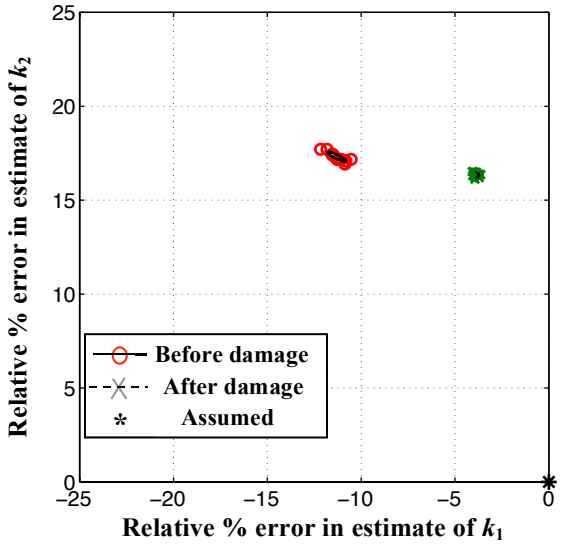

Fig. 6-22. Relative errors in identified stiffnesses of 2DOF structure to assumed ones, before and after damage in 1st story, (BLWN, 6-min samples, Conventional Structure approach)

6.5.2.2 Damage in Second Story

With damage in the second story and using six-minute samples, the VSDD and the conventional structure approaches did well as shown in Fig. 6-23 and Fig. 6-24, but the VSDD approach is clearly superior. With the conventional structure approach, despite very low variations in stiffness estimates as shown in Table 6-15, the first story appears to have stiffened by 1.56% and the damage in the second story has been overestimated, as shown in Table 6-16. The very low standard deviation in the conventional structure approach suggests it may be more accurate, but that is clearly misleading.

Table 6-15. Mean and COV Estimates of the Identified Stiffnesses of the 2DOF Structure for Case of Damage in 2nd Story (BLWN, 6 Min)

	VSDDs Approach				Conventional Structure Approach			
	Before Damage		After Damage		Before Damage		After Damage	
	Mean (N/m)	COV (%)	Mean (N/m)	COV (%)	Mean (N/m)	COV (%)	Mean (N/m)	COV (%)
k_1	613.328	0.895	616.881	0.729	632.408	0.165	642.672	0.282
k_2	800.642	0.157	753.666	0.370	765.509	0.117	708.597	0.180

Table 6-16. Mean and STD Estimates of the Identified Damage for 2DOF Structure, Relative to Assumed Stiffnesses, in Case of Damage in 2nd Story Only (BLWN, 6 min)

	Damage Location	Actual % of Damage	Relative Identified Damage	
			Mean(%)	STD(%)
VSDD App.	1st	0	-0.54	1.08
	2nd	7.39	7.14	0.46
Conventional Structure App.	1st	0	-1.56	0.32
	2nd	7.39	8.65	0.24

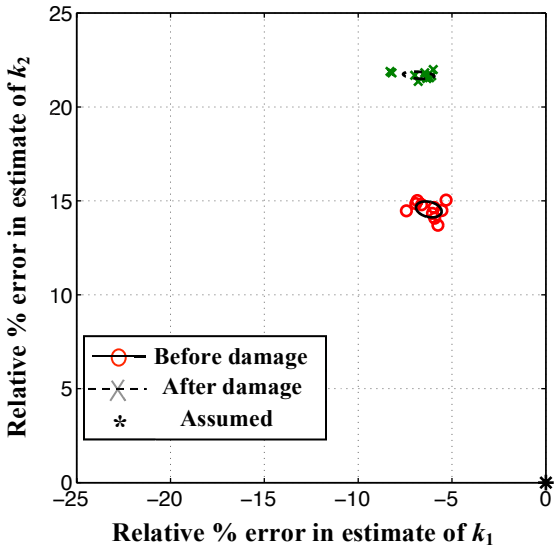

Fig. 6-23. Relative errors in identified stiffnesses of 2DOF structure to assumed ones, before and after damage in 2nd story, (BLWN, 6-min samples, VSDDs approach)

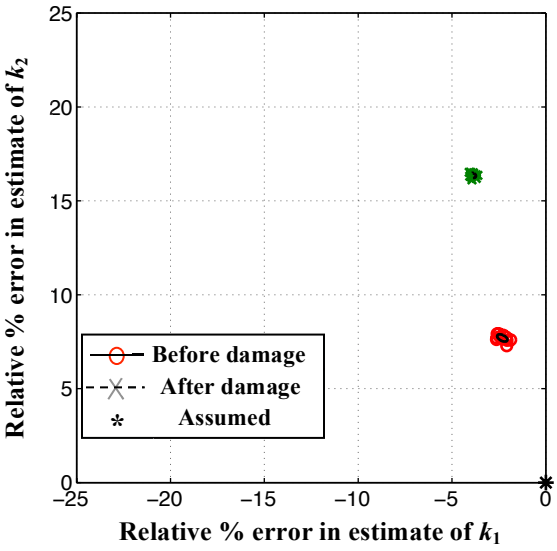

Fig. 6-24. Relative errors in identified stiffnesses of 2DOF structure to assumed ones, before and after damage in 2nd story, (BLWN, 6-min samples, Conventional Structure approach)

6.6 Damage Identification Results for FBLWN Excitation

6.6.1 Two-Minute Data Samples

6.6.1.1 Damage in First Story

Similar to the case of BLWN ground excitation with two-minute samples, the VSDD approach is found, with FBLWN excitation, to be able to identify the damage accurately in the first story whereas the conventional structure approach fails, as is clear from Fig. 6-25 and Fig. 6-26. Table 6-17 also shows that the damage deviations are very large for the conventional structure approach. In addition, from Table 6-18, it can be observed that the damage location is swapped and estimated to be severe in the second story when no damage has actually occurred there.

Table 6-17. Mean and COV Estimates of the Identified Stiffnesses of the 2DOF Structure for Case of Damage in 1st Story (FBLWN, 2 Min)

	VSDDs Approach				Conventional Structure Approach			
	Before Damage		After Damage		Before Damage		After Damage	
	Mean (N/m)	COV (%)	Mean (N/m)	COV (%)	Mean (N/m)	COV (%)	Mean (N/m)	COV (%)
k_1	606.222	1.542	559.180	1.884	629.776	0.481	687.148	17.415
k_2	802.485	0.300	803.340	0.369	764.061	0.264	582.010	28.620

Table 6-18. Mean and STD Estimates of the Identified Damage for 2DOF Structure, Relative to Assumed Stiffnesses, in Case of Damage in 1st Story Only (FBLWN, 2 min)

	Damage Location	Actual % of Damage	Relative Identified Damage	
			Mean(%)	STD(%)
VSDD App.	1st	7.36	7.15	2.14
	2nd	0	-0.13	0.58
Conventional Structure App.	1st	7.36	-8.72	18.19
	2nd	0	27.67	25.32

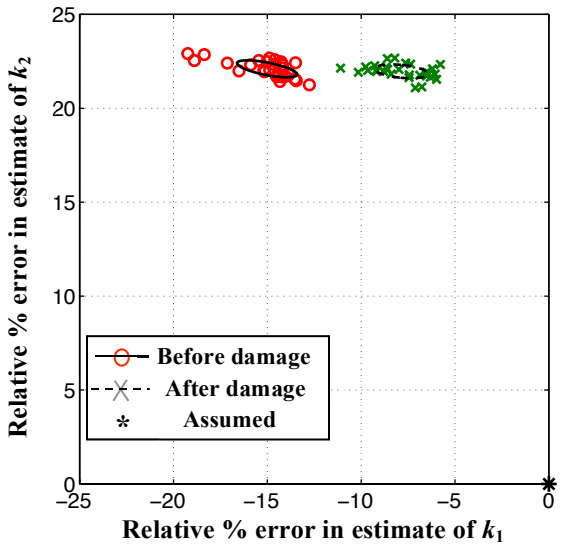

Fig. 6-25. Relative errors in identified stiffnesses of 2DOF structure to assumed ones, before and after damage in 1st story, (FBLWN, 2-min samples, VSDDs approach)

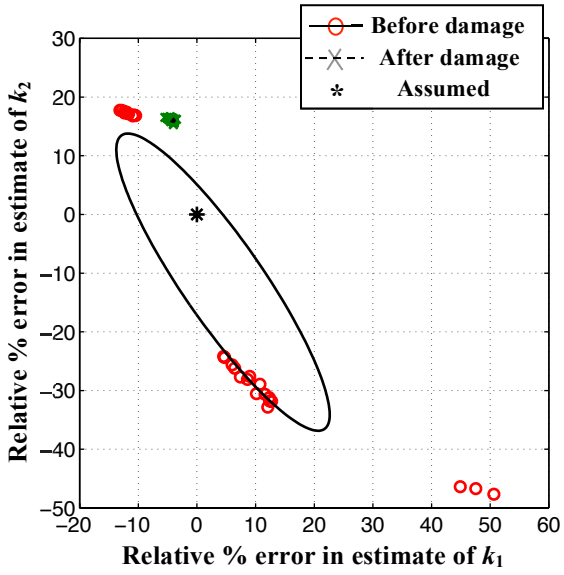

Fig. 6-26. Relative errors in identified stiffnesses of 2DOF structure to assumed ones, before and after damage in 1st story, (FBLWN, 2-min samples, Conventional Structure approach)

6.6.1.2 Damage in Second Story

With damage in the second story, both approaches, the VSDD and the conventional structure, did well also, as shown in Fig. 6-27 and Fig. 6-28. However, the conventional structure approach overestimated the damage in the second story and indicates significant stiffening in the first story, as shown in Table 6-20. However, these are accompanied by very small deviations, which falsely gives credibility to these results and is misleading. On the contrary, the VSDD approach gives a very good estimate of damage in the second story. While the VSDD approach estimates some extra stiffness in the first story, it is less than the deviation, which indicates that this extra stiffness is probably spurious.

Table 6-19. Mean and COV Estimates of the Identified Stiffnesses of the 2DOF Structure for Case of Damage in 2nd Story (FBLWN, 2 min)

	VSDDs Approach				Conventional Structure Approach			
	Before Damage		After Damage		Before Damage		After Damage	
	Mean (N/m)	COV (%)	Mean (N/m)	COV (%)	Mean (N/m)	COV (%)	Mean (N/m)	COV (%)
k_1	606.222	1.542	613.131	1.033	629.776	0.481	638.527	0.658
k_2	802.485	0.300	754.455	0.579	764.061	0.264	708.860	0.435

Table 6-20. Mean and STD Estimates of the Identified Damage for 2DOF Structure, Relative to Assumed Stiffnesses, in Case of Damage in 2nd Story Only (FBLWN, 2 min)

	Damage Location	Actual % of Damage	Relative Identified Damage	
			Mean(%)	STD(%)
VSDD App.	1st	0	-1.05	1.72
	2nd	7.39	7.30	0.76
Conventional Structure App.	1st	0	-1.33	0.79
	2nd	7.39	8.39	0.56

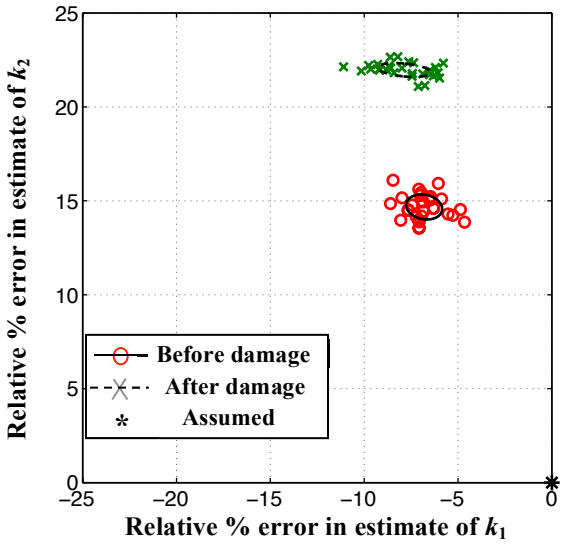

Fig. 6-27. Relative errors in identified stiffnesses of 2DOF structure to assumed ones, before and after damage in 2nd story, (FBLWN, 2-min samples, VSDDs approach)

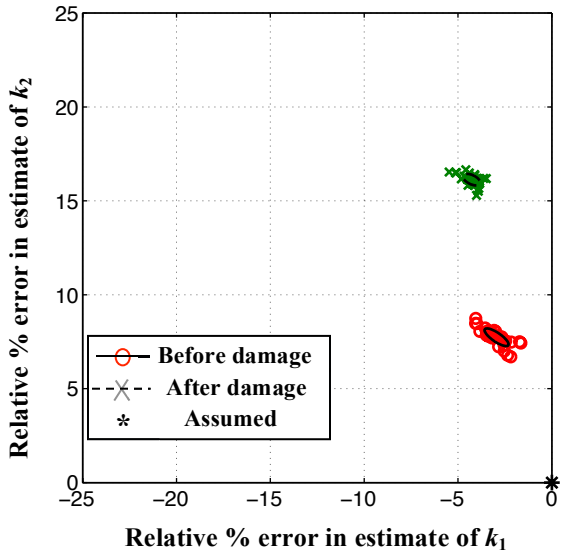

Fig. 6-28. Relative errors in identified stiffnesses of 2DOF structure to assumed ones, before and after damage in 2nd story, (FBLWN, 2-min samples, Conventional Structure approach)

6.6.2 Six-Minute data samples

6.6.2.1 Damage in First Story

Despite the advantage of having the longer duration six-minute samples, the conventional structure approach performs poorly here for damage in the first story with FBLWN excitation. As seen in Fig. 6-30, many of the samples are vastly inaccurate for the undamaged case. The VSDD approach, on the other hand, is able to identify damage quite well and with very small deviations. Table 6-21 and Table 6-22 show that the conventional structure approach gives heavily biased estimates together with large deviation, in contrast with the VSDD approach which gives very good estimates with small deviations.

Table 6-21. Mean and COV Estimates of the Identified Stiffnesses of the 2DOF Structure for Case of Damage in 1st Story (FBLWN, 6 min)

	VSDDs Approach				Conventional Structure Approach			
	Before Damage		After Damage		Before Damage		After Damage	
	Mean (N/m)	COV (%)	Mean (N/m)	COV (%)	Mean (N/m)	COV (%)	Mean (N/m)	COV (%)
k_1	608.854	1.013	562.272	0.940	630.632	0.193	645.830	10.809
k_2	801.958	0.156	803.143	0.249	763.864	0.132	623.723	25.013

Table 6-22. Mean and STD Estimates of the Identified Damage for 2DOF Structure, Relative to Assumed Stiffnesses, in Case of Damage in 1st Story Only (FBLWN, 6 min)

	Damage Location	Actual % of Damage	Relative Identified Damage	
			Mean(%)	STD(%)
VSDD App.	1st	7.36	7.08	1.23
	2nd	0	-0.18	0.36
Conventional Structure App.	1st	7.36	-2.31	10.61
	2nd	0	21.30	23.71

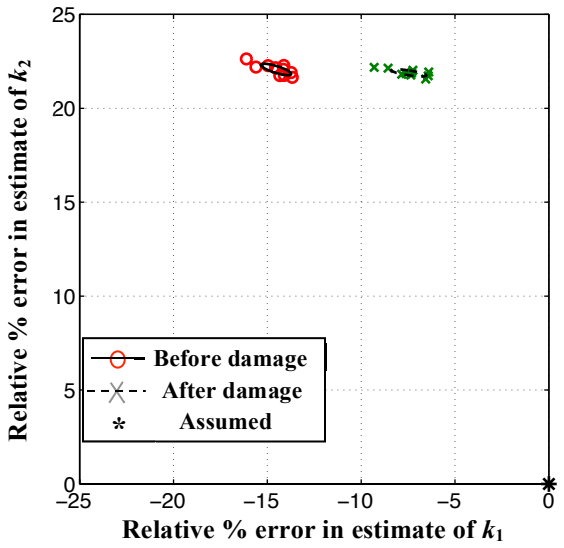

Fig. 6-29. Relative errors in identified stiffnesses of 2DOF structure to assumed ones, before and after damage in 1st story, (FBLWN, 6-min samples, VSDDs approach)

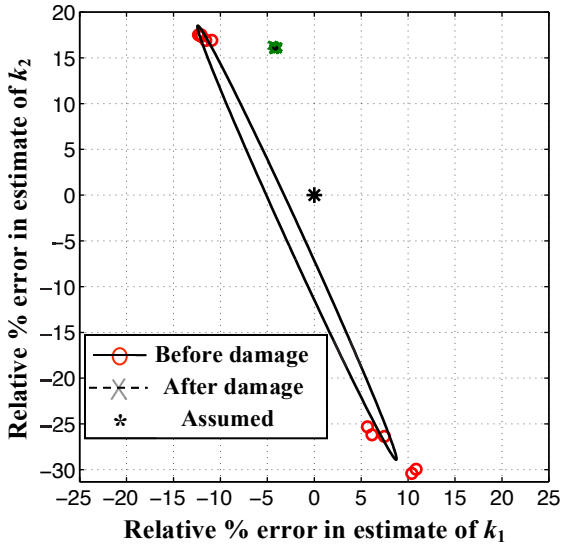

Fig. 6-30. Relative errors in identified stiffnesses of 2DOF structure to assumed ones, before and after damage in 1st story, (FBLWN, 6-min samples, Conventional Structure approach)

6.6.2.2 *Damage in Second Story*

Fig. 6-31 and Fig. 6-32 indicate that both the VSDD and the conventional structure approaches did well in identifying the damage in the second story for six-minute samples with FBLWN excitation. However, the conventional structure approach overestimated the damage in the second story, and gave statistically significant stiffening in the first story, as shown in Table 6-24. This is, again, accompanied with very small variations in stiffness and damage estimates, which is misleading about the credibility of such results. In the meantime, the VSDD approach is successful in estimating the damage more accurately.

Table 6-23. Mean and COV Estimates of the Identified Stiffnesses of the 2DOF Structure for Case of Damage in 2nd Story (FBLWN, 6 min)

	VSDDs Approach				Conventional Structure Approach			
	Before Damage		After Damage		Before Damage		After Damage	
	Mean (N/m)	COV (%)	Mean (N/m)	COV (%)	Mean (N/m)	COV (%)	Mean (N/m)	COV (%)
k_1	608.854	1.013	614.052	0.417	630.632	0.193	638.790	0.286
k_2	801.958	0.156	753.929	0.322	763.864	0.132	709.058	0.168

Table 6-24. Mean and STD Estimates of the Identified Damage for 2DOF Structure, Relative to Assumed Stiffnesses, in Case of Damage in 2nd Story Only (FBLWN, 6 min)

	Damage Location	Actual % of Damage	Relative Identified Damage	
			Mean(%)	STD(%)
VSDD App.	1st	0	-0.79	1.02
	2nd	7.39	7.30	0.42
Conventional Structure App.	1st	0	-1.24	0.33
	2nd	7.39	8.33	0.24

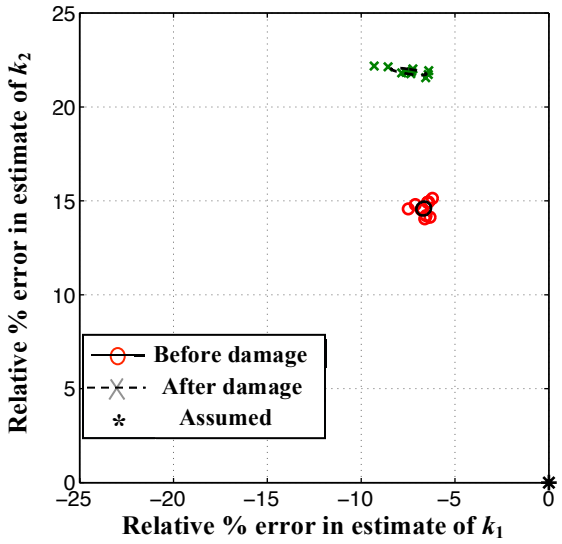

Fig. 6-31. Relative errors in identified stiffnesses of 2DOF structure to assumed ones, before and after damage in 2nd story, (FBLWN, 6-min samples, VSDDs approach)

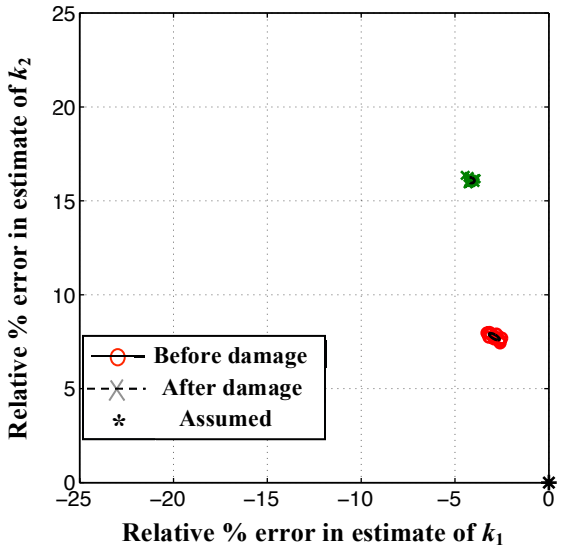

Fig. 6-32. Relative errors in identified stiffnesses of 2DOF structure to assumed ones, before and after damage in 2nd story, (FBLWN, 6-min samples, Conventional Structure approach)

6.7 Overview of results and comments

Comparing the identified stiffness results obtained using the VSDD and the conventional structure approaches, it can be observed that the VSDD approach performed significantly better. This is particularly demonstrated with shorter duration data samples. With two-minute data samples, the VSDD approach is found to be successful in identifying the damage accurately, whether damage exists in either the first or the second story. The identified damage is accompanied with small deviations giving credibility to the results. Meanwhile, for the same case of two-minute data samples, the conventional structure is found to be unsuccessful in identifying damage in the first story. While damage identification is more successful when the damage is in the second story, the conventional structure approach often overestimates the damage and assigns statistically significant extra stiffness to undamaged stories.

With longer duration data samples (six-minute), the VSDD approach gives even better damage means with much smaller variations. For the conventional structure approach, the identified results are improved in some cases compared to the two-minute samples, but often with biased mean damage estimates represented by overestimating damage.

Based on these observations, one can conclude that using the VSDD approach helps overcome the noise in the data more efficiently than the conventional structure approach. This result confirms experimentally the conclusions in the analytical part of this research comparing the two approaches.

7 CONCLUSIONS AND RECOMMENDATIONS

The research introduced in this report studies the improvements in the health monitoring of structures that are available by using semiactive variable stiffness and damping devices (VSDDs). The work here demonstrates the effectiveness of using VSDDs to improve the estimates of structural parameters for SHM and damage detection.

In general, the research herein is divided into two major parts. The first part focuses on the improvements in the identification of the structural parameters when using frequency domain identification techniques. The Iterative Least Squares Numerator (ILSN) method is summarized. This method approximates the more complicated conventional error in the transfer function and, finally, minimizes this error to give fairly accurate estimates through least squares optimization. It is shown that, using the ILSN technique in identification of parameters, the variable stiffness and damping induced by the semiactive device in the structure helps reduce the variation of the estimates of the structural parameters. This was shown in METRANS 01-10 (Johnson and Elmasry, 2003) to be the case when using relatively small additional stiffnesses (a fraction of the corresponding stories stiffnesses) induced by the semiactive devices. However, when using larger induced stiffnesses and damping coefficients than those of the corresponding stories, the means of the structural parameter estimates are more effectively improved and their variations are found to be substantially reduced. The test beds in the research herein are a 2DOF bridge model and two-story and six-story shear building models.

Moreover, the first part introduces another newly modified technique, INVFLS, which identifies the coefficients of the numerator and denominator polynomials of the transfer function and uses the resulting values in identifying the stiffnesses and the damping coefficients of the structure. The resulting identified parameters from applying this technique consistently confirm the improvements obtained in the identification process of the structural parameters in terms of reduced variations when using VSDDs. However, the results are not as impressive as those obtained from the ILSN technique. In addition, the improvements in the identification of the structural parameters are studied in the context of the Eigensystem Realization Algorithm (ERA). The ERA is applied with and without the semiactive devices. The results indicate that the root mean square error in the identified parameters is clearly reduced by using semiactive devices in the structure.

The second part of this report studies the effect of using variable stiffnesses in an experimental structure for improving identified structural parameters. A 2DOF shear building structure, composed of horizontal plexi-glass plates, vertical aluminum plates and two pairs of soft springs as bracings, is used in the lab experiment. Stiff springs are used in pairs to replicate the effect of VSDDs in the structure. The structure is excited through a small-scale shaking table in the SHM and Control Lab at the University of Southern California. The excitation takes two forms: a band limited white noise and a filtered band limited white noise. The absolute accelerations of the shake table and the first and second stories of the experimental structure are measured using one accelerometer fixed to each of the three levels. It is assumed that the masses and the damping coefficients are known *a priori*. Damage is incurred in the structure by removing a pair of the weak springs. The resulting estimates of the reduction in the story stiffness due to damage in the structure indicate more accuracy in the mean estimates when using four different configurations of additional stiffnesses (replicating the effect of VSDDs) compared to the case of the conventional structure. In addition, using the conventional structure approach shows more sensitivity to noise such that the variation in the identified parameters is sometimes

much larger than using the VSDD approach. In general, the results of the experimental work are consistent with the results from the analytical work since they indicate better mean estimates and sometimes considerably less variations when VSDDs are used in the structure.

Future research studying the improvements in identification of structural parameters, using VSDD approach, should study realtime controlled monitoring application in the context of time-domain techniques such as linear black box models (ARMA, ARMAX models, etc.). The 2DOF bridge model can be a good start for such an application. A quadratic cost function, that includes the error in the estimated system parameters and the force exerted by the actuator, can be used. Further, data from real structures should also be considered, if available. Also, more complicated structures should be examined, in order to generalize the VSDD approach.

Further, some new approaches for using VSDDs to change structural behavior have been recently developed by the PI. This approach uses a substructure identification approach (Zhang and Johnson, 2006a), that has an accompanying error approximation, to identify the structural parameters. Further, the approach is directly applicable for using control devices such as VSDDs to exploit the source of error, directed by the error approximation, to change the structural behavior to dramatically improve the accuracy of structural parameter identification (Zhang and Johnson, 2006b).

APPENDIX

This appendix shows the testing reports, by the supplier, of the springs used in the laboratory experiments.

Weak Steel Springs Report (spring #80039)

Century Spring
212 E. 16 USA

Larson Systems Inc. Tester

Model : Super DHT
Version Number : 2.54
Load Cell : 110.000 lb
Date : 06/11/04
Time : 02:25:09 pm
Operator : _____

Two Point with Rate Mode

Test Number	Tp 1 Length (in)	Tp 1 Force (lb)	Tp 2 Length (in)	Tp 2 Force (lb)	Rate (lb/in)
1	3.0000	-0.152	3.9995	-0.620	0.468
2	3.0000	-0.156	3.9995	-0.632	0.476
3	3.0000	-0.190	3.9995	-0.672	0.482
4	3.0000	-0.190	3.9995	-0.660	0.470

END OF DATA

SUMMARY DATA

Test Number	Tp 1 Length (in)	Tp 1 Force (lb)	Tp 2 Length (in)	Tp 2 Force (lb)	Rate (lb/in)
Mean	3.00000	-0.1720	3.99950	-0.6460	0.4740
Std Dev	0.00000	0.0208	0.00000	0.0241	0.0063
Maximum	3.0000	-0.152	3.9995	-0.620	0.482
Minimum	3.0000	-0.190	3.9995	-0.672	0.468
Range	0.0000	0.038	0.0000	0.052	0.014

END OF SUMMARY

Stiff Steel Springs Report (spring #80222)

Century Spring
212 E. 16 USA

Larson Systems Inc. Tester

Model : Super DHT
Version Number : 2.54
Load Cell : 110.000 lb
Date : 06/02/04
Time : 08:43:23 am
Operator :_____

Two Point with Rate Mode

Test Number	Tp 1 Length (in)	Tp 1 Force (lb)	Tp 2 Length (in)	Tp 2 Force (lb)	Rate (lb/in)
1	3.5000	-5.224	3.9995	-8.042	5.642
2	3.5000	-4.980	3.9995	-7.756	5.558
3	3.5000	0.002	3.5000	0.002	0.000
4	3.5000	0.002	3.5000	0.002	0.000
5	3.5000	0.000	3.5000	0.000	0.000
6	3.5000	-4.670	3.9995	-7.412	5.489
7	3.5000	-5.012	3.9995	-7.798	5.578
8	3.5000	-4.972	3.9995	-7.796	5.654
9	3.5000	-4.982	3.9995	-7.744	5.530
10	3.5000	0.004	3.5000	0.004	0.000
11	3.5000	-5.036	3.9995	-7.866	5.666
12	3.5000	-5.066	3.9995	-7.860	5.594
13	3.5000	-5.006	3.9995	-7.800	5.594
14	3.5000	-5.016	3.9995	-7.768	5.510
15	3.5000	-5.112	3.9995	-7.856	5.493
16	3.5000	-5.130	3.9995	-7.886	5.518

END OF DATA

SUMMARY DATA

Test Number	Tp 1 Length (in)	Tp 1 Force (lb)	Tp 2 Length (in)	Tp 2 Force (lb)	Rate (lb/in)
Mean	3.50000	-3.7623	3.87463	-5.8485	4.1766
Std Dev	0.00000	2.2475	0.22338	3.4908	2.4910
Maximum	3.5000	0.004	3.9995	0.004	5.666
Minimum	3.5000	-5.224	3.5000	-8.042	0.000
Range	0.0000	5.228	0.4995	8.046	5.666

END OF SUMMARY

Tests 1–2, 6–9, and 11–16 correspond to spring samples 1–2, 3–6, and 7–12 in Table 4-8.

REFERENCES

Ang, A.H-S., and W.H. Tang (1975). Probability Concepts in Engineering Planning and Design, Basic Principles, Vol. I. Wiley, NY.

Arizona Dept. of Transportation (ADOT) (2001). "Superstition Freeway," web page http://www.superstitionfreeway.com/

Au, S.K., K.V. Yuen and J.L. Beck (2000). "Two-Stage System Identification Results for Benchmark Structure." Proceedings of the 14th ASCE Engineering Mechanics Conference, Austin, Texas, 21–24 May 2000.

Battaini, G. Y., G. Yang and B.F. Spencer, Jr., (2000). "Bench-Scale Experiment for Structural Control." *Journal of Engineering Mechanics*, **126**(2), 140–148.

Beck, J.L. (1978). Determining Models of Structures from Earthquake Records. Report EERL78-01, California Institute of Technology.

Beck, J.L. (1990). "Statistical System Identification of Structures." In A.H-S. Ang, M. Shinozuka and G.I. Schuëller (eds.), *Structural Safety and Reliability* (ASCE, New York)**,** 1395–1402.

Beck, J.L., B.S. May and D.C. Polidori (1994a). "Determination of Modal Parameters from Ambient Vibration Data for Structural Health Monitoring." *First World Conference on Structural Control*, Los Angeles, California, 3–5 August 1994.

Beck, J.L., M.W. Vanik and L.S. Katafygiotis (1994b). "Determination of Stiffness Changes from Modal Parameter Changes for Structural Health Monitoring." *First World Conference on Structural Control*, Los Angeles, California, 3–5 August 1994.

Beck, J.L., S. Au and M.W. Vanik (2001). "Monitoring Structural Health using a Probabilistic Measure." *Computer-Aided Civil and Infrastructure Engineering*, **16**, 1–11.

Béliveau, J.G., and S. Chater (1984). "System Identification of Structures from Ambient Wind Measurements." *Proceedings of the Eighth World Conference on Earthquake Engineering*, Prentice-Hall, Inc., Englewood Cliffs, New Jersey, 1984, **IV,** 307–314.

Bendat, J.S., and A.G. Piersol (2000). *Random Data: Analysis and Measurement Procedures*. Wiley, NY.

Bernal, D., and B. Gunes (2000). "Observer/Kalman and Subspace Identification of the UBC Benchmark Structural Model." *Proceedings of the 14th ASCE Engineering Mechanics Conference*, Austin, Texas, 21–24 May 2000.

Bernal, D., and B. Gunes (2004). "Flexibility Based Approach for Damage Characterization: Benchmark Application." *Journal of Engineering Mechanics*, ASCE, **130**(1), 61–70.

Bodeux, J.B., and J.C. Golinval (2001). "Application of ARMAV Models to the Identification and Damage Detection of Mechanical and Civil Engineering Structures." *Smart Materials and Structures*, **10**, 479–489.

Brincker, R., L. Zhang and P. Anderson (2001). "Modal Identification of Output-Only Systems using Frequency Domain Decomposition." *Smart Materials and Structures*, **10**, 441–445.

Brownjohn, J.M.W. (2003). "Ambient Vibration Studies for System Identification of Tall Buildings." *Earthquake Engineering and Structural Dynamics*, **32,** 71–95.

Caicedo, J.M., S.J. Dyke and E.A. Johnson (2004). "Natural Excitation Technique and Eigensystem Realization Algorithm for Phase I of the IASC-ASCE Benchmark Problem: Simulated Data." *Journal of Engineering Mechanics*, ASCE, **130**(1), 49–60.

Capecchi, D., and F. Vestroni (1999). "Monitoring of Structural Systems by Using Frequency Data." *Earthquake Engineering and Structural Dynamics*, **28**, 447–461.

Chang, F.-K. (1999). Structural Health Monitoring 2000. Proceedings of the 2nd International Workshop on Structural Health Monitoring, Stanford University, 8–10 September 1999, Technomic Publishing Co., Lancaster, PA.

Chen, C.-T. (1999). *Linear System Theory and Design, 3rd Edition*. Oxford University Press, New York.

Chopra, A.K. (1995). Dynamics of Structures, Theory and Applications to Earthquake Engineering. Prentice Hall, Englewood Cliffs, New Jersey.

Christenson, R.E., B.F. Spencer, Jr., N. Hori and K. Seto (2001). "Coupled Building Control Using Acceleration Feedback." *Computer-Aided Civil and Infrastructure Engineering*, accepted, **18**, 3–17, 2003.

Corbin, M., A. Hera and Z. Hou (2000). "Locating Damage Regions Using Wavelet Approach." *Proceedings of the 14th ASCE Engineering Mechanics Conference*, Austin, Texas, 21–24 May 2000.

Doebling, S.W., C.R. Farrar and M.B. Prime (1998). "A Summary Review of Vibration-Based Damage Identification Methods." *The Shock and Vibration Digest*, **30**(2), 91–105.

Doebling, S.W., C.R. Farrar, M.B. Prime and D.W. Shevitz (1996). "Damage Identification and Health of Structural and Mechanical Systems from Changes in their Vibration Characteristics: A Literature Monitoring Review." Los Alamos National Laboratory Report, LA-13070-MS, Los Alamos, New Mexico.

Dyke, S.J., B.F. Spencer, Jr., M.K. Sain and J.D. Carlson (1996a). "Modeling and Control of Magnetorheological Dampers for Seismic Response Reduction." *Smart Materials and Structures*, **5**, 567–575.

Dyke, S.J., B.F. Spencer, Jr., P. Quast, D.C. Kaspari, Jr., and M.K. Sain (1996b). "Implementation of an Active Mass Driver using Acceleration Feedback Control." *Microcomputers in Civil Engineering: special issue on active and hybrid structural control*, **11**, 304–323.

East Bay Business Times (EBBT) (2002). State Budget Deficit Could Hit $20 billion." http://eastbay.bizjournals.com/eastbay/stories/2002/04/01/daily48.html, Web page, 3 April 2002.

Ehrgott, R.C., and S.F. Masri (1992). "Modeling the Oscillatory Dynamic Behavior of Electrorheological Materials in Shear." *Smart Materials and Structures*, **1**(4)**,** 275–285.

Elmasry, M.I.S., and E.A. Johnson (2002). "Parametric Frequency Domain Identification in Multiconfiguration Structures." *15th ASCE Engineering Mechanics Conference (EM2002*), Columbia University, New York, 2–5 June 2002.

Elmasry, M.I.S., and E.A. Johnson (2004a). "Health Monitoring of Structures Under Ambient Vibrations Using Semiactive Devices." *American Control Conference 2004 (ACC2004*), Boston Sheraton Hotel, Boston, 30 June - 2 July 2004.

Elmasry, M.I., and E.A. Johnson (2004b). "Improvements in Structural Parameter for SHM using VSDDs." *9th ASCE Specialty Conference on Probabilistic Mechanics and Structural Reliability (PMC2004*), Albuquerque, NM, 26–28 July 2004.

Erkus, B., A. Masato and Y. Fujino (2002). "Investigation of Semiactive Control for Seisimic Protection of Elevated Highway Bridges." *Engineering Structures*, **24**, 281–293.

Federal Highway Administration (FHWA) (2002). "National Bridge Inventory." Web pages, http://www.fhwa.dot.gov/bridge/britab.html

Gavin, G.P., R.D. Hanson and F.E. Filisko (1996a). "Electrorheological Dampers. Part I: Analysis and Design." *Journal of Applied Mechanics*, **63**, 669–675.

Gavin, G.P., R.D. Hanson and F.E. Filisko (1996b). "Electrorheological dampers. Part I: Testing and Modeling." *Journal of Applied Mechanics*, **63**, 676–682.

Hall, J.F., ed. (1995). "Northridge Earthquake of January 17, 1994, Reconnaissance Report." *Earthquake Spectra*, **11** supplement C.

Hera, A., and Z. Hou (2004). "Application of Wavelet Approach for ASCE Structural Health Monitoring Benchmark Studies." *Journal of Engineering Mechanics*, ASCE, **130**(1), 96–104.

Ho, B.L., and R.E. Kalman (1965). "Effective Construction of the Linear State-variable Models from Input/Output Data." *3rd Annual Allerton Conference on Circuit and System Theory*, 449–459; also *Regelungstechnik*, **14**, 545–548.

Housner, G.W., L.A. Bergman, T.K. Caughey, A.G. Chassiakos, R.O. Claus, S.F. Masri, R.E. Skelton, T.T. Soong, B.F. Spencer, Jr. and J.T.P. Yao (1997). "Structural Control: Past Present, and Future." *Journal of Engineering Mechanics*, ASCE, **123**, 897–971.

Housner, G.W., T.T. Soong and S.F. Masri (1994). "Second Generation of Active Structural Control in Civil Engineering." *Proceedings of the 1st World Conf on Structural Control*, Pasadena, Panel: 3–18.

Housner, G.W., T.T. Soong and S.F. Masri (1994b). "Second Generation of Active Structural Control in Civil Engineering." *Microcomp. in Civil Eng.*, **11**(5), 289–296.

Ikonen, E., and K. Najim (2002). *Advanced Process Identification and Control*. Marcel Dekker, New York.

Inman, D.J. (1989). *Vibration: with Control, Measurement, and Stability*. Prentice Hall, Englewood Cliffs, New Jersey.

Johnson, E.A., and M.I.S. Elmasry (2003). Parametric Frequency Domain Identification Using Variable Stiffness and Damping Devices, METRANS Report, Research Project 01-10.

Johnson, E.A., H.F. Lam, L.S. Katafygiotis and J.L. Beck. (2004). "Phase I IASC-ASCE Structural Health Monitoring Benchmark Study Using Simulated Data." *Journal of Engineering Mechanics*, ASCE, **130**(1), 3–15.

Johnson, E.A., L.A. Bergman and P.G. Voulgaris (1997). *Online Modal State Monitoring of Slowly Time-Varying Structures*, NASA Contractor Report 198057.

Johnson, E.A., R.E. Christenson and B.F. Spencer, Jr. (2003). "Semiactive Damping of Cables with Sag." *Computer Aided Civil and Infrastructure Engineering*, **18**(2), 132–146.

Juang, J. (1994). *Applied System Identification*. Prentice Hall, Englewood Cliffs, New Jersey.

Juang, J., and M.Q. Phan (2001). *Identification and Control of Mechanical Systems*. Cambridge University Press, New York.

Juang, J., and R.S. Pappa (1985). "An Eigen System Realization Algorithm for Modal Parameters Identification and Model Reduction." *Journal of Guidance*, **8**(5), 620–627.

Juang, J., J.E. Cooper and J.R. Wright (1988). "An Eigen System Realization Algorithm using Data Correlations (ERA/DC) for Modal Parameter Identification." *Control-Theory and Advanced Technology*, **4(**1), 5–14.

Kanai, K. (1957). "Semi-emperical Formula for the Seismic Characteristics of the ground." *Bulletin of Earthquake Research Inst.*, University of Tokyo, **35**, 309–325.

Katafygiotis, L.S., and K. Yuen (2001). "Bayesian Spectral Density Approach for Modal Updating using Ambient Data." *Earthquake Engineering and Structural Dynamics*, **30**(8) 1103–1123.

Katafygiotis, L.S., H.F. Lam and N. Mickleborough (2000). "Application of a Statistical Approach on a Benchmark Damage Detection Problem." *Proceedings of the 14th ASCE Engineering Mechanics Conference*, Austin, Texas, 21–24 May 2000.

Kiremedjian, A.S. (1999). "Vulnerability and Damage of Structures from Earthquakes." Presentation, *Uncertaininty of Damageability Conference*, Risk Prediction Initiative, web page: http//:www.bbsr.edu/rpi/meetpart/Nov99

Kobori, T., and M. Takahashi (1993). "Seismic Response Controlled Structure with Active Variable Stiffness System." *Earthquake Engineering and Structural Dynamics*, **22**(12), 925–941.

Kurata, N., T. Kobori, S.M. Takahashi, T. Ishibashi, N. Niwal, J. Tagami and H. Midorikawa (2000). "Forced Vibration Test of a Building with Semiactive Damper System." *Earthquake Engineering and Structural Dynamics*, **29**, 629–645.

Lam, H.F., L.S. Katafygiotis and N.C. Mickleborough (2004). "Application of a Statistical Model Updating Approach on Phase I of the IASC-ASCE Structural Health Monitoring Benchmark Study." *Journal of Engineering Mechanics*, ASCE, **130**(1), 34–48.

Levy, E. (1959). "Complex Curve Fitting." *IRE Transactions on Automatic Control*, **AC-4**(1), 37–44.

Ljung, L. (1999). *System Identification: Theory for the User* (2nd ed.), Prentice Hall, Englewood Cliffs, New Jersey.

Luş, H., and R. Betti (2000). "Damage Identification in Linear Structural Systems." *Proceedings of the 14th ASCE Engineering Mechanics Conference*, Austin, Texas, 21–24 May 2000.

Luş, H., R. Betti and R. W. Longman (1999). "Identification of Linear Structural Systems Using Earthquake-Induced Vibration Data." *Earthquake Engineering and Structural Dynamics*, **28**, 1449–1467.

Luş, H., R. Betti, J. Yu and M. De Angelis (2004). "Investigation of a System Identification Methodology in the Context of the ASCE Benchmark Problem." *Journal of Engineering Mechanics*, ASCE, **130**(1), 71–84.

Lutes, L.D., and S. Sarkani (2004). *Random Vibrations, Analysis of Structural and Mechanical Systems*. Elsevier, Burlington, Massachusetts.

Makris, N., S.A. Burton, D. Hill and M. Jordon (1996). "Analysis and Design of ER Damper for Seismic Protection of Structure." *Journal of Engineering Mechanics*, ASCE, **122**(10), 1003–1011.

MATLAB® (1999). The Math Works Inc., Natick, Massachusetts.

Mita, A. (1999). "Emerging Needs in Japan for Health Monitoring Technologies in Civil and Building Structures." In F.-K. Chang (ed.), *Structural Health Monitoring 2000: Proceedings of the 2nd International Workshop on Structural Health Monitoring*, Stanford University, 8–10 September 1999 (Technomic Publishing Co., Lancaster, PA), 56–67.

Moses, F., C.G. Schilling and K.S. Raju (1987). "Fatigue Evaluation Procedures for Steel Bridges." National Cooperative Highway Research Program, Report (**299)**, Transportation Research Board, National Research Council, Washington, DC, ISSN 0077-5614.

Nagarajaiah, S., and X. Ma (1996). "System Identification Study of a 1:10 Scale Steel Model Using Earthquake Simulator," *Proc. of Eng. Mech. Conf.,* ASCE, **2**, 764–767.

Nagarajaiah, S., and X. Sun (2001). "Base-Isolated FCC Building: Impact Response in Northridge Earthquake." *Journal of Structural Engineering*, ASCE, **127**(9), 1063–1075.

Patten, W.N., S. Jinghui, L. Guangjun, J. Kuehn and G. Song (1999). "Field Test of an Intelligent Stiffener for Bridges at The I-35 Walnut Creek Bridge." *Earthquake Engineering and Structural Dynamics,* **28**, 109–126.

Quanser Consulting Inc. (1995). *User Manuals*. Ontario, Canada.

Quek, S.T., W. Wang and C.G. Koh (1999). "System Identification of Linear MDOF Structures Under Ambient Excitation." *Earthquake Engineering and Structural Dynamics*, **28**, 61–77.

Rabinow, J. (1948). "The Magnetic Fluid Clutch." *AIEE Trans.*, **67**, 1308–1315.

Ramallo, J.C., E.A. Johnson and B.F. Spencer, Jr. (2002). "'Smart' Base Isolation Systems." *Journal of Engineering Mechanics*, ASCE, **128**, 1088–1099.

Ray, L.R., and L. Tian (1999). "Damage Detection in Smart Structures through Sensitivity Enhancing Feed-back Control." *Journal of Sound and Vibration*, **227**(5), 987–1002.

Ribakov, Y., and J. Gluck (1999). "Active Control of MDOF Structures with Supplemental Electrorheological Fluid Dampers." *Earthquake Engineering and Structural Dynamics*, **28**, 143–156.

Sanayei, M.S., W. Doebling, C.R. Farrar, S. Wadia-Fascetti and B. Arya (1998). "Challenges in Parameter Estimation for Condition Assessment of Structures." *Structural Engineering World Wide*, *Proc. Structural Engineers World Congress*, San Francisco, CA, July 1998, Elsevier, New York, paper ref. T216-5.

Simiu, E., and R.H. Scanlan (1996). *Wind Effects on Structures* (3rd Ed.), Wiley & Sons, New York, England.

SIMULINK® (1999). The Math Works Inc., Natick, Massachusetts.

Smith, J.W. (1988) Vibration of Structures: Applications in Civil Engineering Design, Chapman & Hall, London, England.

Sohn, H., and C. R. Farrar (2001). "Damage Diagnosis using Time Series Analysis of Vibration Signals." *Smart Materials and Structures*, **10**, 446–451.

Sohn, H., and K.H. Law (2000). "Bayesian Probabilistic Damage Detection of a Reinforced Concrete Bridge Column." *Earthquake Engineering and Structural Dynamics*, **29**, 1131–1152.

Soong, T.T., and B.F. Spencer, Jr. (2002). "Supplemental Energy Dissipation: State-of-the-Art and State-of-the-Practice." *Engineering Structures*, **24**, 243–259.

Soong, T.T., and G.F. Dargush (1997). *Passive Energy Dissipation Systems in Structural Engineering*, Wiley & Sons, Chichester, England.

Soong, T.T., and M. Grigoriu (1993). *Random Vibration of Mechanical and Structural Systems*. Prentice Hall, Englewood Cliffs, New Jersey.

Spencer, B.F., Jr., and M.K. Sain (1997). "Controlling Buildings: A New Frontier in Feedback." *IEEE Control Systems Magazine*, **17**(6), 19–35.

Spencer, B.F., Jr., G.Q. Yang, J.D. Carlson and M.K. Sain (1998). "Smart Dampers for Seismic Protection of Structures: a Full-Scale Study." *Proceedings of the 2nd World Conference on Structural Control*, Kyoto, Japan, 417–426.

Spencer, B.F., Jr., S.J. Dyke, M.K. Sain and J.D. Carlson (1997). "Phenomenological Model for Magnetorheological Dampers." *Journal of Engineering Mechanics*, ASCE, **123**(3), 230–238.

Symans, M.D., and M.C. Constantinou (1997). "Seismic Testing of a Building Structure with a Semiactive Fluid Damper Control System." *Earthquake Engineering and Structural Dynamics*, **26**, 759–777.

Symans, M.D., and M.C. Constantinou (1999). "Semiactive Control Systems for Seismic Protection of Structures: a state-of the-art review." *Engineering Structures*, **21**, 469–487.

Tajimi, H. (1960). "A Statistical Method of Determining the Maximum Response of a Building Structure during an Earthquake." *Proceedings of 2nd World Conference on Earthquake Eng.*, Japan, 781–797.

Takewaki, I., and M. Nakamura (2000). "Stiffness-Damping Simultaneous Identification using Limited Earthquake Records." *Earthquake Engineering and Structural Dynamics*, **29**, 1219–1238.

Vanik, M.W., J.L. Beck and S.K. Au (2000). "Bayesian Probabilistic Approach to Structural Health Monitoring." *Journal of Engineering Mechanics*, ASCE, **126**(7), 738–745.

Varadarajan, N., and S. Nagarajaiah (2000). "Semi-Active Variable Stiffness Tuned Mass Damper for Response Control of Wind Excited Tall Buildings: Benchmark Problem." *Proceedings of the 14th ASCE Engineering Mechanics Conference*, Austin, Texas, 21–24 May 2000.

Wang, C.S., and F.-K. Chang (1999). "Built-In Diagnostics for Impact Damage Identification of Composite Structures." In F.-K. Chang (ed.), *Structural Health Monitoring 2000: Proceedings of the 2nd International Workshop on Structural Health Monitoring*, Stanford University, 8–10 September 1999 (Technomic Publishing Co., Lancaster, PA), 612–621.

Winslow, W.M. (1949). "Induced Vibration of Suspensions." *J. Applied Physics*, **20,** 1137–1140.

Xu, Y.L.,W.L. Ku and J.M. Ko (2000). "Seismic Response Control of Frame Structures using Magnetorheological/Electrorheological Dampers." *Earthquake Engineering and Structural Dynamics*, **29**, 557–575.

Yang, G., B.F. Spencer, Jr., J.D. Carlson and M.K. Sain (2002). "Large-Scale MR Fluid Dampers: Modeling and Dynamic Performance Considerations." *Engineering Structures*, **24**, 309–323.

Yang, J.N., J.C. Wu and Z. Li (1996). "Control of Seismic-Excited Buildings Using Active variable Stiffness Systems." *Engineering Structures*, **18**(8), 589–596.

Yang, J.N., Y. Lei, S. Lin and N. Huang (2004). "Hilbert-Huang Based Approach for Structural Damage Detection." *Journal of Engineering Mechanics*, ASCE, **130**(1), 85–95.

Yuen K.-V., S.K. Au and J.L. Beck (2004). "Two-Stage Structural Health Monitoring Approach for Phase I Benchmark Studies." *Journal of Engineering Mechanics*, ASCE, **130**(1), 16–33.

Zhang, D.-Y., and E.A. Johnson (2006a). "Substructure Parameter Identification Method for Shear Type Structures," *4th World Conference on Structural Control and Monitoring (4WCSCM)*, San Diego, CA, July 11–13, 2006. CD-ROM Proceedings (E. Johnson and A. Smyth, eds.), paper 4WCSCM-371.

Zhang, D.-Y., and E.A. Johnson (2006b). "Controlled Substructure Identification Method for Shear Type Structure," *4th World Conference on Structural Control and Monitoring (4WCSCM)*, San Diego, CA, July 11–13, 2006. CD-ROM Proceedings (E. Johnson and A. Smyth, eds.), paper 4WCSCM-372.